DEVELOPMENT AND EVALUATION OF AN INTRAORAL TONGUE OPERATED ASSISTIVE TECHNOLOGY FOR PEOPLE WITH QUADRIPARESIS

A Dissertation
Presented to
The Academic Faculty

by

Fanpeng Kong

In Partial Fulfillment
of the Requirements for the Degree
Doctor of Philosophy in the
School of Electrical and Computer Engineering

Georgia Institute of Technology
May 2020

DEVELOPMENT AND EVALUATION OF AN INTRAORAL TONGUE OPERATED ASSISTIVE TECHNOLOGY FOR PEOPLE WITH QUADRIPARESIS

Approved by:

Dr. Gregory D. Durgin, Advisor
School of Electrical and Computer Engineering
Georgia Institute of Technology

Dr. Ying Zhang
School of Electrical and Computer Engineering
Georgia Institute of Technology

Dr. Omer Inan
School of Electrical and Computer Engineering
Georgia Institute of Technology

Dr. Hoseon Lee
Department of Electrical Engineering
Kennesaw State University

Dr. Andrew F. Peterson
School of Electrical and Computer Engineering
Georgia Institute of Technology

Date Approved: March 9, 2020

To my family and friends

ACKNOWLEDGEMENTS

This dissertation would not have been possible without the support of the people who have helped and inspired me during my Ph.D. life at Georgia Tech. I would like to thank all of them.

First, I would like to express my deepest gratitude to my advisor, Dr. Gregory D. Durgin. All these accomplishments could not be possible without his valuable advice, insightful guidance and support. He is an outstanding scientist, mentor and leader. What I have learnt from him will be my lifetime treasure. I would also like to extend my gratitude to the committee members, Dr. Omer Inan, Dr. Andrew F. Peterson, Dr. Ying Zhang, and Dr. Hoseon Lee, for their time and effort in serving on my committee.

I would like to give my special thanks to my colleagues in Georgia Tech: Yaoyao Jia, Gwangrok Jung, Pyungwoo Yeon, Nazmuz Sahadat, Nordine Sebkhi, Zhenxuan Zhang, Byunghun Lee, Jaemyung Lim, and Abdollah Mirbozorgi. Their help and support were with me through my whole Ph.D. journey. My thanks also extend to all the researchers and students I worked with. Especially, I would like to give my thanks to all of my friends. They shared my happiness and sadness with me through my entire Ph.D. life and encouraged me to go over every difficulty in my life.

I would like to especially thank my family. Without the endless love, guidance and support from my parents, I would not be here. They are always the source of my strength and motivation.

TABLE OF CONTENTS

LIST OF TABLES

LIST OF FIGURES

SUMMARY

The objective of this research is to develop a wireless intraoral tongue operated assistive technology (AT) for the people with disabilities, such as quadriplegia to improve the quality of their lives and do daily activities more efficiently and independently. Comparing with the tongue operated AT, the current ATs, such as EEG, EMG, and speech recognitions, are lack of robustness and intuitiveness. For example, the speech recognition technology is very sensitive to the outside noise. The focus of this work has been designing a system, called intraoral Tongue Drive System (iTDS) that captures the tongue motions and convert them to a set of the user-defined commands to interact with devices such as computers, smartphones, and wheelchairs. In this work, a new intraoral antenna operating at 2.4 GHz will be proposed to solve the weak wireless communication between inside and outside the mouth. Many research works have been focused on the implantable antennas; therefore, this work provides a novel antenna design and analysis in the intraoral environment. Considering the noisy surroundings and the dynamic mouth environment that adversely affects the wireless communication, this work will also focus on solving these issues by developing a triple-band transmitter application-specific integrated circuits (ASIC) chip equipped with an adaptive matching network. It also provides a method to improve the robustness of the wireless link quality in the presence of dynamic environment, not only for the intraoral application. Besides these, a high accuracy signal processing algorithm will be implemented in the iTDS, making it as a stand-alone device, to process users' inputs which are efficient to compute in a limited resource embedded hardware. This research will also focus on designing

experiments to evaluate the learning abilities, pros and cons of this intraoral tongue operated assistive technology in accessing computers, using smartphones and driving the wheelchairs efficiently. During the experiments, it was observed that the proposed iTDS has demonstrated a robust wireless communication link and better performance compared with other tongue operated assistive technologies. In conclusion, this research work proposes a new intraoral AT, at the same time, it contributes several key innovations regarding the wireless communication in the presence of intraoral environment.

CHAPTER 1. INTRODUCTION

1.1 Background and Motivation

Across the United States, nearly 1 in 5 people live with some form of paralysis during their lifetime, of which 29% is caused by stroke, 23% by spinal cord injury (SCI), and 17% by multiple sclerosis [1][2]. To improve the quality of life of these and other people with severe physical disabilities and enhance their independence, engineers have developed various assistive technologies (ATs) [2]-[7]. However, the choices are quite limited as many ATs do not provide sufficient flexibility for the patients or they require frequent caregivers' assistance. Others are not sufficiently robust, intuitive, or compatible with various environments.

For example, the EEG-based brain computer interfaces (BCI) [8][9] are suitable for people who have severe paralysis, but they are difficult to wear and set up and susceptible to motion artifacts, making them inappropriate for outdoor environments. Another group of ATs operate with electromyography (EMG) signals. The EMG-controlled switches provide users with computer access, but they are limited by the number of commands and muscle fatigue in long-term operation [11]. The speech recognition system is a popular AT [12][13]. Even though people with disabilities can issue simple commands and type efficiently using this technology in a quiet environment, it cannot provide efficient cursor control nor is it reliable enough for wheelchair navigation because of noise sensitivity and difficulties in outdoor environments [13][14].

To addess these problems, GT researchers have developed the Tongue Drive System (TDS) to tap into the inherent abilities of the human tongue together with added system robustness, simplicity, and high flexibility through customized tongue command definition [15][16]. Tongue and oral muscles have a strong representation in the human motor cortex, which results in sophisticated motor control needed for speech and ingestion with many degrees of freedom [17]. The tongue is directly connected to the brain through the hypoglossal nerve, which often escapes SCIs and major neurological diseases[18]. Therefore, a tongue operated AT can offer broad coverage among people with severe physical disabilities, who can move their tongues without difficulty. TDS detects a number of user-defined commands by monitoring the position of a small magnetic tracer, which is attached near the tip of the tongue with tissue adhesive, in real time. Several versions of the TDS have been developed, including external TDS (eTDS), multimodal TDS (mTDS). The eTDS has been evaluated clinically, with the results presented in [16]. However, in certain conditions, such as driving a powered wheelchair (PWC) or riding in a vehicle in rough terrain, the users may experience mechanical stability issues with the head-worn versions of the TDS [19]. This is because the headset position on the head, and consequently the magnetic sensor positions near the mouth may shift with respect to the position of magnetic tracer on the tongue during the training phase. Also, the result of a survey on eTDS indicated that the majority of potential users are sensitive to their appearance when using their ATs [20]. They prefer devices that can be completely hidden from sight, and provide them with a higher degree of privacy.

The intraoral Tongue Drive System (iTDS) was introduced alternative solutions by completely hiding inside of the mouth, while also being more mechanically stable by

clasping on the teeth to be a potential solution to these issues of the TDS. The objective of this research is to develop a fully functional wireless iTDS. The focus of this work includes designing the proposed intraoral system to interact with smart devices, also on establishing a robust wireless communication between the inside mouth device and outside the mouth surroundings. Considering the moisture environment of the mouth, a hermetical sealing technique to protect the intraoral device is also included in this research. In addition, this work will include designing general human computer interaction (HCI) experiments to evaluate the performance of the proposed intraoral assistive technology. The outcomes of this research are to test the hypothesis that the proposed iTDS has better performance compared to other tongue operated ATs in accessing and controlling smart devices and to realize a robust wireless communication between in- and outside the mouth. This research proposes a new AT to improve the life quality of people with disabilities, and also provides ideas on establishing a robust wireless communication for wireless intraoral devices, such as the inductive tongue computer interface (ITCI) AT, the intraoral device to quantify real time sodium intake, the mouth guard to monitor concussions, and other general intraoral devices such as sleep apnea oral devices [21]-[24]. Nowadays, a large amount of intraoral devices have entered the market or under development [21]-[24]. Considering this fact, this research is necessary at the moment to meet the needs of the growing intraoral devices market.

1.2 Related Work

Spinal cord injuries (SCI), stroke, cerebral palsy, and other neuromuscular disorders may lead to quadriplegia, a condition that results in loss of sensor and motor functions of all limbs and torso. The annual incidence of SCI that leads to quadriplegia,

not including those who die at the scene of the accident, is approximately 7400 new cases each year. The number of people in the U.S. who are alive in 2014 and are quadriplegic caused by SCI has been estimated to be approximately 163,000 persons. Various research has been done to develop computer interfaces for individuals without upper limb mobility based on different functional parts of the body such as head tracking, gaze tracking, speech recognition, chin/mouse-operated joysticks, Sip-n-puff, and brain-controlled interfaces.

Those remaining abilities, such as speech recognition and brain-controlled interfaces, are required to be operated in a less noisy environment. The head tracking requires head and neck movement, which have limited coverage because some quadriplegics have limited or no head mobility or they cause fatigue in weakened cervical/shoulder muscles. Tongue-operated ATs have shown superior advantages in terms of robustness, noninvasiveness, and simplicity. In addition, the tongue muscle is similar to the heart muscle in that it does not fatigue easily. Therefore, it is the most suitable remaining ability for AT.

Balance between functionality, performance, and ease of use must be found for the design of a good computer interface. A good computer interface should not only be easy to use, but also have good performance. Some of the key aspects of successful ATs are the ease of setup/removal, maintenance, learning, and usability particularly in long intervals, unobtrusiveness, physical comfort, noninvasiveness, number of direct commands that can be issued by the user, information transfer rate from the user to the computer or the environment (input speed), accuracy (error rate), rate of perceived exertion, versatility and adaptation to user's particular needs and disabilities, robustness,

cost, and aesthetics. Tongue movement based assistive technology can become an excellent computer interface.

Among existing ATs, some are designed to operate inside the mouth which are completely hidden providing the privacy issues of the end users. Operating inside mouth also increases the mechanical stability to provide a more robust system. However, one of the biggest design considerations is the communication of intraoral tongue operated ATs since most of the ATs are operated wirelessly, which increases the design difficulties. Considering the noisy operation environment and the dynamic mouth environment, realizing a robust wireless link becomes more challenging. Some methods, such as designing a high gain transmission antenna and providing dynamic antenna impedance matching, are proposed to improve the robustness of the wireless link. However, most of these proposed methods are not dedicated for the intraoral tongue operated ATs.

In the rest of this chapter, some of the existing tongue controlled ATs with different design principles will be presented and some wireless link quality improvement methods will be discussed.

1.2.1 Tongue-Operated Assistive Technologies

Figure 1a shows the Tongue Drive System, which uses a magnetic field generated by a magnetic tracer attached to user's tongue to detect commands issued by the participant [25]. Four sensors around the face are used to capture the magnetic field issued by the subject. The analog magnetic field is digitized and sent to a control unit to transmit wirelessly using 2.4GHz

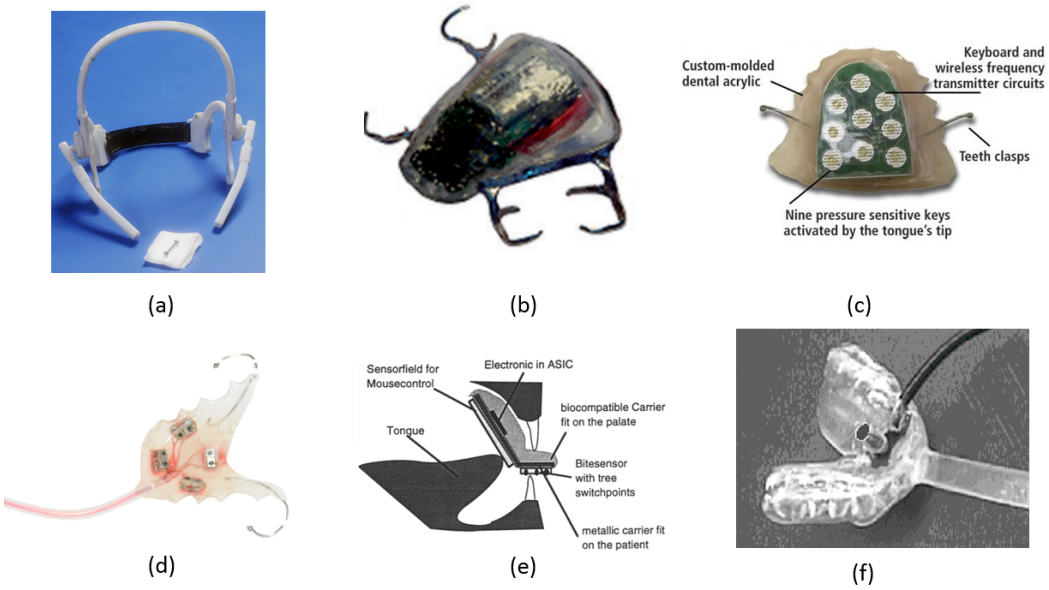

Figure 1 (a) Tongue Drive System (TDS)[15] (b) Inductive Tongue Control System (ITCS)[30] (c) Tongue Touch Keypad (TTK)[35] (d) Optically Tongue Gesture Sensing Device (oTGS)[36] (e) Tongue Mouth[37] (f) Tongue Pointing Device (TPD)[38].

Texas instrument's proprietary RF protocol to the receiver [26]. The receiver unit receives the signal and sends it to a PC or phone for further processing to find the assigned tongue commands [27]. A LabVIEW interface is used to find the proper signal capture by the system by observing the signal waveform [28]. After confirming the functionality of the system, the system goes through a calibration procedure where the earth magnetic field (EMF) is attenuated to remove unwanted magnetic signal other than the magnetic field generated by the user's magnetic tracer [29]. The user needs to go through a training procedure, where a k-nearest neighbor (KNN) classifier is trained after dimension reduction using principle component analysis (PCA) for 70 issued tongue commands (10 times each 6 commands and a neutral).

An intraoral Tongue operated AT, ITCS, is shown in Figure 1b. This device uses the change of inductance by placing a ferromagnetic material attached to the tongue on

the inductive switch [30]. This causes change of inductance because of changing the core material of the inductor, detected from the voltage change induced by it. The system PCB uses 18 inductor switches attached to the pallet of the user [31]. This is an inductive switch based assistive technology driven by the tongue. Using this device, participants can drive a wheelchair [32] as well as control a computer [33].

Another tongue operated AT named Tongue Touch Keypad (TTK) is shown in Figure 1c. TTK is an assistive technology that uses the pressure of the tongue tip to activate 9 pressure sensitive switches mounted on the pallet of the user [34]. The device PCB is molded with custom acrylic to avoid saliva leaking in the electronics. Based upon the activated switch, a command transmits wirelessly from mouth cavity to the receiver either to drive a wheelchair or to control a computer [35].

Researchers at University of Washington have developed an optical sensing technique to detect the tongue gestures [36], which is shown in Figure 1d. The optical tongue gesture sensor (oTGS) is made as a palatal dental retainer, which embedded four infrared light emitting diodes (LED) and four infrared photodiodes in the mouth. When the tongue approaches these sensors, the amount of light from an LED reflecting back to the photodiode varies, allowing it to sense the proximity of the tongue to these sensors. Another tongue computer interface was developed using piezoelectric sensors, shown in Figure 1e [37]. The user bites on the device, and the tongue directly touches the sensor plate, which is similar to a touchpad. The piezoelectric sensors form a matrix, which can detect the pressure and position of the tongue tip. The tongue-pointing device (TPD), shown in Figure 1f, is based on the IBM track point technology. One of the advantages of

the device is providing proportion control, which is realized by using the tongue touching the track point to move the mouse pointer [38].

1.2.2 Wireless link quality enhancement

To improve the performance of the wireless link, in [39] and [40], the authors have presented a dipole antenna for intraoral devices and discussed its propagation characteristics, respectively. However, their discussions are devoid of any system implementation. In addition, some similar types of antennas which are for the biomedical implants were proposed [41]. Even though, these antennas require only a small space but the gain is not enough for intraoral communication. A dedicated intraoral antenna needs to be designed to meet this requirement.

Multiple adaptive antenna impedance matching techniques have been published to overcome the dynamic operation environment. In [42] the authors presented an off-chip impedance matching by adding additional four capacitors, resulting 16 combinations of possible matching for an intraoral device. By detecting the phase and amplitude of the output signal of the power amplifier (PA), [42] provided on chip matching and realized a tuning range up to $|\Gamma| = 0.5$. In another literature [44], an integrated antenna impedance mismatch correction system at 2.4 GHz was proposed. In this design, the signal amplitude of the PA output was picked up as the mismatch information. Two pi-matching networks were integrated at the output PA to provide the antenna impedance matching. With this design, the realized tuning range can be up to $|\Gamma| = 0.3$. A method of choosing the optimal matching capacitance values has been presented in [45]. Different matching networks have been analyzed, and an optimal matching network was selected with the

guidance for the capacitance selection. Measurement results were also provided to prove the proposed method.

1.3 Summary of Contributions

The objective of this dissertation is to develop a wireless intraoral tongue operated assistive technology for the people with disabilities, such as quadriplegia to improve the quality of their lives and do daily activities more efficiently and independently. To reach this ultimate goal, several research topics need to be addressed such as establishing a robust wireless communication for wireless intraoral device, developing an advanced signal processing algorithm to process the data efficiently, and evaluate the system performance and generating the learning ability of the device. All of these tasks are consist of the contributions of this dissertation which are listed as bellow:

1. The most important intellectual property of this work is to propose a brand new intraoral tongue motion tracking system, which are able to converted to user defined commands for people with severe disabilities.
2. Proposed a human mouth model in CST to design a high-gain intraoral antenna operating at 2.4 GHz with fully characterization and integration with the proposed system.
3. Designed a first version of ASIC that operates at three different bands wirelessly transmit data. In this ASIC, we integrated analog biasing blocks used as power supplies and three types of transmitters with power amplifier (PA) and voltage-controlled oscillator (VCO). Most important is that an adaptive matching network is implemented at the end of the PA to compensate the mismatching effect.

4. Designed a second version of ASIC which improves the performance based on the first one in terms of transmission power and matching capability. Moreover, in this version of ASIC, a super-regenerative receiver has been implemented to realize the bi-direction transmission.
5. Implemented the intraoral system with an advanced signal processing algorithm that is able to process the tongue commands locally in micro-controller instead of in the personal computer, reducing the power consumption of the system. In addition, this new system is accessible to all of the smart devices in the market.
6. A new typing method dedicated to this device has been proposed to improve the typing experience of the user, increasing the typing speed and reducing the typing error rate.
7. Several general human computer interaction (HCI) tasks have been developed to evaluate the learning ability and the performance of this system, comparing with other ATs which are developed in the labs and markets.

The second chapter of this dissertation describes the detailed design of the intraoral antenna along with the first version of the intraoral Tongue Drive System (iTDS), with antenna and system level characterization. In chapter three, the first ASIC equipped with dynamic matching system is demonstrated with measurement results. Chapter four presents the design of the second ASIC with improved functionality and performance compared to the first one. A new iTDS with an advanced signal processing algorithm along with a new typing method will be presented in chapter five. In addition, the general human interaction tasks are developed for the system to evaluate the performance. Finally, chapter six presents the summary of this dissertation followed by the future work.

CHAPTER 2. ANTENNAS FOR INTRAORAL TONGUE DRIVE SYSTEM AT 2.4 GHZ: DESIGN, CHARACTERIZATION, AND COMPARISON

2.1 Introduction

The Tongue Drive System (TDS) is developed to provide a kind of Assistive Technology (AT) that is flexible, easy to use, and robust. The TDS taps into the inherent abilities of the human tongue together with added system robustness, simplicity, and high flexibility through customized tongue command definition. TDS allows users to employ a set of unique tongue gestures to issue a set of user-defined commands for accessing computers, navigating wheelchairs, and controlling their environment. A small permanent magnetic tracer, the size of a lentil, is affixed near the tip of the tongue, via tissue adhesives, implantation, or tongue piercing, to generate a magnetic field pattern for each tongue gesture [46]. This magnetic signature is recorded by an array of magnetic sensors inside the mouth or near the cheeks on the outside and wirelessly delivered to a processing unit that runs a real-time pattern recognition algorithm to infer the user's intended command [47].

Tongue and oral muscles have a strong representation in the human motor cortex, which results in sophisticated motor control needed for speech and ingestion with many degrees of freedom [48]. The tongue is directly connected to the brain through the hypoglossal nerve, which often escapes SCIs and major neurological diseases [49]. Therefore, a tongue-operated AT can offer broad coverage among people with severe

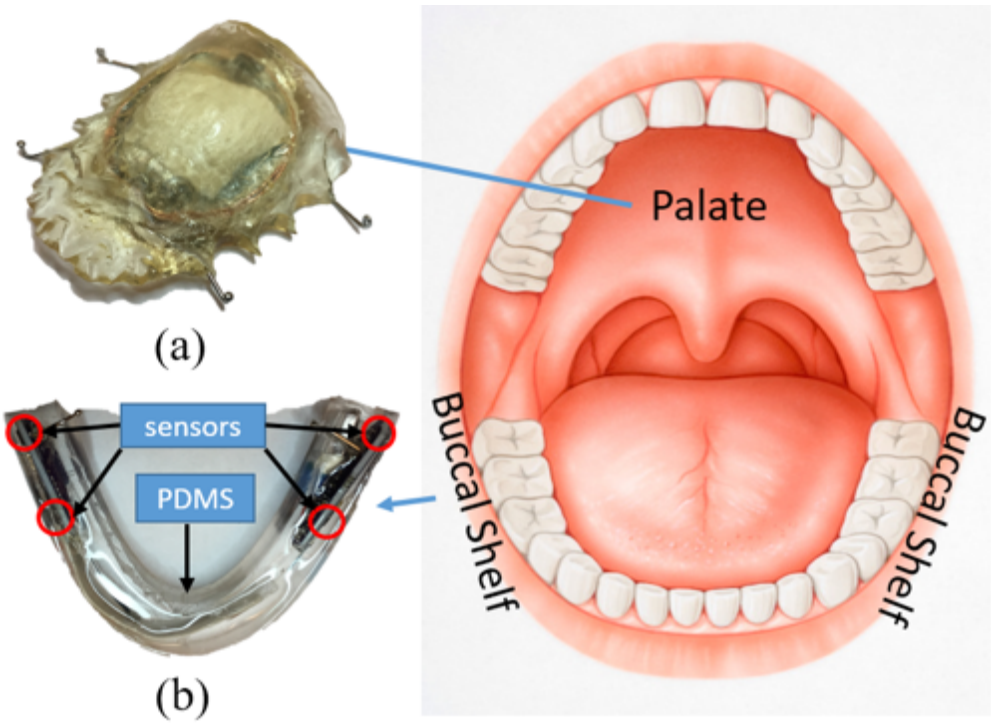

Figure 2 Two versions of the iTDS: (a) iTDS-p, located at the palate place; and (b) iTDS-a, located at the buccal shelf place.

physical disabilities, who can move their tongues without difficulty. In addition, unlike the brain, the tongue is easily accessible without any surgical procedure, and being hidden inside the mouth offers the end users an intraoral AT with a certain degree of privacy.

Several versions of the TDS have been developed, including external TDS (eTDS) [15] multi-model TDS (mTDS) [50], and intraoral TDS (iTDS) [51] [52]. The eTDS has even been evaluated clinically, with the results presented in [20]. The iTDS has no externally worn component, such as a headset, and provides its users the highest level of mechanical stability and privacy. However, like most dental retainers, it should be customized based on the user's oral anatomy for maximum comfort level. Two different shapes have been considered for the iTDS so far; the iTDS-p in the form of a palatal

retainer (Figure 2a) [51], and the iTDS-a in the form of an arch-shaped retainer (Figure 2b) [52]. Even though iTDS-p is simpler to construct, has been adopted for prior intraoral ATs [53] [54], and offers more space for the electronics and battery, iTDS-a has the advantage of not occupying the intraoral space, where the tongue moves, thus providing the user more freedom to issue tongue commands. Therefore, iTDS-a is our preferred shape for which we have designed and analyzed antennas in this study. The new iTDS-a prototype is built using commercial off-the-shelf components (COTS) that are located in the buccal shelf space of the mouth.

The intraoral device presented in [54] uses wires to send information which are inconvenient and unattractive to users. Therefore, one of the important design considerations for the iTDS is wireless communication from inside the mouth to the outside receiver (Rx). However, the design of wireless communication for intraoral devices is challenging because the mouth absorbs power in the high radio frequency (RF) range, de-tunes antennas, and has a dynamically changing environment because of the varying jaw and tongue positions. Normally, basic wireless communication methods for intraoral devices can be adopted from wearable and implantable medical devices (IMD), such as short-range RF and body channel communication (BCC) [52]. Because BCC requires special operating conditions that have been discussed in [52], and is not as reliable, RF communication is the preferred method for the iTDS. Since most the intraoral devices use commercialized transceivers that operate at 2.4 GHz, a critical component is the antenna, which needs to be small and also address the changing environment of the mouth with additional loss imposed by the surrounding tissue.

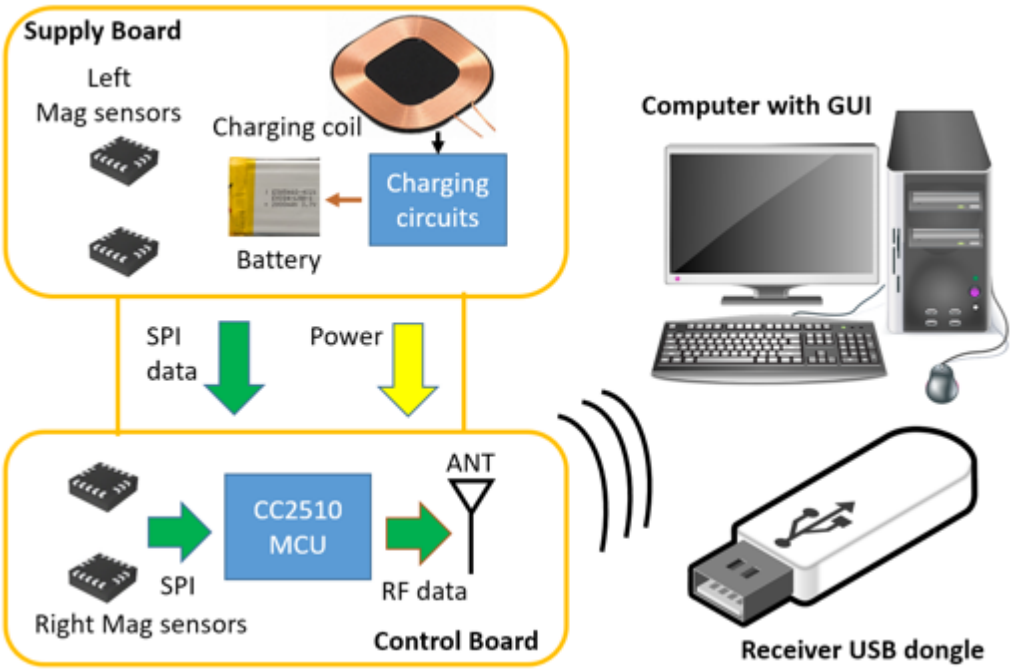

Figure 3 System block diagram of the iTDS, including the printed circuit boards and the universal user interface.

In [39] and [40] the authors have presented a dipole antenna for intraoral devices and discussed its propagation characteristics, respectively. However, their discussions are devoid of any system implementation. Furthermore, several studies include wireless intraoral devices [55]-[58], but none of them provide detailed antenna designs or evaluate the wireless communication aspect of the systems. In particular, communication robustness and radiative performance are unclear. A number of articles focus on implantable antenna design [59]-[61]. However, the gain of most implantable antennas is small and insufficient for intraoral applications. Previously, we studied the performance of COTS antennas in three operating frequencies, 27 MHz, 432 MHz, and 2.48 GHz for the iTDS-p. Those antennas were not designed for intraoral application and suffered from impedance mismatch and small gain. Furthermore, we designed a planar inverted-F

antenna (PIFA) that works at 432 MHz for an earlier version of iTDS-a. However, the antenna was not fully characterized and had a low radiation efficiency.

In this chapter, to ensure robust wireless communication for iTDS-a, we have designed and presented three types of 2.4 GHz antennas: a patch antenna, a dipole antenna, and a PIFA with proper size for operation inside the mouth. We have characterized these antennas and tested their robustness within an actual iTDS-a prototype.

2.2 iTDS-A Implementation

2.2.1 System Overview

The iTDS-a block diagram is shown in Figure 3. The system has two printed circuit boards (PCB), connected by a ten-wire flat cable [62] which houses the control and supply circuitry as well as two 3-axial magnetic sensors (LSM303D, STMicro-electronics, Switzerland). In practice, the entire device will be coated with medical-grade polydimethyl -siloxane (PDMS), which is biocompatible and approved for intraoral appliances. A receiver USB dongle connected to a PC established the wireless communication link with the iTDS-a inside the mouth

2.2.2 Control Board

A CC2510 microcontroller unit (MCU) (Texas Instrument, Dallas, TX) reads the digitized magnetic sensor data, sampled at 100 Hz, via serial peripheral interface (SPI). The four magnetic sensors are placed at the corners of the control board and the supply board, respectively. The MCU has a built-in 2.4 GHz transceiver, which RF transmitter port presents 80+74j Ω impedance. We chose a COTS balun (2450BM15B0003) to

realize the matching, while connecting the MCU to the antenna. A micro-strip line was considered from the balun to the feed of the antenna. Another design challenge is the connection between the PCB and antenna. Because the size of intraoral devices are limited, a mini Hirose U. FL connector was chosen to connect the antenna to the PCB [63]. This is a male surface-mount device (SMD) connector with a height of 1.25 mm. A female connector on coaxial cable was used to connect the PCB to the antenna. These connectors and cables are designed to have 50 Ω characteristic impedance to minimize the power loss from impedance mismatch.

The buccal shelf area is bounded on the medial side by the crest of the residual ridge, in the mesial area by the buccal frenulum, and on the distal side by the masseter muscle [64]. The nominal length of the buccal shelf area includes the length of three consecutive molar teeth, which is ~33mm on average, as reported in [65].The height of the area is also defined by the heights of molar teeth. It was reported in [66] that the heights of the 1st, 2nd, and 3rd molars are 19.3 mm, 18.4 mm, and 17.2 mm, respectively, from 46 healthy adult measurements. The depth of the buccal shelf is considered to be ~3 mm over the 1st and 2nd molars and 6.3 mm over the 3rd molar [67]. Therefore, 30 mm × 22 mm set the upper limit of the size of two iTDS-a PCBs. In the current prototype, the PCB size is 26.7 mm by 13 mm to ensure the device is comfortable when placed in a customized mold. We also understand that the size of buccal shelf area is different among various individuals depending on their oral anatomy, particularly between males and females. Therefore, it is necessary to minimize the size of the electronics and customize the device based on the user's dental impression.

2.2.3 Supply Board

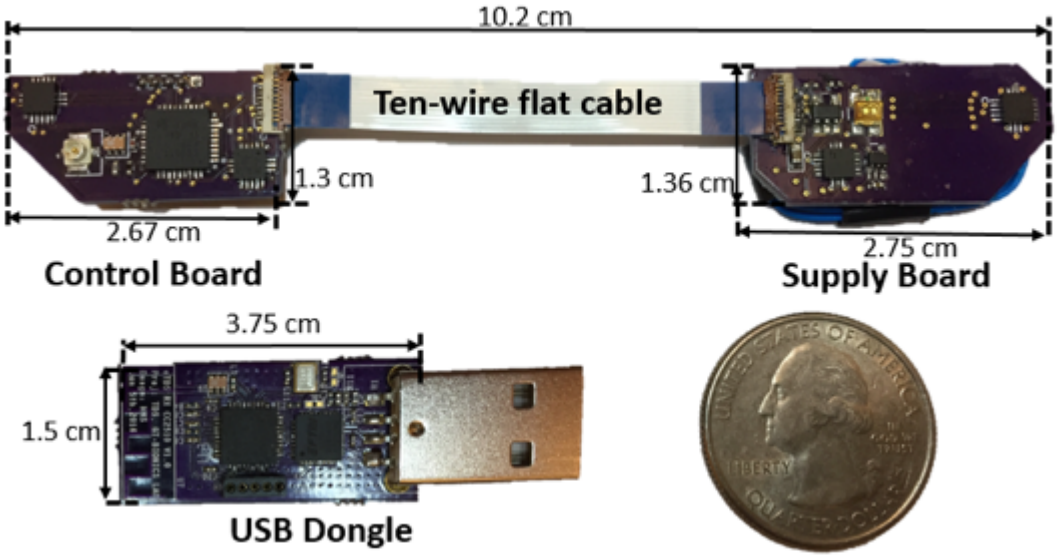

Figure 4 iTDS system prototype with a control board, a supply board, and a USB dongle.

To ensure a stable supply voltage, the battery is followed by a low dropout (LDO) regulator (TPS71730), which generates a stable 3 V supply. A wireless charging coil is used to charge the battery, since the device must be hermetically sealed to protect against saliva in the mouth. The coil is followed by a rectifier (BAS4002A) and a 5 V regulator (MCP1730T), which enables a charging circuit (LTC4054) to charge the battery. Once the battery is fully charged, the charger is disabled and the battery resupplies the system.

2.2.4 USB Dongle

The USB dongle receives data wirelessly and transfers it to a PC via the Universal Asynchronous Receiver/Transmitter (UART). A similar CC2510 MCU with inverted-F antenna pairs with the one on the controller board in the mouth. We have also added a USB-to-UART controller (CY7C64225) to the dongle, which receives magnetic sensor

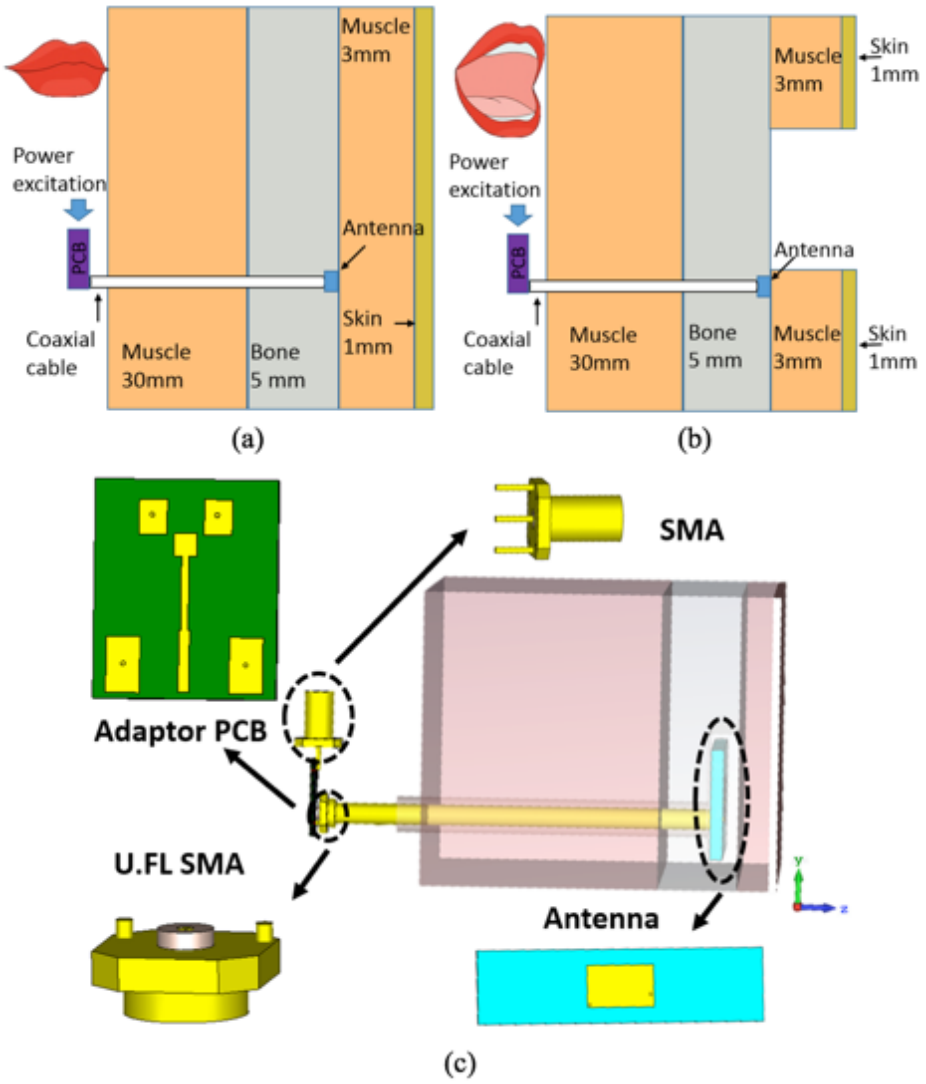

Figure 5 (a) Simple four-layer geometry of the human closed mouth model for the antenna design. (b) Simple four-layer geometry of the human open mouth model of the antenna design. (c) Simulation components used in CST.

data from the MCU. The data is transferred to the PC via a USB port at a baud rate of 921.6 kbps. The complete iTDS-a system prototype is shown in Figure 4.

2.3 Intraoral Antenna Design

To ensure successful communication between the Tx-Rx, we have designed three types of antennas, all operating at 2.4 GHz. The design details and simulation results are presented in the following.

2.3.1 Simulation Model

Considering placement of the iTDS-a in the mouth, the surrounding tissue consists of the teeth, tongue, and chin, which are simulated as bone, muscle, and a combination of muscle and skin, respectively [68]. RF properties of these human tissue materials are provided in the CST Microwave Studio, which was used to design and analyze the

custom antennas according to the simple human mouth model, shown in Figure 5a. The model has four layers, 1 mm for the chin skin over 8 mm of muscle according to [67]. The thickness of the bone layer is 5 mm, based on dimensions of the teeth, over a 30 mm muscle layer that represents the tongue. The length and the width of this model are 60 mm and 14 mm, based on the dimensions of the human teeth [66]. The antenna is placed between the bone (teeth) and the muscle of the chin (lips). To prevent exposure to saliva, we seal the antenna inside a biocompatible silicone, which is also known as polydimethyl-siloxane (PDMS).

2.3.2 Antenna Design

In the physical setup, the iTDS antenna is fed through a female U. FL coaxial cable. To make the simulation profile similar to the physical setup, we created a coaxial cable model in CST, one side of which is connected to the antenna and the other side to a small female SMA model. A male U. FL, which is also used on the PCB for the iTDS, connects

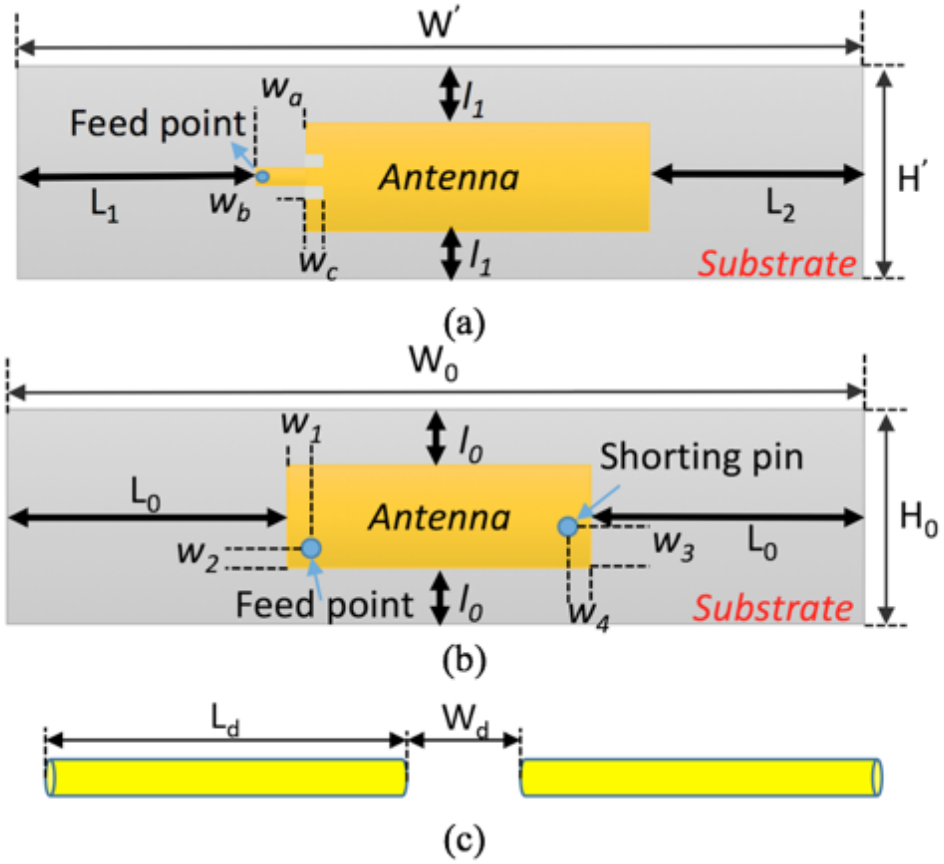

Figure 6 Top view of the three types of antennas: (a) the patch antenna, (b) PIFA, and (c) the dipole antenna.

to the RF cable. A small PCB adaptor, imitating the antenna feed line of the iTDS, was designed with a 7 mm micro-strip line to convert the male U. FL to a regular SMA connector, which connects to the Vector Network Analyzer (VNA) for measurements. The micro- strip line in the PCB adaptor is also modeled in the CST PCB studio to ensure that it has 50 Ω impedance at 2.4 GHz. All of these structures are included in the model, as shown in Figure 5c, and simulated in CST.

The design procedure has three steps: 1) the antenna is optimized in the air for 2.4 GHz with the feed components, which are a coaxial cable, SMA, and adaptor PCB. 2) PDMS material is added on the coaxial cable and antennas in the model, and the antenna

is re-tuned to resonate at 2.4 GHz. 3) the antenna with PDMS coating is placed within the mouth model in Fig. 4a and re-optimized at 2.4 GHz. Finally, we compare the simulation and measurement results.

We used Roger 3003 (Rogers Corporation, Rogers, CT), which has electrical permittivity of $\varepsilon_r = 3.0$, as a flexible substrate material with 0.75 mm thickness [69]. The width of the antenna needs to be less than 19 mm, and the length is defined according to oral anatomy. The backside of the substrate was used as a ground plane for the patch antenna. The antenna was placed in the center of the substrate to reduce the coupling effect between the antenna and the ground plane. The geometry of the patch antenna on

the top layer of the substrate is shown in Figure 6a. A feed line at the center is inserted into the antenna. The antenna impedance is controlled by the width and depth of the feed line. Due to the space limitation in the retainer, a traditional patch antenna cannot easily fit inside the mouth. Instead, an alongated patch antenna has been designed based on [70][71]. The operating frequency, f of a patch antenna in a homogeneous medium can be found from [72]. However, the antenna is surrounded by high-permittivity, conductive human tissue, which decreases the effective length of the antenna. Therefore, the actual resonance frequency differs from the one predicted in [72]. To design the patch antenna in human tissue, we first optimized the length of the antenna to reach the desired frequency. Then, the width and the depth of the feed line into the antenna needed to be optimized. By changing these parameters, the antenna with S_{11} parameter less than -10 dB at 2.4 GHz was designed. Table 1 summarizes the dimensions of the patch and other antennas.

The PIFA antenna has a structure similar to the patch antenna on the same substrate material, with a smaller size as it is operating at a quarter wavelength. The geometry of the PIFA antenna is presented in Fig. 5b, which is achieved by following a design procedure similar to that of the patch antenna. However, we directly use a probe to feed

Table 1 – Key parameters of three custom-designed antennas.

Symbol	*Value (mm)*	*Symbol*	*Value (mm)*
W_0	60	H'	13
H_0	13	l_1	2.9
l_0	3.7	L_1	13.6
L_0	23.8	L_2	17.4
w_1	1	w_a	4
w_2	1.47	w_b	0.6
w_3	2.4	w_c	1
w_4	0.8	L_d	7
W'	60	W_d	2

the PIFA antenna instead of a feed line. Another component of the PIFA is the shorting pin, which is placed on the corner of the antenna, with 0.5 mm in diameter. Compared to the length and width of the PIFA antenna, the size of the shorting pin is negligible. Therefore, the resonant frequency depends on the width and the length of the antenna, which are optimized to operate at 2.4 GHz. The impedance of the PIFA is controlled by the feeding pin position. By changing the position of the probe, we achieve a reflection coefficient below -10 dB. The dipole antenna consists of two copper wires connected to the signal and ground feeds of the coaxial cable, which distance is defined by diameter of the cable. The dimensions of the dipole antenna in the tissue are smaller than those in the air because the electrical properties of the surrounding human tissue reduce the effective wavelength of radiation. The total length of the dipole was optimized in CST to operate at 2.4 GHz. The antenna is initially embedded inside the Figure 5a model to simulate the

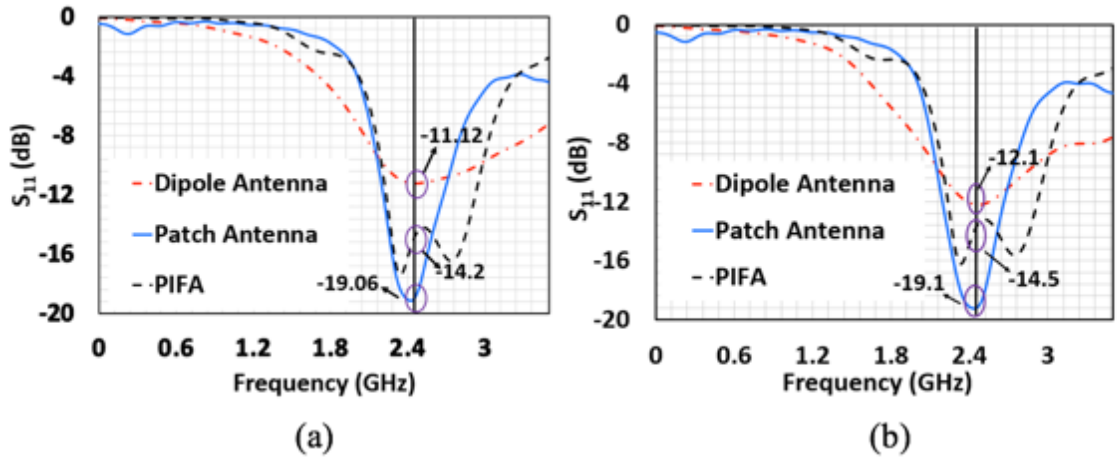

Figure 7 S_{11} simulation of the three antennas under (a) closed-mouth and (b) open-mouth scenarios.

case of a closed mouth. In addition, the open mouth model, shown in Figure 5b, was created, by removing the upper part of the skin and muscle in front of the antenna. Using the open mouth model, we re-simulated all antennas. The return loss (S_{11}) simulation results of the three antennas in closed- and open-mouth scenarios are shown in Figure 7a and Figure 7b, respectively. All simulations indicate that the antennas have sufficiently low power reflection at 2.4 GHz. Based on these simulation results, the -10 dB bandwidths of the patch, PFIA, and dipole antennas are 580 MHz, 778 MHz, and 750 MHz, respectively. Antennas in lossy materials, such as human tissue, often exhibit unusual wideband behavior [73]. Compared with the results of the closed mouth scenario, the center frequency does not shift much, though the S_{11} value has changed.

We also simulated the realized gain radiation pattern (co-polarization) of three antennas in the human mouth model. Because the antennas are embedded in the tissue, considerable power is lost. The realized gain is below zero in every direction in azimuth. The realized gain radiation patterns in the closed- and open-mouth scenarios are shown in Figure 8a and Figure 8b, respectively. The reference in this simulation is the horizontal

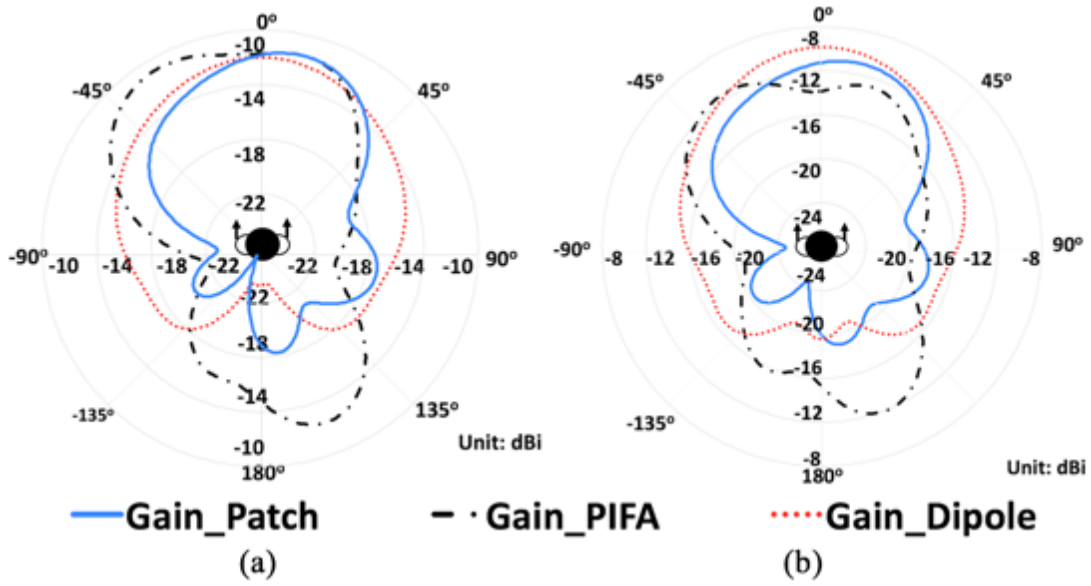

Figure 8 Simulated antenna realized gain radiation pattern using a self-created human mouth model in two scenarios: (a) closed mouth, and (b) open mouth.

plane, parallel to ground. The human top view in the center of the pattern indicates its orientation. In section IV, the measurement radiation patterns have the same orientation and reference plane as these simulations. Based on the simulation results, when the mouth is closed, the peak realized gains of the patch, PIFA, and dipole antennas are -11.4 dBi, -11.5 dBi, and -12 dBi, respectively. The peak realized gains in the open-mouth case increase to -11 dBi, -11 dBi, and -9.8 dBi, respectively. Here, the dipole antenna exhibits the largest improvement in gain. The simulation results of the radiation pattern show the front sides of the antennas have larger realized gain compared to backside. This is because in the simulation model, there is a large amount of tissue, such as the tongue body and the spinal column, on the backside, which absorbs a significant part of the radiated power. Moreover, when the mouth is open, because of the omnidirectional pattern of dipole and PIFA, some of their radiated power towards the upper part of the antenna face less tissue loss. The patch, on the other hand, is a directional antenna, and

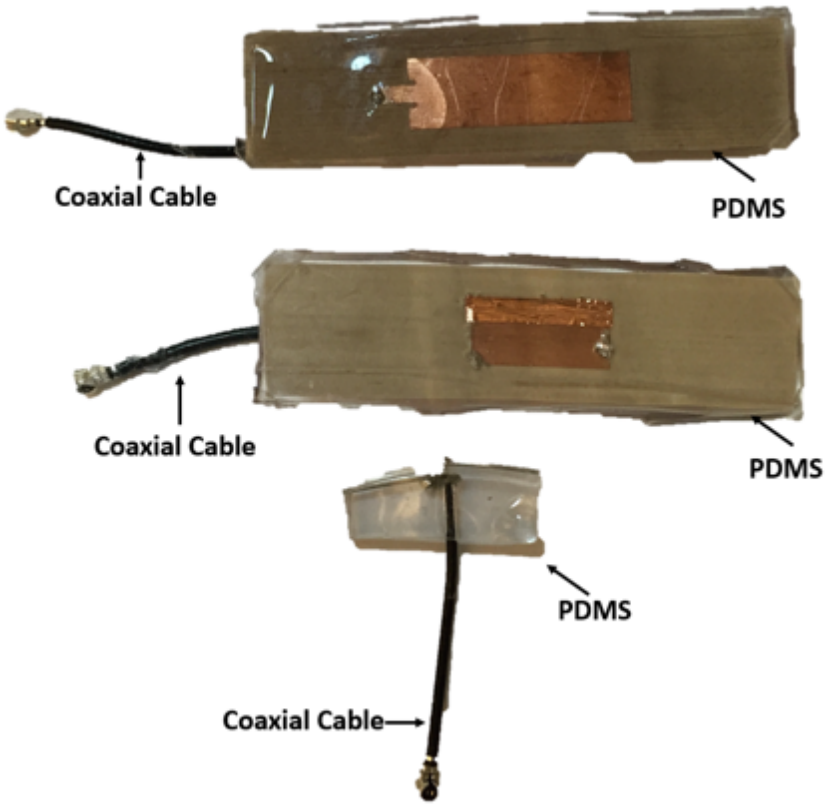

Figure 9 Photograph of the three types of fabricated antennas from the top to the bottom with the PDMS coating material: the patch antenna, PIFA, and the dipole antenna.

most of its power is radiated in front of the antenna through the lips, regardless of whether the mouth is open or closed. Thus, the realized gain of the patch antenna does not change much in the open mouth scenario.

2.4 Results

The three antennas were fabricated based on the simulation results, as shown in Figure 9. The patch and the PIFA were fabricated using a milling machine, while the dipole antenna was made manually. The antenna and cable were coated with PDMS (Sylgard 184 Silicone Elastomer Kit, Dow Corning), after which it was de-gassed using a vacuum pump. The antenna and PDMS were heated in an oven to cure more rapidly. All

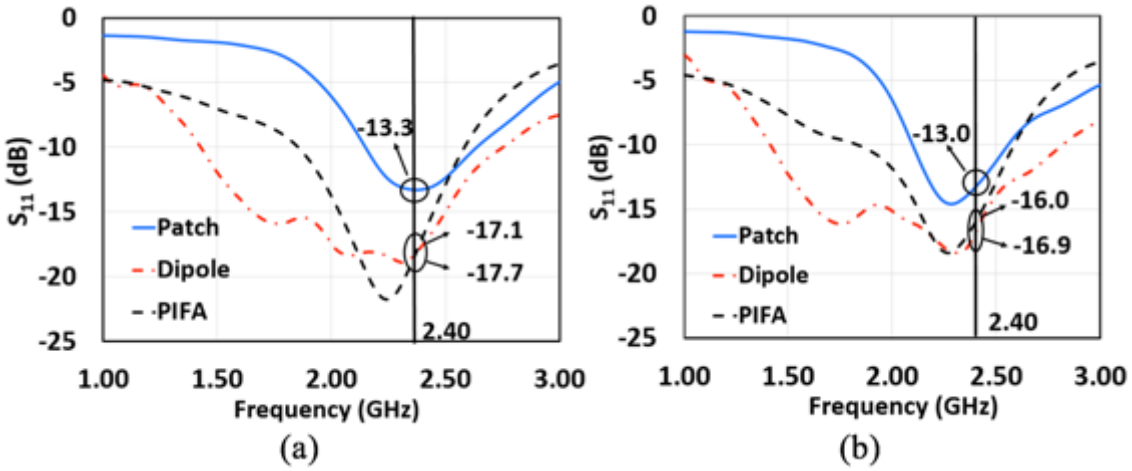

Figure 10 Measurement results of the S_{11} parameter of the three types of antennas in (a) closed-mouth and (b) open-mouth scenarios.

antennas were soldered to coaxial cable, and then the PDMS around the antennas was trimmed with 1 mm margin around the boundaries of the antennas.

2.4.1 Antenna Characterization Results

The experimental setup was quite similar to the simulation setup, including the U. FL cable, U. FL male connector, adaptor PCB, and regular SMA. Antennas were immersed in alcohol, rinsed with tap water, and placed inside the mouth of a 24-year-old male subject with part of the coaxial cable extending out of the subject's mouth to connect to the PCB. The SMA on the adaptor PCB connects to a vector network analyzer (VNA) which was used to measure the S_{11} and S_{21} parameters under open- and closed-mouth scenarios. Since the iTDS is going to be eventually operated in the human mouth along with the antenna, it is better to conduct the measurements in the most realistic fashion, which is inside the human mouth. The results of the return loss are shown in Figure 10. At 2.4 GHz, all antennas reflect much less than -10 dB, very close to the simulation results. The human mouth is a complex environment that includes saliva,

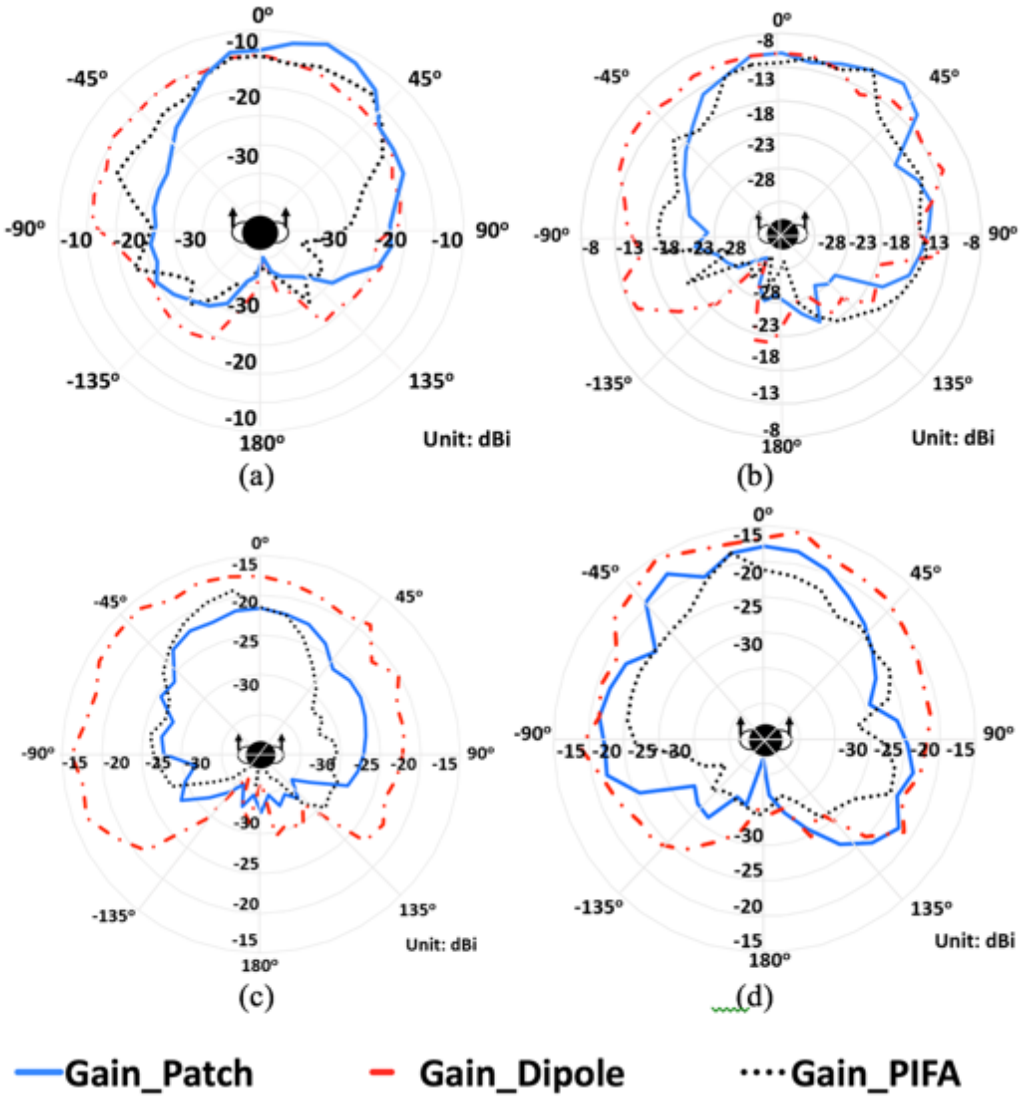

Figure 11 Measurement results of realized gain radiation pattern (co-polarization and cross-polarization) when the three antennas inside the subject mouth: (a) closed-mouth, co-polarization, (b) open-mouth, co-polarization, (c) closed-mouth, cross-polarization, and (d) open-mouth, cross-polarization.

movements of the tongue, and surrounding oral muscles, as well as temperature variations when eating food and various anatomies among different users. These differences cannot be simulated with high accuracy in a software model. It can be seen that in the measurements, the center resonance frequencies have slightly shifted to lower frequencies compared to the simulations. To measure the radiation pattern and realized

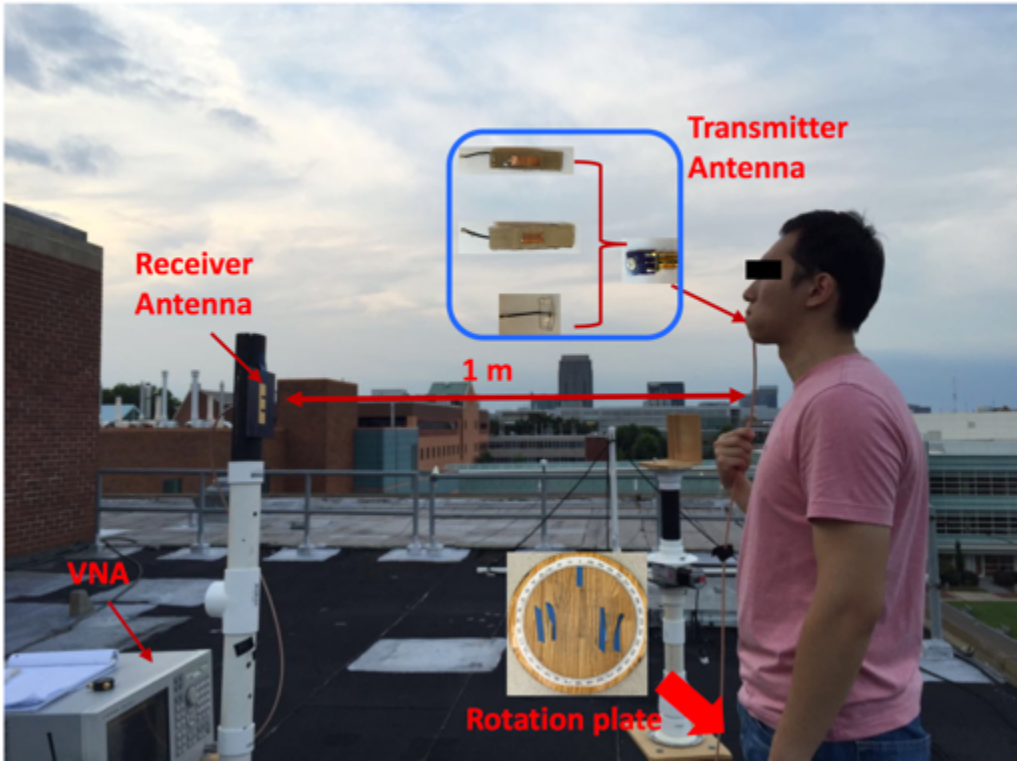

Figure 12 Radiation pattern measurement setup with the Tx antenna inside the subject's mouth.

gain of these antennas, the subject stood on a rotating plate, with the Tx antenna in his mouth. The Rx antenna was an E-shape patch antenna, described in [73]. At 2.4 GHz, the E-patch antenna has 6 dBi gain and relatively large bandwidth. Moreover, it has been well-characterized at 2.4 GHz, similar to other reference antennas in the laboratory environment. The Rx antenna was placed in front of the subject, 1 m away from the Tx. The Tx and Rx antennas were connected to VNA ports, and the subject was rotated 10° at a time, while S_{21} measurements were recorded manually for a complete 360° rotation. To eliminate multi-path effects, which are caused by the indoor subjects that can absorb or reflect radio waves, the experiment was conducted in a calibrated rooftop antenna range. If present, multi-path effects will cause multipath fading, resulting in reduced signal strength and antenna measurement errors. However, in our application, the multi-

Table 2 – Benchmarking Custom-Designed Antenna Performance.

Ref. Ant	Frequency (GHz)	Area (mm^2)	BW (MHz)	Gain (dBi)	Efficiency (%)
[59]	2.4-2.48	144	200	-28	0.5
[60]	2.4-2.5	321	135	-18.5	0.605
[61]	2.45	221	100	-23.98	NA
[74]	2.4-2.48	127	190	-22	NA
[40]	2.45	Monopole: NA Loop: NA	Monopole:300 Loop: 250	Monopole:-18 Loop: -21	Monopole:NA Loop: NA
This work	2.4	Patch:208 PIFA: 69 Dipole:16	Patch:450;PIFA: 700 Dipole:1400	Patch:-10.6;PIFA: -14 Dipole:-14.4	Patch:2.9PIFA: 4.46 Dipole:2.68

path effects cannot be eliminated. To overcome the possibility of the reduction of the signal strength, resulting from the multi-path effects, we can adjust the output power from the microcontroller accordingly. The gain was solved using the Friis formula. The VNA transmitted power was fixed at 0 dBm. The Rx antenna gain is known, and the received power, which is the S_{21} parameter, is measured by the VNA. Therefore, the gain of the Tx antenna can be found. We conducted realized gain radiation pattern (co-polarization and cross-polarization) measurements under closed- and open-mouth scenarios, with results shown in Figure 11, using the experimental setup in Figure 12. In the co-polarization scenario, the peak realized gains of the patch, PIFA, and dipole antennas are -10.6 dBi, -14 dBi, and -14.4 dBi, respectively when the mouth is closed,

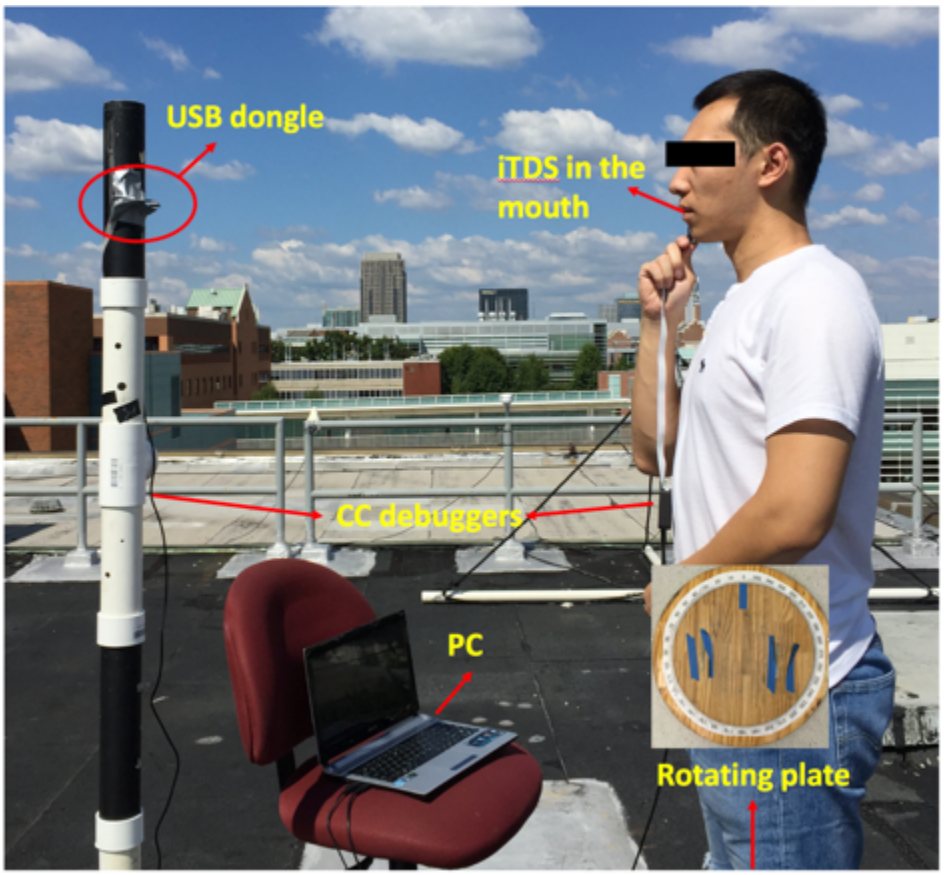

Figure 13 Measurement setup for measuring the radiation pattern of the antennas with the iTDS inside the mouth.

and -9 dBi, -11.1 dBi, and -9.8 dBi, when the mouth is open. In the cross-polarization scenario, the peak realized gains of the patch, PIFA, and dipole antennas are -21.6 dBi, -19.1 dBi, and -16.2 dBi, respectively, when the mouth is closed, and -17.1 dBi, -16.9 dBi and -15.2 dBi, when the mouth is open. Based on the measurement results, the dipole antenna experiences more de-polarization compared to patch antenna and PIFA. This is likely because there is no ground plane shielding the de-polarizing scattering structures in the head. In the measurement, all of the proposed antennas show a directional pattern because a large portion of muscle is at the backside of the antennas, which shields the antennas radiated power. In Table 2, these three antennas are compared with other

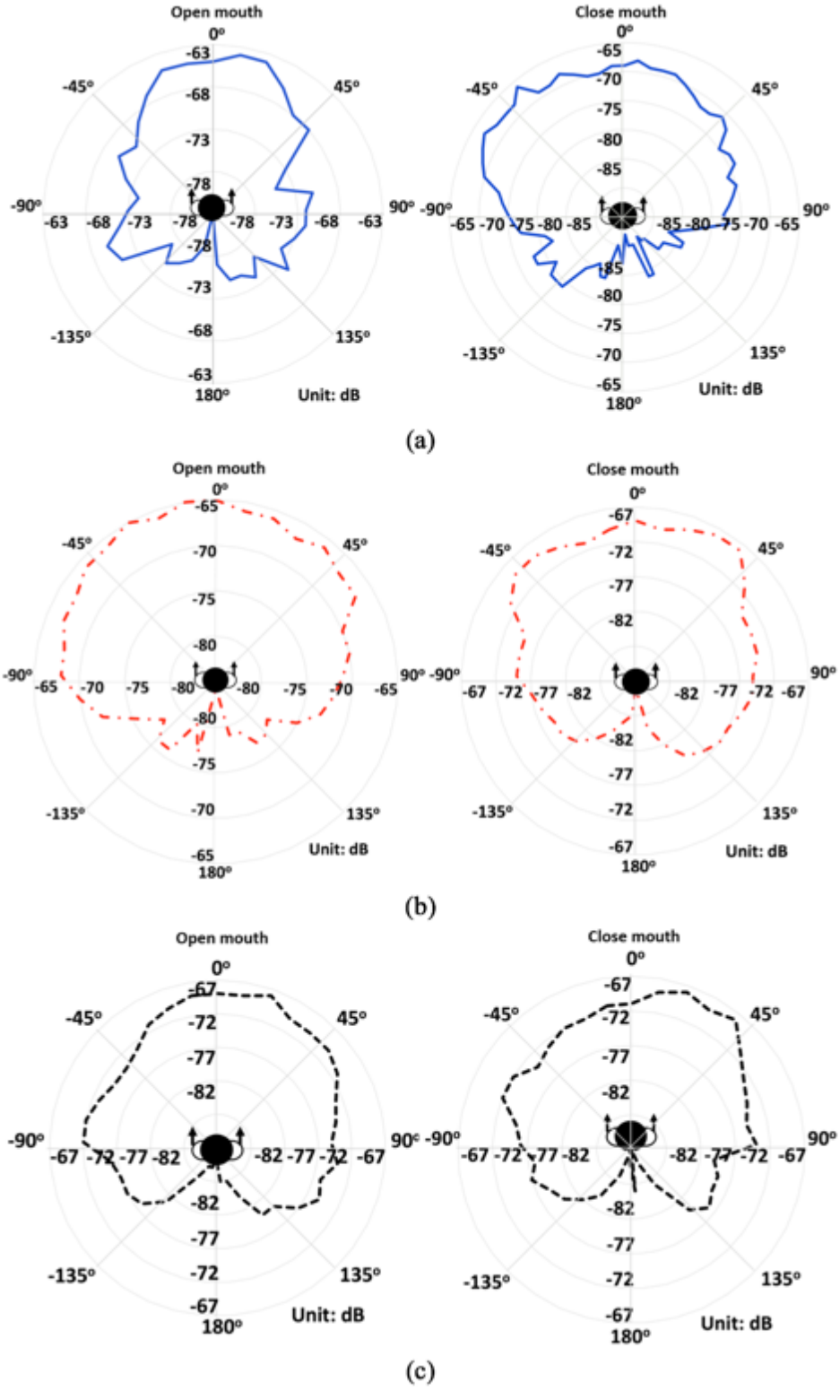

Figure 14 Measured radiation patterns in closed- and open-mouth scenarios of the three antennas connected with the system inside the mouth: (a) the patch antenna, (b) the dipole antenna, and (c) PIFA.

implantable and intraoral antennas in the literature. The most important finding is that the patch antenna displays the highest realized gain among these designs in the co-polarization scenario. The PIFA and patch antennas employ the same type of substrate,

resulting in the similar ε_{eff} in both antennas. However, the patch antenna has larger physical area compared to PIFA, which contributes to its higher gain.

2.5 System Level Evaluation of the Antennas

The radiation pattern was measured at the system level to realistically evaluate the antenna performance within the iTDS-a. The measurement setup in Figure 13 is similar to the antenna radiation pattern measurement setup, but the antenna is now embedded within the iTDS-a prototype and placed inside the subject's mouth. According to the antenna measurement results, the proposed antennas are linearly polarized in the mouth, therefore in this system, The Rx, located 1 m away in front of the subject, was the USB dongle, discussed in Section II. Both iTDS-a (Tx) and USB dongle (Rx) were connected to a PC, running SmartRF Studio 7 (TI, Dallas, TX) [75], via two CC debuggers (TI, Dallas, TX) [76]. On the SmartRF Studio 7, the transmission power, operating frequency, data rate, and modulation scheme were set to 0 dBm, 2.4 GHz, 250 kpbs, and minimum-shift keying (MSK), respectively. The subject was rotated 360°, 10^{o} at a time. The received power on the Rx side was recorded after the power reading on SmartRF was stabilized. Sometimes the received power reading had small fluctuations, in which case, the average received power was recorded. The experiment was repeated with both closed- and open-mouth conditions.

Table 3 – Packet Error Rate (PER) in Open- and Closed-Mouth Conditions At Different Head Orientations

	Patch Ant.	*PIFA*	*Dipole Ant.*
0°o-m[*]	0.2%	0.7%	0.6%
0°c-m[**]	0.4%	1.5%	0.7%
90°o-m	0.3%	1.5%	1.9%
90°c-m	0.4%	1.7%	2%
-90°o-m	0.3%	1%	1.6%
-90°c-m	0.5%	1.1%	1.8%

[*]o-m: open-mouth [**]c-m: closed mouth

The antenna characterization section showed the realized gain value in the radiation pattern of the antenna. The iTDS-a system radiation patterns, shown in Figure 14, exhibit the power received at the Rx. The shapes of the system level radiation patterns are similar to those with antennas only. Measurement results show that the USB dongle received more power when the subject opened his mouth because of higher antenna gain. Compared to the S_{21} measurements by VNA when the antennas were characterized, the Rx received less power because both Rx and Tx PCBs have power loss. In particular, the Tx PCB is coated with PDMS and surrounded by tissue, which also contribute to power loss. The antenna that has a high gain in the front side of the mouth ensures enough power can be delivered to the Rx, resulting in a high SNR and low bit error rate (BER). The iTDS is meant to allow users to issue commands to control their environment. Therefore, reliability in safety critical tasks such as driving a powered wheelchair is paramount, and we need to ensure system robustness by maintaining a high SNR and very low BER. Based on these results, the patch antenna in the system has the highest gain in both closed- and open-mouth conditions. Moreover, the radiation patterns in Fig.

13 show similar power received by the dongle at 1 m Tx-Rx separation, compared to [42] in which the Tx-Rx distance is only 22 cm.

We also measured the package error rate (PER) in SmartRF Studio 7 at three different angles: 0^0, $+90^0$, and -90^0, for each antenna, as an indicator of the system robustness. Random packets, each containing 30 bytes, were generated by SmartRF Studio 7 and transmitted to the Rx, where the SmartRF Studio 7 reads the incoming packets in real time, compares them with the transmitted packets, and calculates the PER. We used the same setup as in system radiation pattern measurement. In addition, at every angle, the subject was asked to open and close his mouth. 50,000 packets (1.2×10^7 bits) were sent and the PERs were recorded for every scenario. The results are listed in the **Table 3**, where the PER of the three antennas are presented at three angles. These results show that the patch antenna has the lowest PER among these three antennas, and results in the most robust link for the iTDS-a, because of its high gain.

The last step of the experiment was to test the complete iTDS-a wireless data transmission functionality in a setup similar to [42]. The subject placed the iTDS-a inside the mouth, running a firmware that packetized the raw magnetic sensor data from four 3-axial magnetic sensors in the CC2510 MCU, and send those packets to the USB dongle, connected to a PC. The distance between the Rx dongle and iTDS-a inside the mouth was 1 m, similar to the other measurements. A custom user interface in LabVIEW was able to display the raw data on the computer similar to the eTDS headset without any noticeable data loss [50].

2.6 Summary

We designed three types of antennas (patch, PIFA, and dipole) at 2.4 GHz to establish a wireless link between an iTDS-a inside the mouth and an external receiver implemented as a USB dongle. The antenna performance was compered for establishing the most robust connection. The antennas were designed in CST using a simple human mouth model, and fabricated on Roger substrate. Simulation and measurements were conducted in similar conditions by placing the prototypes inside a subject's mouth. Measurement results showed that the patch antenna has the highest gain in both closed- and open-mouth conditions, with -10.6 dBi and -9 dBi received power at 1 m Tx-Rx separation, respectively when it is co-polarized. The dipole antenna, on the other hand, demonstrated the widest bandwidth and best performance in the cross-polarization scenario. To match the impedance of the antennas where they connect to the PCB, mini-SMA and thin coaxial cable were used with careful design of the RF traces on the PCB. All custom-designed antennas were also tested within the iTDS-a system in a realistic measurement setup, where the transmitter antennas and receiver antenna maintain the same polarization and the superiority of the patch antenna was further confirmed by demonstrating the lowest PER measured in the SmartRF Studio 7 environment.

CHAPTER 3. ADAPTIVE MATCHING TRANSMITTER WITH DUAL BAND ANTENNA FOR INTRAORAL TONGUE DRIVE SYSTEM

3.1 Introduction

A key objective in design of the iTDS is maintaining a robust wireless communication with the external Rx, particularly for safety-critical tasks such as wheelchair navigation, while keeping the power consumption low to extend the small battery operating time beyond one day. The main challenges are the considerable power loss in the tissue, which is affected by the choice of carrier frequency, the compromise between the user comfort and the size of battery, antenna, and iTDS electronics, and dealing with the dynamic environment of the mouth, which results in detuning the Tx antenna because of the movements of the jaw and the tongue. Moreover, there are always external sources of noise and interface that can disrupt the wireless link by lowering the signal-to-noise ratio (SNR) on the Rx side. As a measure of safety and robustness, it is more suitable to have multiple bands instead of only one band. Because if operation of one band is severely affected by the external interference, another band would be available to switch to, and continue the system operation.

Previously, we developed a version of the iTDS using only commercial-off-the-shelf (COTS) components, plus a custom high-gain intraoral antenna for 2.4 GHz carrier frequency to achieve a robust wireless communication [77]. However, 2.4 GHz is a crowded band and suffers from considerable loss in the tissue, which result in a low

specific absorption rate (SAR) limit [78][79]. In our previous work, we identified better choices within the Industrial-Scientific-Medical (ISM) band, and presented a dual band system which operated at 27 MHz and 433 MHz [51][52]. This system had only one far-field operating frequency, at 433 MHz, which in the absence of an external 27 MHz receiver coil, is still prone to interference. We present a Tx ASIC with a secondary far-field operating frequency in 915 MHz, which is away from the busy 2.4 GHz band, and offers an alternative, even in the absence of a near-field external Rx coil.

To address the dynamic intraoral environment, an adaptive matching mechanism is implemented on the ASIC to compensate for the changes in the antenna impedance due to jaw and tongue movements. Adding dynamic matching components, such as capacitors, ahead of the antenna is common. However, these discrete components occupy a large space, and provide a limited number of matching combinations. For instance, four discrete capacitors used in the matching network of offer only 16 matching options, which might be too coarse for this application. Even though fully-integrated matching networks are reported in the literature, these implementations are rather too complex and occupy large chip area for the iTDS application.

In this work, we present a triple-band Tx ASIC with hybrid adaptive matching, assisted by a COTS ultra-low power MCU to achieve sufficient resolution, while reducing the on-chip footprint by avoiding complexity. We are also presenting a dual-band Tx antenna, operating at 433 MHz and 915 MHz, which dimensions are specifically suitable for intraoral applications.

3.2 System Architecture

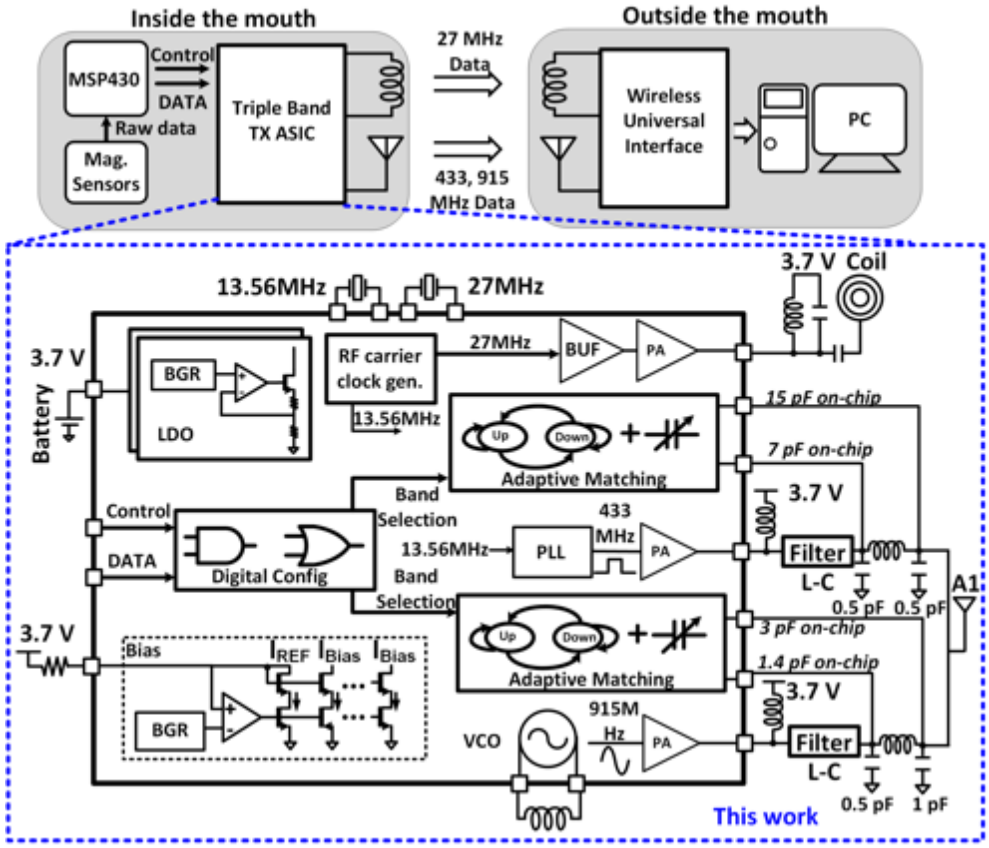

Figure 15 Block diagram of the iTDS triple-band transmitter ASIC with its off-chip components.

Block diagram of the triple-band Tx ASIC with its off-chip components is shown in Figure 15. Two low dropout (LDO) linear regulators convert the rechargeable Li-Po battery voltage to 1.8 V, one for analog blocks and the other for digital blocks, and a band- gap reference (BGR) generates the required bias currents. Twelve magnetic sensors (3-axes × 4 LSM303) are sampled at 100 Hz each, with each sample being 2-bytes, and packetized in the MCU to generate raw data packets that are 30 bytes long. The ASIC includes a digital control block for buffering the data packets and generating control signals to select different bands. Data packets are serially loaded onto an on-chip shift register at a rate of 24 kb/s, while an additional 2 command lines between the MCU and the ASIC activate the desired Tx band. In this early prototype, switching from one band

to another will be done by the iTDS users, who can switch the active band by placing their tongues at a specific position, e.g. holding the tongue against the right cheek for >3 s. This will trigger a special tongue command that is detected locally in the MCU by simply elevating the absolute value of a designated magnetic sensor output above a certain threshold for a designated period. When the original connection is lost, the external SDR-Rx keeps searching for the handshaking packet from the iTDS in different bands at initialization. Once the handshaking signal is captured at a specific band, the communication between the iTDS and SDR-Rx will be established in that band. If the connection is lost again, the SDR-Rx goes back to the searching state until another handshaking packet is detected.

3.2.1 Transmitter

Three transmitters operating at 27 MHz, 433 MHz, and 915 MHz, respectively, are included on-chip, all of which utilize on-off-keying (OOK) modulation scheme. In 27 MHz band, signal is transmitted through a coil for near field communication. The other two transmitters share the same dual-band antenna that is discussed in section III. The default band for the iTDS is 27 MHz because it shows the lowest attenuation in human body, and consumes minimum power for near-field communication [52]. However, some citizen radios and short-distance applications, such as remote-controlled toys and Walkie-Talkies, also use this band, presenting possible sources of external interference for the iTDS. The 433 MHz band was selected because of its proximity to the Medical Implant Communication Service (MICS) band, which is within 402–405 MHz, and utilized in some implantable medical devices (IMD) and yet it does not interfere with this band.

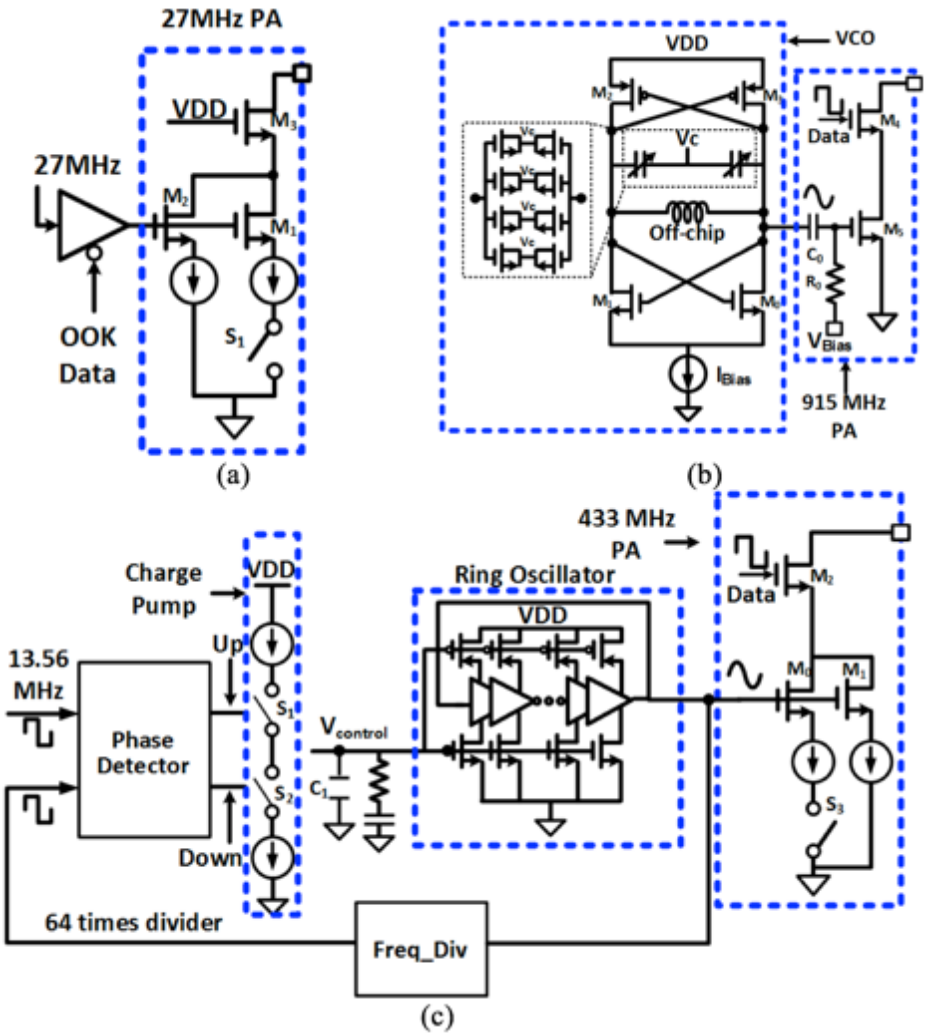

Figure 16 Schematic diagram of the transmitters at (a) 27 MHz, (b) 915 MHz, and (c) 433 MHz.

Finally, 915 MHz was also adopted in occasions when the other two bands are occupied because it is less crowded than 2.4 GHz, while more power transmission is permitted.

The three-band Tx schematics are shown in Figure 16. The 27 MHz Tx consists of a power amplifier (PA) and a buffer to realize the OOK by turning it on and off. A higher power option is implemented by adding an additional current source in parallel. The 433 MHz Tx is shown in Figure 16c, including a phase locked loop (PLL), followed by a PA. A frequency divider divides the carrier signal, which is generated by the voltage

controlled ring oscillator (VCRO) in the PLL, by a factor of 64 before it is compared with a crystal-based 13.56 MHz reference clock. A control voltage, $V_{control}$, varies the pull up and pull down currents of each inverter in the VCRO to adjust its delay, and consequently the carrier frequency. The phase difference between the carrier signal and the reference clock is produced by a phase detector, controlling a charge pump. $V_{control}$ is generated by charging and discharging a capacitor, C_1, at the output of the charge pump. An off-chip resistor in series with a capacitor is added at the output of the charge pump to maintain stability of the PLL. These components form a feedback loop that keeps the output and input signals in phase, locking the carrier frequency at 433 MHz. The 433 MHz PA has the same topology as 27 MHz.

The main component of the 915 MHz Tx is a voltage control LC-oscillator (VCO) with an off-chip inductor, followed by a PA. Compared to 433 MHz band, which is more likely to be interfered by other medical or implantable devices around the end users, 915 MHz band is less noisy, allowing for a larger frequency tolerance. Therefore, at 915 MHz, a VCO has been adopted instead of adding PLL, which increases power consumption as well as chip and PCB areas by requiring another reference frequency generator. Four pairs of NMOS transistors are connected across the VCO output as varactors. The capacitances of the varactors are controlled by an external voltage, which is used to oppose the carrier frequency drifts. OOK is realized by turning on and off the cascode transistor, M_4, on top of the PA.

3.2.2 Adaptive Matching

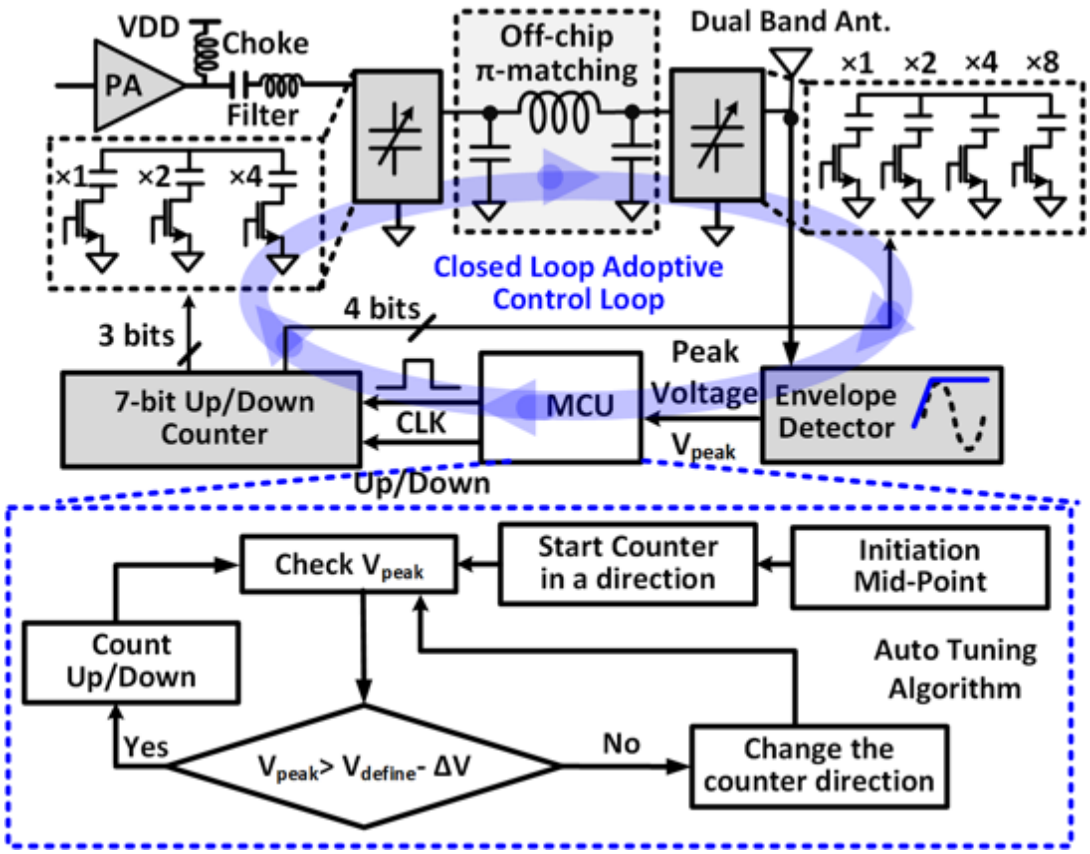

Figure 17 Schematic diagram of the adaptive matching network, including the capacitor banks, feedback control loop, and matching algorithm flowchart.

The dynamic intraoral environment detunes the antenna, increasing the reflected power and reducing the desired power transmitted from the iTDS. Unlike many other transmission scenarios, in which Tx operates in a stable environment, or its output power is increased to satisfy minimum SNR at the Rx input in the worst case condition, it is necessary to implement an adaptive matching mechanism between the Tx and antenna to compensate for the effects of detuning.

In the proposed Tx design, we have added two adaptive matching networks for 433 MHz and 915 MHz, but not for the 27 MHz because the human body, with all the dynamic changes in the intraoral environments, is transparent to magnetic field at this

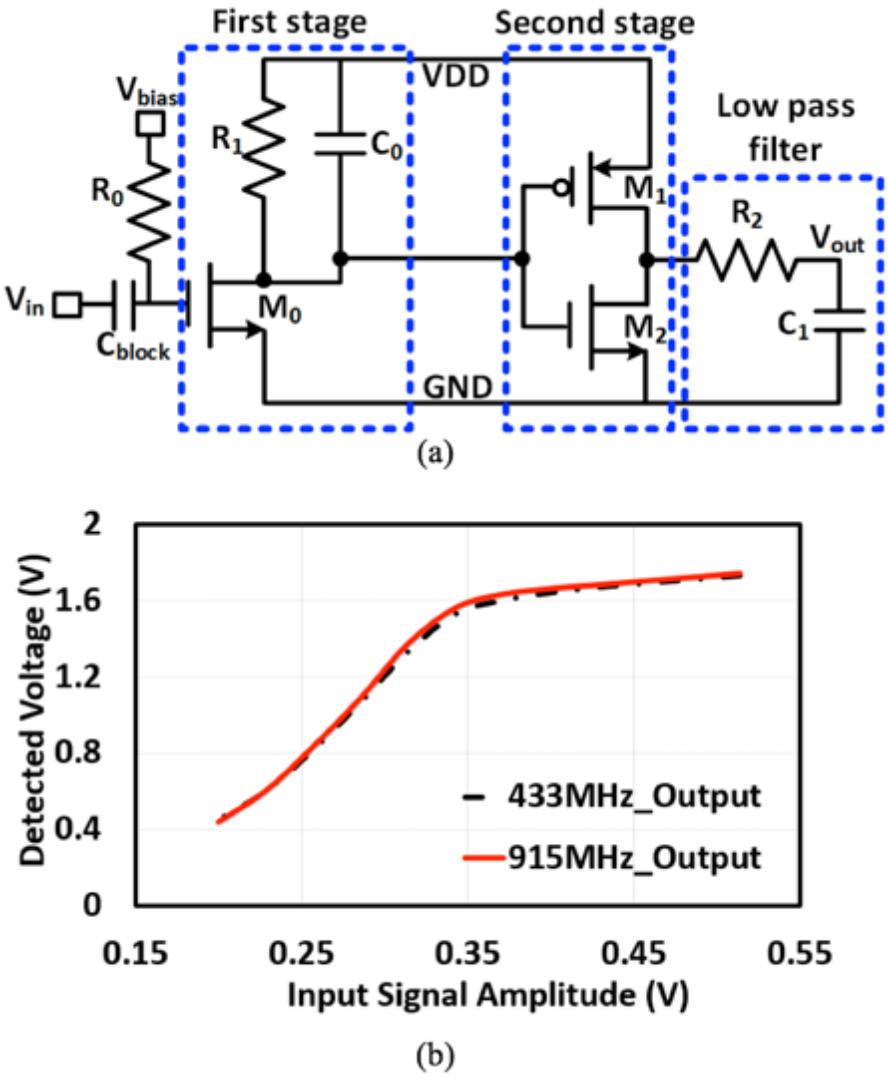

Figure 18 Schematic diagram of the peak detector block. (b) Simulated transfer function of the peak detector at 433 MHz and 915 MHz.

frequency, and has a small effect on near-field inductive coupling. The 433 MHz and 915 MHz transmitters have similar output matching topologies, shown in Figure 15 and Figure 17, consisting of a choke inductor, a series LC-filter, and a variable π-matching network, which in turn includes two capacitor banks, an up-down counter, and an peak detector. The capacitor banks provide 1 pF and 0.2 pF matching resolution for 433 MHz and 915 MHz, respectively. Three-bit and four-bit binary-weighted on-chip poly-insulator-poly (PIP) capacitor banks are connected at the input and output nodes of the

off-chip π-matching LC-tank, providing a total of 7 pF and 1.4 pF capacitance selection ranges for 433 MHz and 915 MHz at the input nodes, and 15 pF and 3 pF variable capacitance at the output nodes for 433 MHz and 915 MHz, respectively.

Each capacitor bank in the π-network is controlled by a 7-bit up-down counter, which can keep the antenna matched even though it might be detuned, thus improving the output power level. The mismatch detection and correction is based on the amplitude of the output signal fed to the antenna, which is picked up by a peak detector, and digitized

by the MCU. Since the cascode structure has been used in both 433 MHz and 915 MHz PAs, the load impedance variations do not change the input impedance of the PAs much, keeping the voltage swing at the input of the PA constant at the same amount of input power. Therefore, the voltage at the PA output is primarily dependent on its load impedance, which include the matching network and antenna.

The peak detector block is shown in Fig. 5a, which consists of an envelope detector circuit, which uses a blocking capacitor, C_{block}, in series with the gate of M_0, as an envelope detector together with an RC-network in the drain, a common-source envelope amplifier as the second stage, followed by a low pass filter to reduce ripples in the output voltage, V_{peak}. When the input signal increases, the output of the M_0 decreases from VDD, and the PMOS transistor M_1 begins to charge C_1. On the other hand, once input signal decreases, M_2 starts to discharge C_1 to a specific level. In this application, the peak detector should provide large input impedance to avoid degradation of the PA performance, and fast detection time. The simulated input impedance of the peak detector was 13.67 kΩ and 11.74 kΩ for 433 MHz and 915 MHz, respectively. Fig. 5b shows the

simulated output voltage of the detector, showing its linear range, based on the input amplitude.

Since every matching adjustment takes multiple steps, such as V_{peak} detection, comparison, and counter sweep, it is necessary to minimize the detection time of the peak detector. However, there is a trade-off between the detection time and the output voltage ripple. A large C_1 reduces the output ripple, but increases the detector response time by taking longer to charge and discharge. Another possible solution is to increase the sizes of M_1 and M_2. It is suggested that 2 mV output voltage ripple and 0.5 μs detection time are suitable, which are the values adopted for this design in order to strike a balance between the voltage ripple and detection time. The simulation shows the actual detection time is 0.45 μs.

The adaptive matching mechanism is depicted in Figure 17, which is implemented in the MCU. A short initialization period is required for the adaptive tuning, in which the up/down counter starts from the mid-point, while the MCU continuously samples V_{peak} across the antenna via the peak detector block. The 7-bit counter counts in a certain direction until V_{peak} at the antenna reach within the vicinity of V_{define}, which is the voltage correlated with the transmitted power in matched condition. The MCU changes counter direction when V_{peak} drops by ΔV, which is 20 mV in this case, below V_{define}. This simple tracking mechanism ensures the Tx antenna is always tuned near the original transmitted power level (not necessarily the optimal matching condition), despite dynamic changes in the oral environment, thus reducing the power loss and improving the wireless link robustness. An arrays of NMOS transistors are used to switch the capacitor banks.

According to [80], if the Q-factor of switched capacitors is lower than 20, the power loss on these capacitors will be substantial. Therefore, we sized the switches to have Q-factor of binary scaled capacitor in the on-state to be >30 to minimize the power loss. The capacitor values of each bank were selected based on the method in [81].

Based on post layout simulation results, the actual detection time for the envelope detector is 0.45 μs. We have long rising and falling times since large NMOS transistors are adopted as switches for the capacitor banks. From simulations, 1.82 μs is needed for a capacitor to switch on and off completely. Comparison is done in the MSP430 MCU, which has 120 ns as the response time for its internal comparator [82]. Therefore, it is required 2.39 μs to check one capacitor combination. We can assume 3 μs to check one matching combination. Therefore, a total of 0.38 ms is required to check all possible 128 combinations.

3.3 Dual Band Antenna Design

Considering the limited intraoral space, a small dual-band antenna at 433 MHz and 915 MHz was designed to achieve reliable communication between iTDS and SDR-Rx. To fit the arch-shaped iTDS, the planar antenna was designed within a rectangular space on flexible substrate to be placed in front of the incisors.

3.3.1 Antenna Design

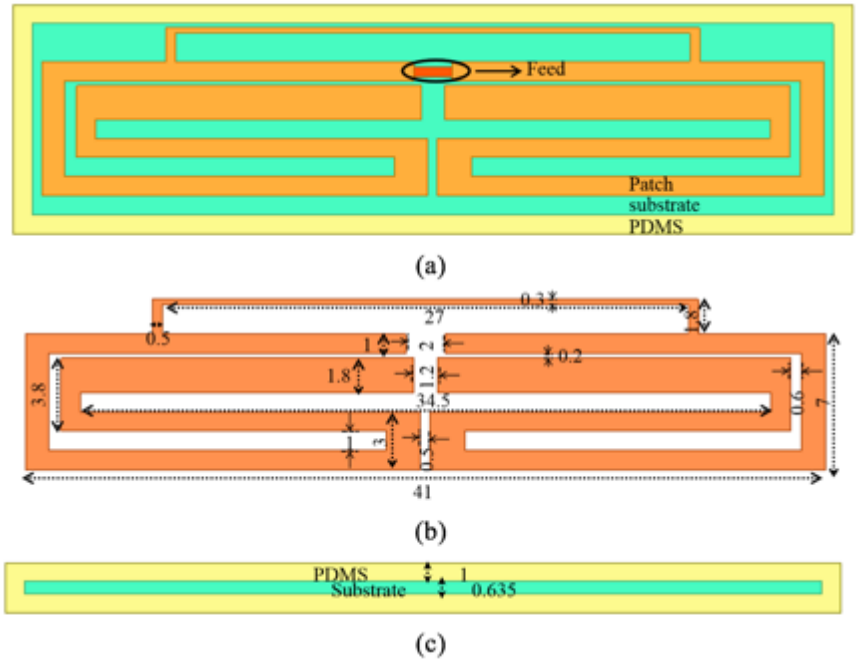

Figure 19 Geometry of the proposed dual band antenna (unit: mm): (a) top view, (b) radiating patch, and (c) Side view.

The structure and dimensions of the proposed antenna are depicted in Figure 19a-c, presenting the front view, radiating patch, and top view of the antenna, respectively. The dielectric material, Roger RT/duriod 6010 (ε_r = 10.2, tan δ = 0.0035, thickness = 0.63 mm), is chosen as the substrate because of its flexibility and high relative permittivity. To hermetically seal the antenna, it is coated with a 1 mm-thick silicone (Polydimethylsiloxane or PDMS) layer, which has relative permittivity of 2.68 and tangent loss of 0.04. The dimension of the antenna is optimized based on the human oral anatomy which have been investigated in [77], occupying 266.7 mm^3 (42 × 10 × 0.635 mm^3) space within the iTDS. The radiating patch consists of two symmetrical spiral arms, which extend the antenna current path, and are connected through a 0.3 mm-thick strip, miniaturizing the size of the antenna. The width of the meandered strips plays an important role in the impedance matching. By carefully varying the width, the antenna is

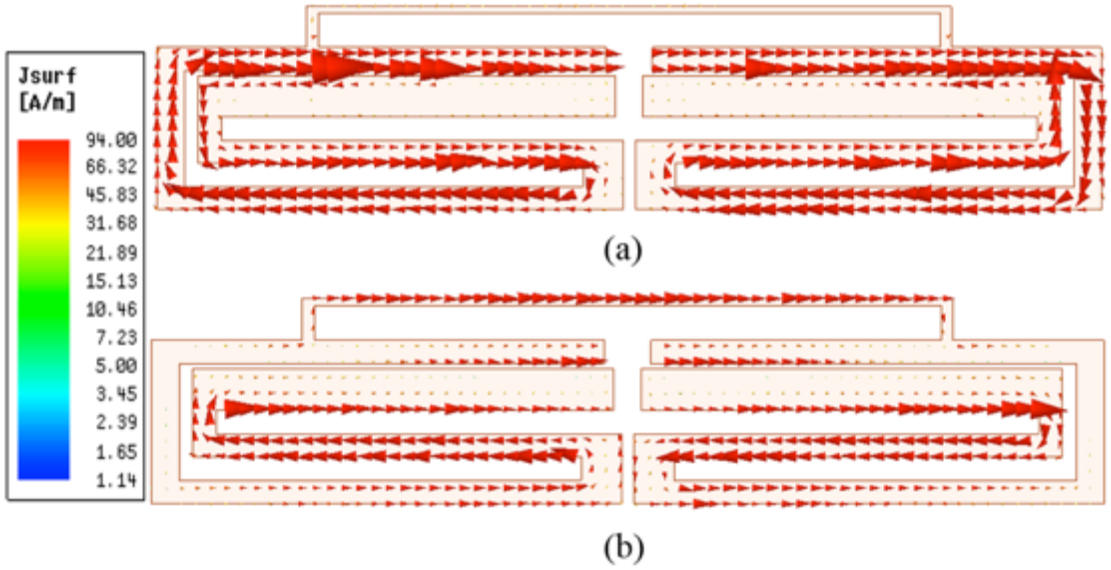

Figure 20 Surface current distribution on the proposed dual band antenna at: (a) 433 MHz. (b) 915 MHz.

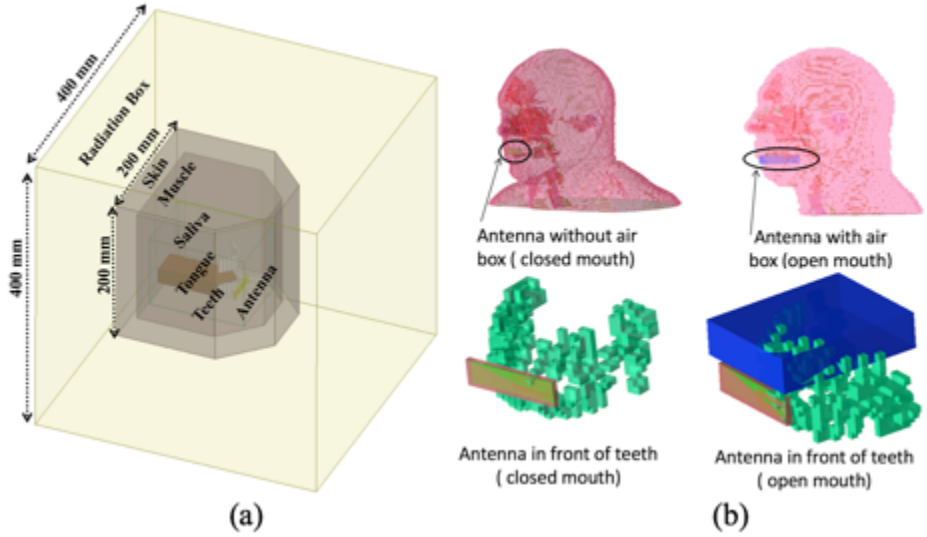

Figure 21 Simulation setup for the proposed antenna: (a) human mouth model in HFSS, (b) human head phantom in Remcom for open- and closed-mouth conditions.

matched at desired ISM bands. A 50 Ω coaxial feed, shown in Figure 19a, merges the ends of the two arms. The current distribution in the proposed dual-band antenna in 433MHz band, shown in Figure 20a, shows that the entire path contributes to the

Table 4 – Dielectric properties of the tissues

Tissue Type	433 MHz		915 MHz	
	ε_r	σ[S/m]	ε_r	σ[S/m]
Skin	46.08	0.702	41.33	0.872
Muscle	56.87	0.805	54.99	0.948
Tongue	57.38	0.783	55.23	0.942
Teeth	13.074	0.094	12.44	0.145
Saliva	77.3	0.738	76.00	0.818

radiation, while in the 915 MHz band, shown in Figure 20b, only the middle portion of the radiating patch contributes.

3.3.2 Simulation Setup

The dual-band antenna is designed and simulated in Ansoft HFSS in a 200 × 200 mm^2 multi-layer heterogeneous custom mouth model, shown in Figure 21 Simulation setup for the proposed antenna: (a) human mouth model in HFSS, (b) human head phantom in Remcom for open- and closed-mouth conditions.a, which includes different types of tissues materials, including muscle, skin, teeth, tongue, and saliva. Properties of these tissues are depicted in Table 4, and considered frequency-dependent in simulations, as described in [83]. Additionally, to validate the simulation results in our custom HFSS model, the proposed antenna was simulated in a realistic human head model in XFdtd Remcom, shown in Figure 21b. We also simulated the open- and closed-mouth conditions in both models. Since it is not possible to open the mouth in the realistic phantom, an air box (63 × 50 × 15 mm^3) was inserted below the upper jaw of the phantom in the open-mouth model. The return loss (S_{11}) simulation results for the proposed antenna in the HFSS and closed/open-mouth conditions in the XFdtd Remcom

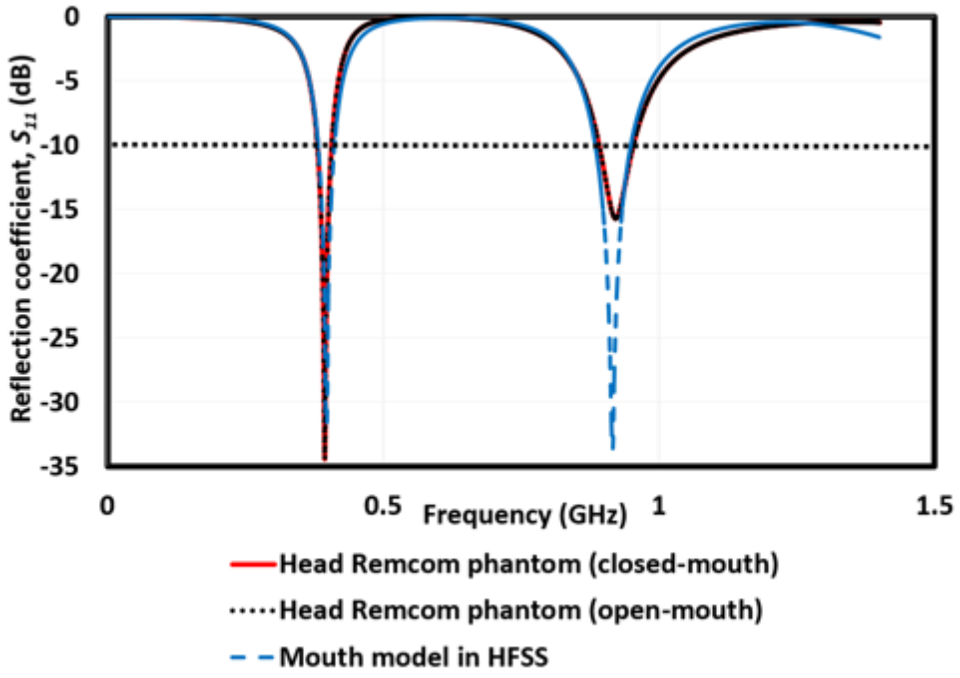

Figure 22 Simulated reflection coefficient of the proposed dual-band antenna in HFSS and Remcom models in the open- and closed-mouth conditions.

are shown in Figure 22, which indicates the antenna has sufficiently low power reflection in both 433 MHz and 915 MHz bands. The -10 dB bandwidths at 433 MHz and 915 MHz are 28 MHz and 99 MHz in the HFSS mouth model, respectively. In the Remcom human head model, the bandwidth at 433 MHz is 26 MHz for open-mouth and 28 MHz for closed-mouth. At 915 MHz, the bandwidth is 61 MHz and 65 MHz for open- and closed-mouth, respectively.

Figure 23 presents the realized gain radiation pattern of the proposed antenna in mouth model in Ansoft HFSS and Remcom at 433 MHz and 915 MHz, including azimuthal (XY plane) and elevation (XZ plane). Because of the power loss in the tissue, the realized gain is below zero in every direction. When the mouth is closed, the peak realized gain at 433 MHz and 915 MHz are -19.59 dBi and -16.99 dBi in the mouth

model in HFSS, respectively. Using the realistic human head model, the peak realized gain in the open-mouth case at 433 MHz and 915 MHz are -25.66 dBi and -15.08 dBi; and for the closed mouth case -26.41 dBi and -17.03 dBi, respectively. According to the

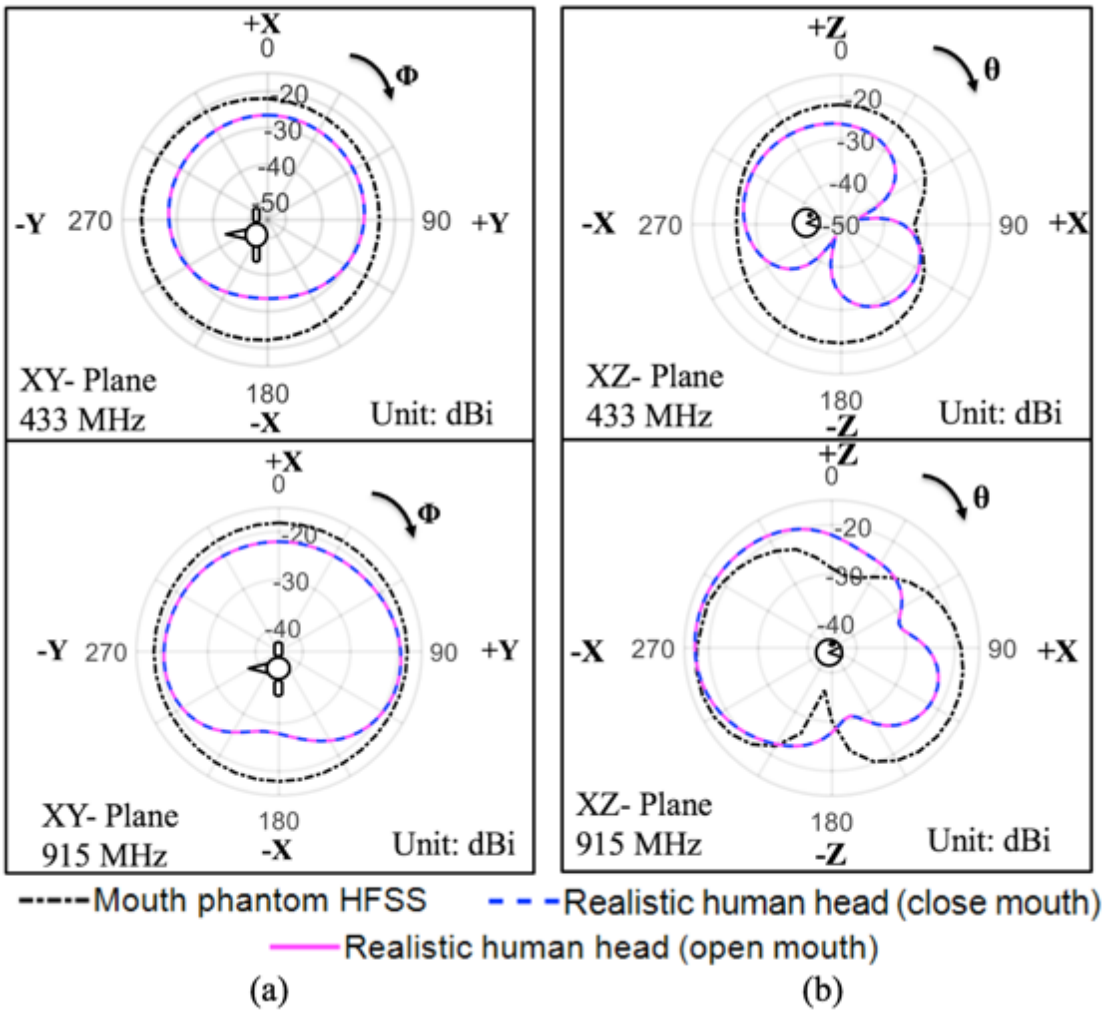

Figure 23 Simulated realized gain radiation pattern of the proposed antenna in HFSS and Remcom human head model at 433 MHz and 915 MHz in: (a) Azimuthal (XY plane) and (b) Elevation (XZ plane).

simulation in the XFdtd Remcom human head model, the open- and closed-mouth show little differences and present similar radiation patterns at the desired frequency bands.

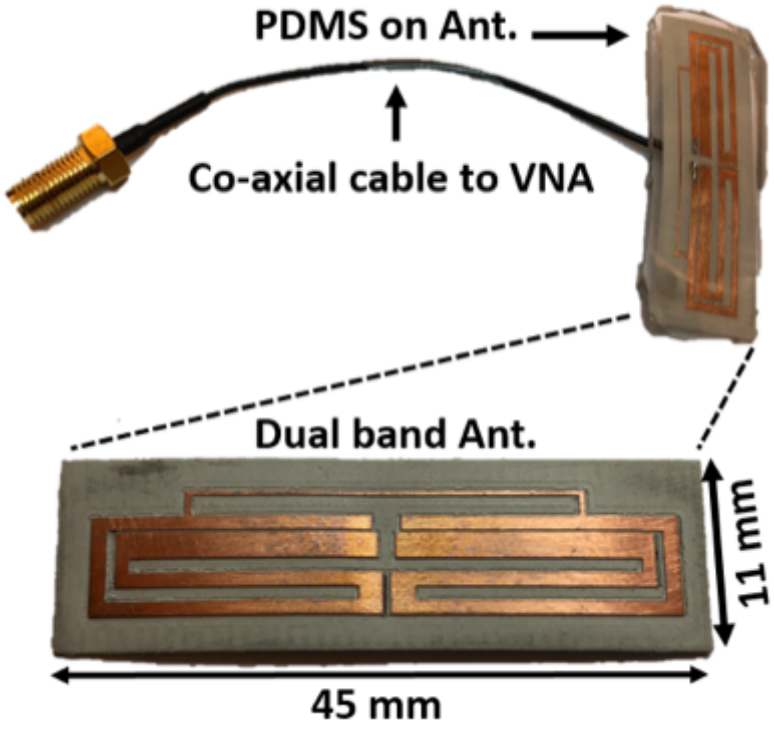

Figure 24 Fabricated dual-band antenna on Roger substrate with PDMS coating and co-axial cable.

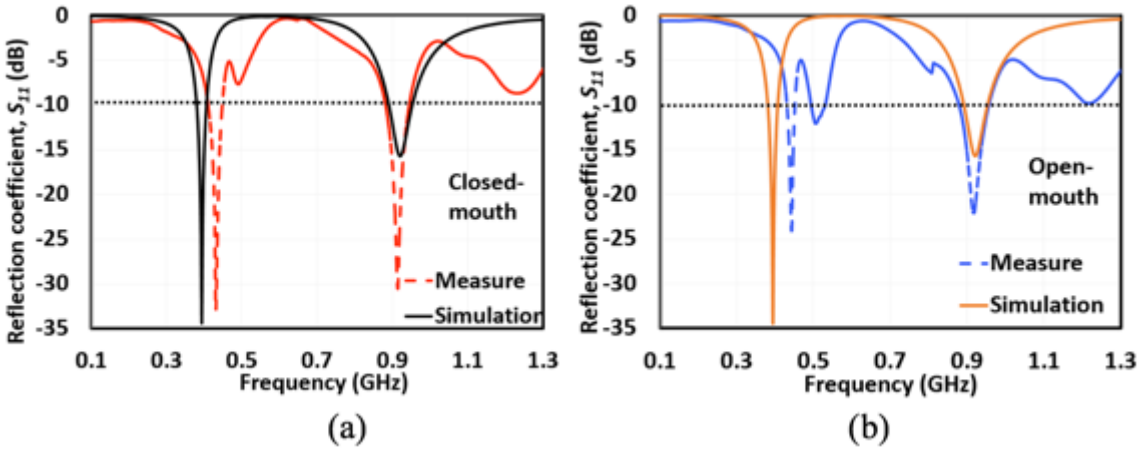

Figure 25 Combining measured and simulated reflection coefficient of the proposed dual band antenna in (a) closed- and (b) open-mouth conditions.

3.4 Measurement Resutls

3.4.1 Dual-Band Antenna

The dual-band antenna was fabricated using a milling machine and coated with PDMS after being degassed in a vacuum chamber. A U.FL to SMA cable is used to feed the antenna and connect it to a vector network analyzer (VNA) for measurement. The fabricated antenna with PDMS coating, shown in Figure 24, was placed inside in human

mouth to perform the reflection coefficient (S_{11}) measurements under open- and closed-mouth scenarios. The simulation and measurement results using XFdtd Remcom for open- and closed-mouth scenarios are compared in Figure 25. At low frequencies, the measurement results show a slight shift from the simulation results, ~30 MHz towards the higher frequencies. At high frequencies there is a very good agreement between simulation and measurement results. Measured results show the -10 dB bandwidth in open-mouth to be 25 MHz and 92 MHz at the 433 MHz and 915 MHz, respectively.

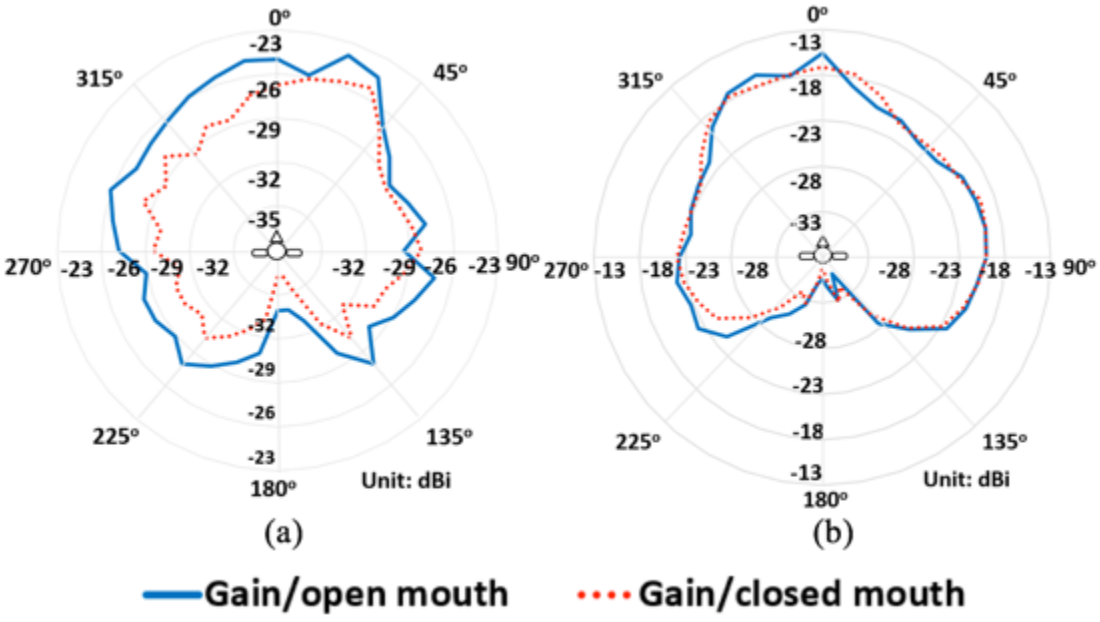

Figure 26 Measured realized gain radiation pattern of the dual-band antenna at (a) 433 MHz and (b) 915 MHz under open- and closed-mouth conditions.

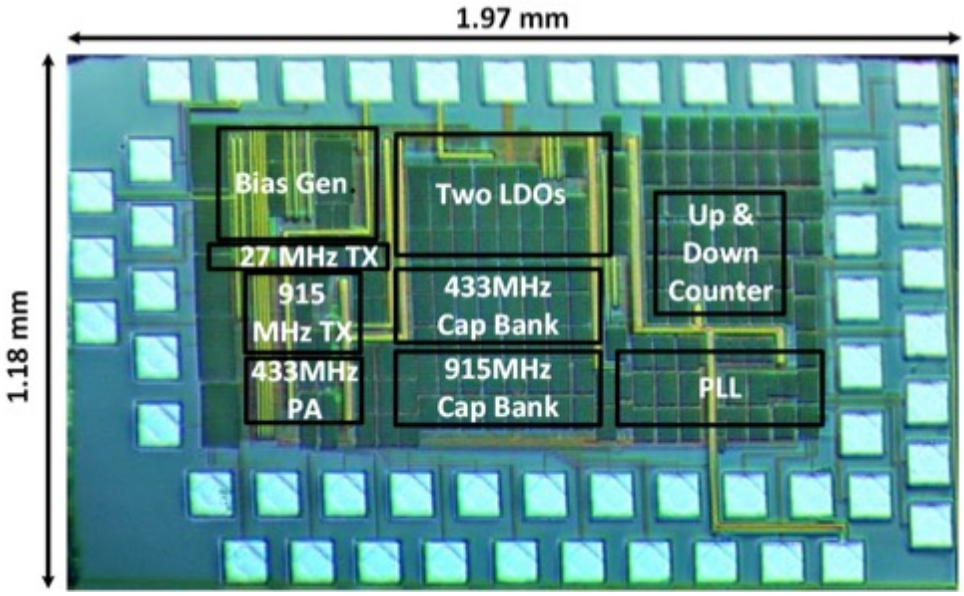

Figure 27 The die photo of the multi-frequency transmitter system which has 1.97 mm length and 1.18 mm width.

When the mouth is closed, the bandwidth is 40 MHz and 65 MHz at 433 MHz and 915 MHz, respectively. These bandwidths can sufficiently cover both lower and higher ISM bands for data transmission.

To characterize the radiation pattern of the antenna, we adopted method similar to [77]. The subject stood on a rotating plate with designated rotation angles on a calibrated rooftop antenna range with the dual-band antenna in the mouth. The Rx antenna, connected to a VNA, was placed in front, 75 cm from the subject. Measurements were conducted under open- and closed-mouth conditions, with the results shown in Figure 26. At 433 MHz, the peak gains of the proposed antenna are -24.4 dBi and -25.27 dBi for open- and closed-mouth, respectively. For 915 MHz, when the mouth was open, the antenna has peak gain of -15.63 dBi and -17.13 dBi for the open- and closed-mouth conditions, respectively.

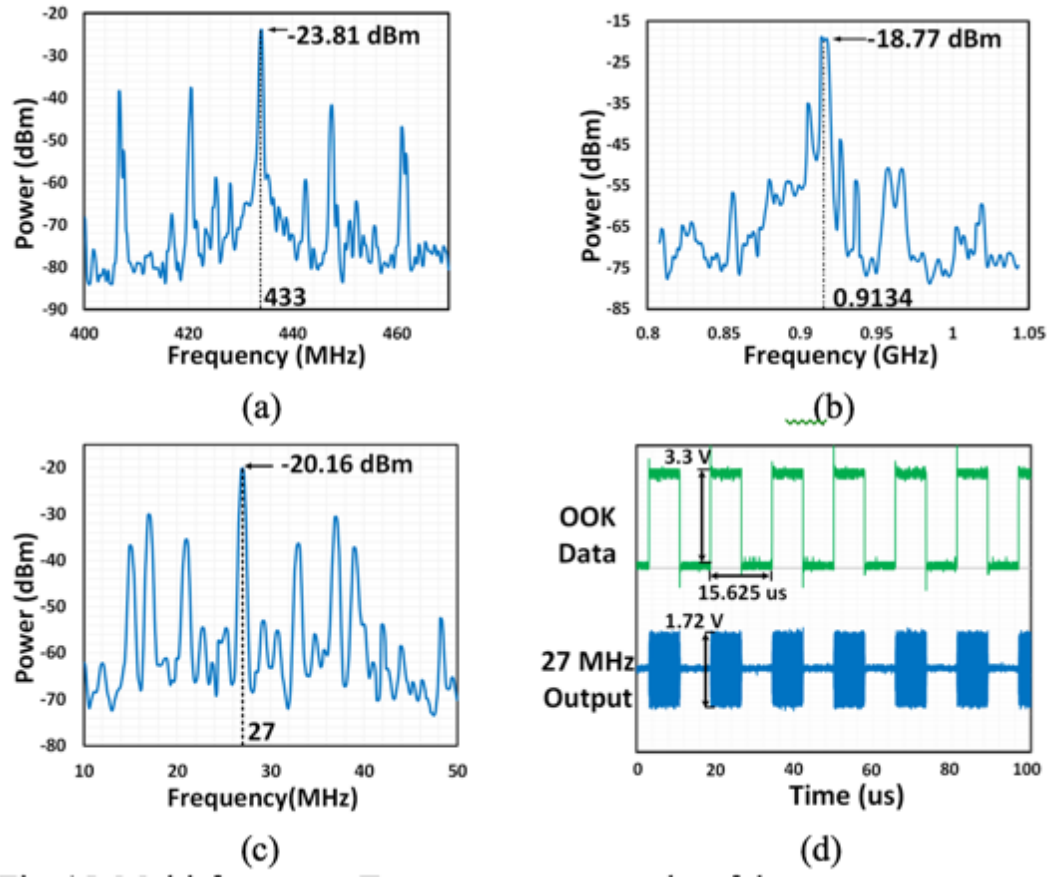

Figure 28 Multi-frequency Tx measurement results of the output spectrums of (a) 433 MHz Tx, (b) 915 MHz Tx, and (c) 27 MHz Tx. (d) Serial data bit stream and 27 MHz OOK carrier signal at the output of the 27 MHz Tx.

3.4.2 Tx Measurement Results

The adaptive multi-frequency Tx ASIC was fabricated in the TSMC 0.35-µm standard CMOS process, occupying 1.97 × 1.18 mm^2 of silicone real estate, as shown in Figure 27. To validate the basic Tx functionality, we measured the output power spectrum of each individual Tx with 50-Ω spectrum analyzer input port loading, as shown in Figure 28. Figure 28d shows the transient OOK signal at 27 MHz. The output power of the Tx at 27 MHz, 433 MHz, and 915 MHz are -20.16 dBm, -23.18 dBm, and -18.77 dBm, respectively, which are lower than simulation results in [84]. Additional

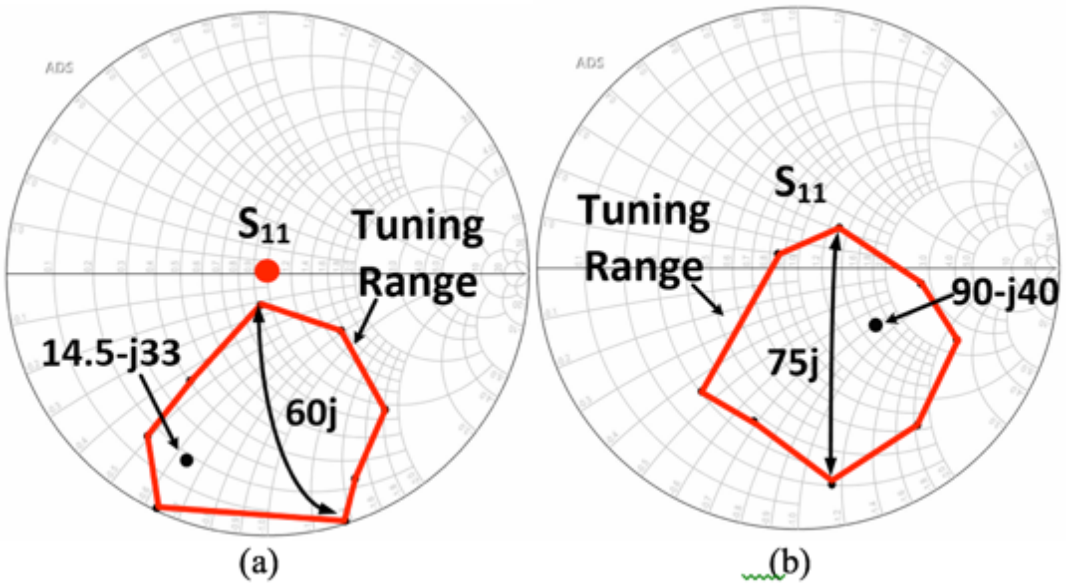

Figure 29 Measured tuning range of the adaptive matching network at a) 433 MHz and b) 915 MHz.

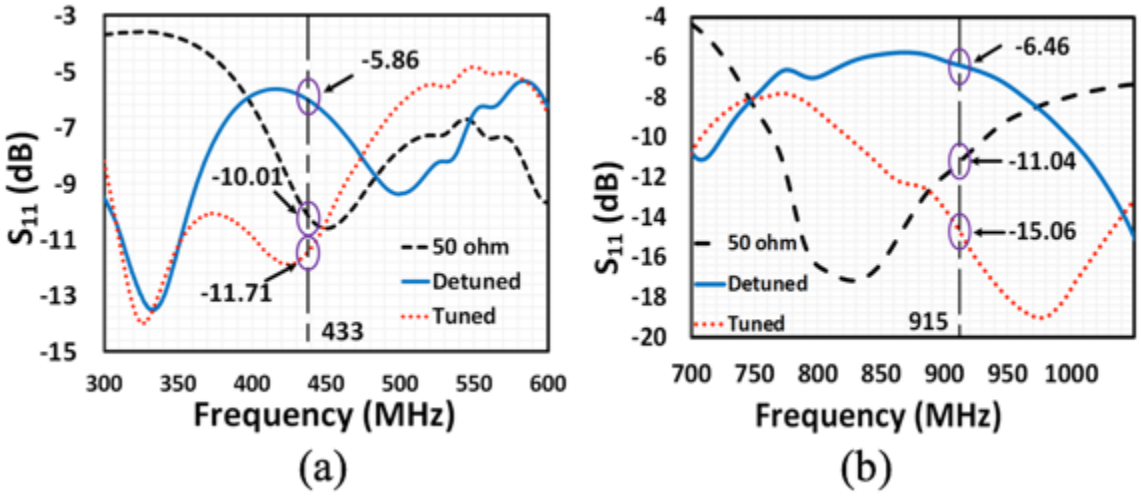

Figure 30 Measured adaptive matching ability of the auto tuning network in response to a shift in the load impedance: (a) from 50 Ω to (14.5-j33) Ω at 433 MHz, and (b) from 50 Ω to (90-j40) Ω at 915 MHz.

parasitic components on the printed circuit board (PCB), deviation from 50-Ω loading, and mismatch with the measurement cable are possible reasons for this discrepancy.

3.4.3 Adaptive matching range

Table 5 – Benchmarking the matching properties

	TBioCAS 2012	TMTT 2014	JSSC 2008	RFIC 2013	TBioCAS 2017	JSSC 2014	This work
Process	0.5-µm std. CMOS	Discrete	RF-MEMS	2-µm HBT	40-nm CMOS	0.18-µm std. CMOS	0.35-µm std. CMOS
Frequency (MHz)	27/433	27, 433, 2480	900	1950	2400	2400	27/433/915
Dynamic matching	No	Yes	Yes	Yes	Yes	Yes	Yes
Matching integration	-	Off-chip	On-chip	Off-chip	On-chip	On-chip	On-chip
Detection target	-	Power	Phase	Polar	Polar	Magnitude	Magnitude
Tuner settings	-	16	32	8	32	128	128
Tuning range	-	-	75j	VSWR of 2.5	VSWR of 3	VSWR of 1.9	60jΩ@433MHz 75jΩ@915MHz
Application	iTDS	iTDS	Mobile	Mobile	Wearable/ Implantable	Mobile	iTDS

Following [43], we have measured the tuning range of the adaptive matching networks and depicted them in Figure 29. These figures show that if the detuned antenna impedance falls within the red polygon in the Smith chart (including 50 Ω), the adaptive tuning network can help return it back to the matched condition with return loss is below -10 dB. To test the adaptive matching performance, a VNA was used to mimic a 50 Ω

antenna. After connecting Tx ASIC to the VNA, the counter in the adaptive matching block was enabled to sweep all of the possible matching conditions, which were recorded to prove the tuning range. To test the matching ability, we selected an exemplar impedance in the matching region in each frequency, here (14.5-j33) Ω and (90-j40) Ω for 433 MHz and 915 MHz, respectively, and monitored the S_{11} measurement results, as shown in Figure 30. In the ideal case, where the load impedance is 50-Ω, the return loss is below -10 dB. To detune the antenna, the load impedance was changed to (14.5-j33) Ω and (90-j40) Ω for 433 MHz and 915 MHz, respectively, resulting in the return losses greater than -10 dB. The PA output power and efficiency at the two exemplar impedances were also measured. Without adaptive matching, at 433 MHz the output power reduced to -23.48 dBm, showing 3.32 dBm difference. This is corresponding with PA efficiency

Table 6 – Link budget analysis for iTDS with dual-band antenna

Parameters	Variables	Value
Frequency (MHz)	f	433/915
Data Rate (kb/s)	B_r	24
Modulation	OOK	100%
Tx Power (dBm)	P_t	-23.81/-18.77
Tx Ant. Gain (dBi)	G_{TX}	-25.27/-17.13[1]
Path loss (dB)	P_L	Adaptive
Rx Noise Figure (dB)	NF	3.5[2]
Rx Ant. gain (dBi)	G_{RX}	1.2/4[3]
Channel Filter BW (kHz)	BW	540
Signal to Noise ratio (dB)	SNR	12.0[4]
Noise power density (dBm/HZ)	N_0	-203.9

dropping from 7.53% to 3.72% after impedance change. With adaptive matching, the output power was improved to -20.4 dBm, and the PA efficiency increased to 4.51%. As for 915 MHz, 2.2 dBm reduction can be seen at the PA output power without adaptive

matching, from -18.77 dBm to -20.97 dBm, dropping the PA efficiency from 8.12% to 5.57%. With the adaptive matching, only 0.18 dBm difference was observed at the output of PA, generating -18.85 dBm output power, corresponding to the PA efficiency of 9.3%. Then the adaptive matching network was allowed to tune the capacitor banks and improve the matching condition. Based on the measurement results, the tuning ranges of the proposed adaptive matching mechanism are up to 60 jΩ and 75 jΩ for 433 MHz and 915 MHz, respectively, as shown in Figure 29. Table 5 summarizes and benchmarks the tuning performance of current Tx ASIC prototype.

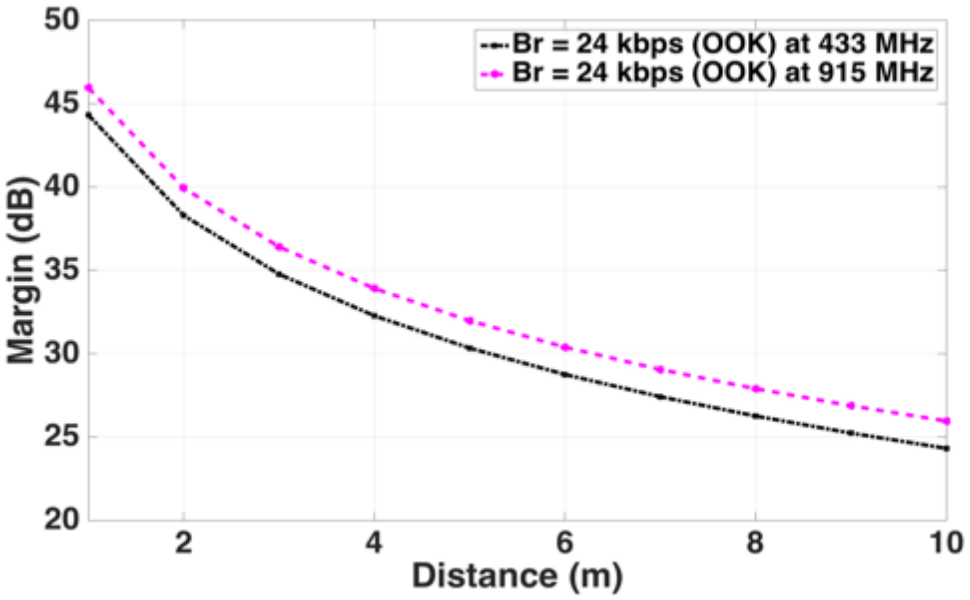

Figure 31. Distance versus link margin of the dual band antenna at 433 MHz and 915 MHz at 24 kbps date rate.

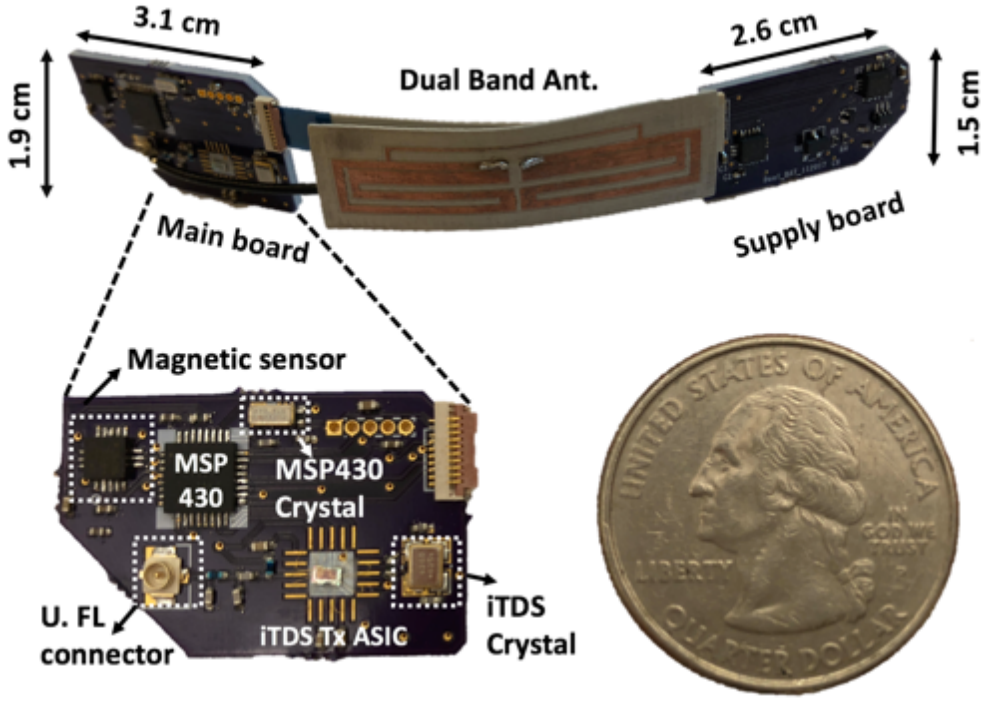

Figure 32 Implementation of iTDS in the form of arch-shaped prototype with the detailed illustration of the main board.

3.4.4 Wireless Communication Link Budget Analysis

To justify if the proposed Tx meets the requirement of our system, a link budget for wireless communication is investigated. The link budget is associated with different losses, such as reflection, absorption, scattering, path loss, and losses due to antenna mismatch [83], [85]. The link margin, L_m, can be calculated using the important parameters listed in Table 6. The Tx power is from the measurements in Figure 28. For reliable communication, [83] suggests maintaining 20 dB link margin. In addition, since

the SDR-Rx is an external unit, COTS antennas were considered for 433 MHz [86] and 915 MHz [87].

Figure 31 shows the distance versus margins for 433 MHz and 915 MHz, which indicates that data can be transmitted from distances up to 5 m with 30 dB margins for low gain value at 433 MHz. Similarly, data can be transmitted at distance up to 6 m with 30 dB margin for high gain value at 915 MHz. In iTDS application, the nominal distance between Tx in the user's mouth and SDR-Rx is ~1 m, which is well within the link budget according to this analysis.

Implementation of an iTDS prototype in the form of an arch-shaped dental retainer is underway, as shown in Figure 32. All electronics are housed on two 4-layer FR4 PCBs, connected by a ten-wire flat cable, which are shaped based on the average adult human oral anatomy. The iTDS Tx ASIC and MCU are mounted on one of the two PCBs, with two LSM303D magnetic sensors, one of which is on the backside of the board. To connect the dual-band antenna, a mini U.FL connector is used. The other two magnetic sensors and power management circuitry are mounted on the other PCB. The entire iTDS will be hermetically sealed with a thin layer of Parylene and medical-grade epoxy. Then

it will be further protected and given mechanical strength by a self-curing acrylic resin, which is shaped based on the user's dental impression, as commonly done in dentistry. At this stage, stainless steel dental clasps are also embedded in the acrylic to perfectly fit and stabilize the iTDS on the lower teeth.

In a preliminary experiment with the iTDS prototype, the dual-band antenna, coated with PDMS, was connected to the rest of the device. A subject placed the sealed iTDS inside the mouth and sat 75 cm away from an Rx antenna, connected to a spectrum analyzer. We asked the subject to open and close the mouth to cause antenna detuning and recorded the received power at 433 MHz and 915 MHz. At 433 MHz, with open and closed mouth, the Rx receives -62.5 dBm and -62.84 dBm signal, respectively. At 915 MHz, the received power is -53.32 dBm and -53.8 dBm for open- and closed-mouth, respectively. The results show that the received power from iTDS is relatively stable under open- and closed-mouth conditions, thanks to the adaptive matching mechanism. In addition, the received power is 30 dB higher than the Rx sensitivity, -106 dBm in this case, from Table 6 and equations.

3.5 Summary

A prototype of adaptive multi-frequency Tx ASIC, operating at 27 MHz, 433 MHz, and 915 MHz is presented with a dual- band antenna for iTDS, a tongue-operated intraoral AT, to establish a robust wireless communication link between the iTDS and an external SDR-Rx. External RF interference can be mitigated by switching the operating frequency from one band to another, which is currently manual, but will be automated in future versions by adding an Rx to this ASIC. Since the Tx antenna is easily detuned in

the dynamic mouth environment, increasing the return loss, an adaptive matching network is included by adjustable capacitor banks in the ASIC. They form a feedback loop with an off-chip low power MCU that monitors the output power level, delivered to the Tx antenna, via an on-chip peak detector, to sense the matching condition, and control an on-chip 7-bit up/down counter to adjust the capacitor banks. A small dual-band antenna at 433 MHz and 915 MHz has also been presented, specifically for this application. It has been simulated in HFSS and XFdtd Remcom with a real human head model under open- and closed-mouth conditions. It has also been experimentally characterized and showed enough gain for a robust wireless link, according to the link budget analysis. In the future, the dynamic matching algorithm will be entirely implemented on-chip, and detects interference and switches to a different band in coordination with the SDR-Rx.

CHAPTER 4. AN ADAPTIVE IMPEDANCE MATCHING TRANSMITTER FOR A WIRELESS INTRORAL TONGUE-CONTROLLED ASSISTIVE TECHNOLOGY

4.1 Introduction

We have been discussed the operation and background of the intraoral Tongue Drive System. Maintaining a robust wireless communication with the external receiver (Rx) for iTDS is critical especially when the users are performing safety-critical tasks, such as wheelchair navigation. One of the challenges is the considerable RF propagation loss through oral tissue. Besides this, the dynamic mouth environment, due to constant movements of the lower jaw and tongue, detunes the intraoral Tx antenna, resulting in antenna impedance mismatch and additional power loss. Moreover, the wireless link can be severely interrupted by external in-band radio frequency (RF) interference, lowering the signal-to-interference ratio (SIR) at the external Rx.

Several techniques have been proposed to solve those issues and establish a robust wireless communication link for the iTDS. A high gain intraoral antenna has been designed for the iTDS, and built with commercial-off-the-shelf (COTS) components at 2.4 GHz, to enhance communication. Even though the custom designed antenna improves the robustness of the wireless link, 2.4 GHz is a crowded band, easily affected by other commercial devices, such as WiFi. In our previous work, a dual-band system was proposed, which operated at 27 MHz and 433 MHz. In the system, once one of the operation bands is disrupted by RF interference, another unused band can be activated to

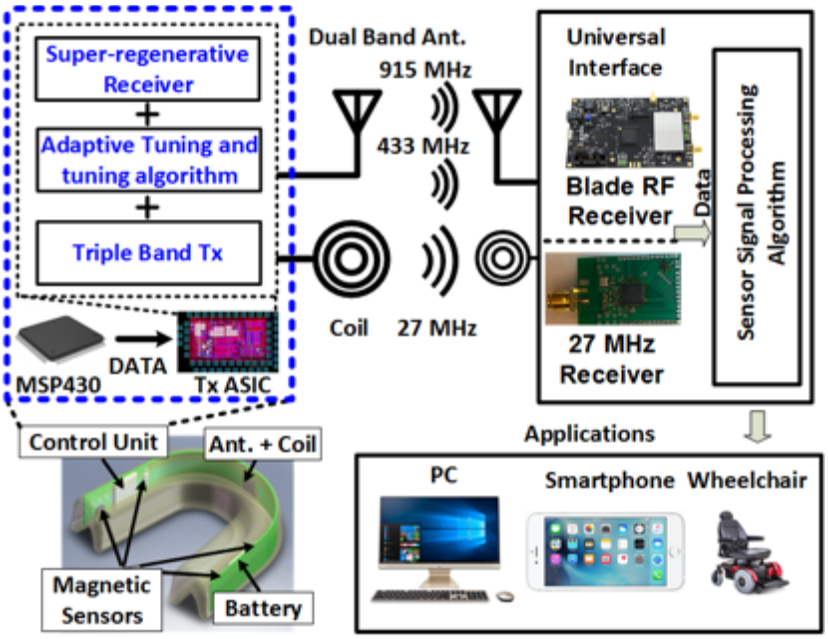

Figure 33 System overview of the intraoral Tongue Drive System (iTDS) with its key components and target applications.

continue the operation. However, in the previous design, only one far-field band, 4MHz, which is close to other medical devices as well, is provided. With only two band options, the radio link is still easily disrupted by interference. To reduce the possibility of being interrupted, another far-field band, 915 MHz, which is not as congested as 433 MHz and 2.4 GHz, was added. Although there are enough operating bands to mitigate external noise in this design, the chip did not have the ability to select the optimal band without the users' involvement.

Dynamic antenna impedance matching can be utilized to compensate antenna impedance variations in the variable mouth environment by adding dynamic components. In another example, four discrete capacitors as a matching network were added ahead of the antenna. However, by utilizing the discrete components, only a limited number of impedance matching combinations can be achieved while avoiding a large circuitry. 128

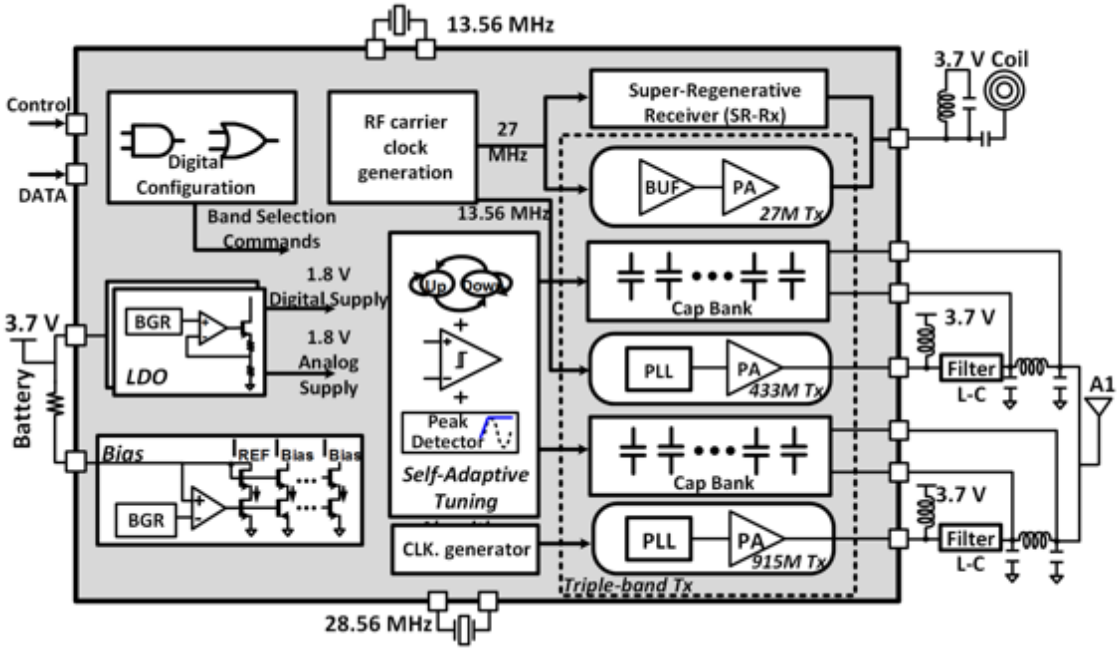

Figure 34 Block diagram of the proposed iTDS triple-band transmitter ASIC.

matching combinations were provided using on-chip capacitors. Even though this design provides enough matching combinations, the output power of the PAs is still low, which needs more optimization. Low output power may result in poor connectivity at longer data transmission distances. In this chapter, we present an application specific integrated circuit (ASIC) with standalone adaptive antenna impedance matching Tx for the iTDS, which adopts the triple-band structure, while integrating the impedance matching algorithm in the ASIC to realize the adaptive antenna impedance matching without any assistance from external components. In addition, a super- regenerative Rx (SR-Rx) is added to the ASIC, presenting the ability to automatically switch the active bands by monitoring the link quality without users' involvement. The system overview of the iTDS is shown in Figure 33, including the Rx which has been implemented by a COTS software define radio (SRD) in this prototype. The off-chip MCU (MSP430) collects magnetic data from sensors at 100 Hz, packetizes them into 30-byte data packets, and

sends them to the ASIC. A dual-band antenna has been designed for the two upper bands, while a coil is used for near-field data transmission at 27 MHz. In following sections, the Tx ASIC design with the self-adaptive antenna impedance matching block and the SR-Rx block are presented, followed by the measurement results and concluding remarks.

4.2 Tx ASIC Architecture

Figure 34 presents the block diagram of the proposed Tx ASIC. Two on-chip low dropout (LDO) regulators convert the 3.7 V rechargeable battery voltage to two 1.8 V supplies, one for digital and the other for analog blocks. In the future, to obtain higher power efficiency, the buck converter can be used instead of the LDO. Bias currents are generated from a band-gap reference (BGR). The matching networks consist of two capacitor banks equipped with the matching algorithm for the upper two bands, 433 MHz and 915 MHz, while sharing a dual-band antenna. As for the 27 MHz Tx, a coil is used for near-field communication, which is shared with the SR-Rx that monitors the link quality.

4.2.1 Triple Band Tx ASIC Structure

All three transmitters use on-off-keying (OOK) to modulate data. The default band for iTDS is 27 MHz since the power has the lowest attenuation in human body at this band. The 27 MHz Tx consists of a power amplifier (PA) and a buffer to realize OOK by turning it on/off based on. The upper two bands transmitters utilize a phase locked loop (PLL) to generate the carrier signal, followed by a PA. In the PLL, the carrier signal, generated by a voltage-controlled ring oscillator, is compared with the crystal-

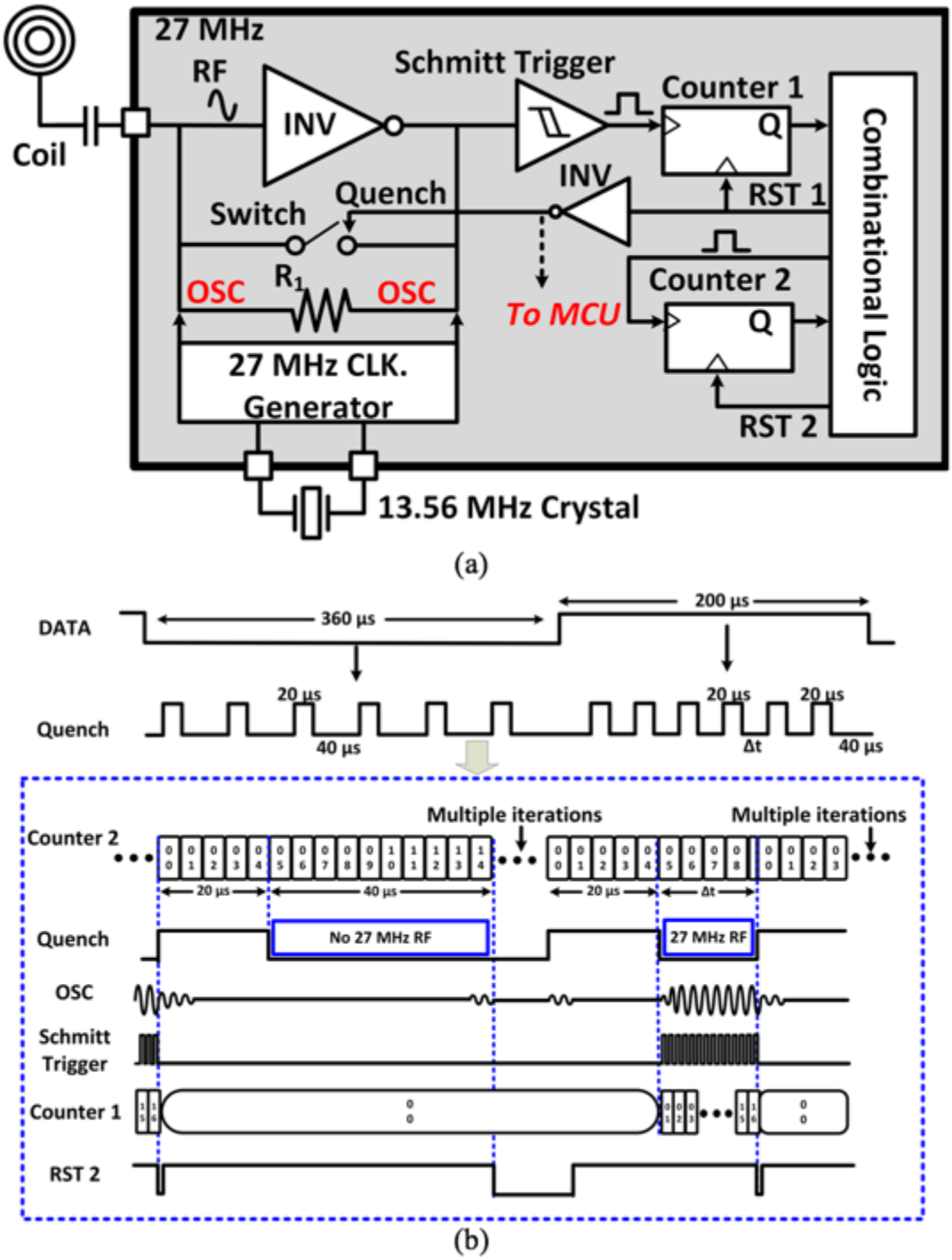

Figure 35 Operational description of the Super-Regenerative Receiver (SR-Rx): (a) block diagram, and (b) timing diagram.

based reference clock after a 64:1 divider. A cascade class-E PA is adopted for bothbands.

4.2.2 Super-regenerative Receiver

In our previous tri-band radio design, users inconveniently needed to issue specific tongue commands to switch the active band. In this ASIC, a SR-Rx is added to overcome the limitation of one-way communication, having the ability to automatically switch the active band without the need for user involvement. The goal of the SR-Rx is to detect the 27 MHz signal which comes from the external receiver and external noise and recover the OOK data. Block diagram of the SR-Rx is shown in Figure 35a. It consists of a 27 MHz clock generator and digital control blocks, including two counters and combinational logic.

Figure 35b describes the SR-Rx functionality. Counter 2 inputs a 250 kHz clock signal from the off-chip MCU. During the first 20 μs, when Counter 2 counts up to 5, the quench signal stays "High" to eliminate previous oscillations. Within the next 40 μs, the quench signal is pulled down to "Low". When there is no 27 MHz RF input coming from the coil, during the 40 μs, there will be no oscillations feeding into the Schmitt trigger. After this 40 μs, Counter 2 is reset. If there are any RF inputs coming from outside environment, and passing through the band-pass LC-tank, it will cause oscillations during this 40 μs. These oscillations are passed through the Schmitt trigger to generate a clock at 27 MHz for Counter 1. After Counter 1 counts to "16", the 27 MHz input will be recognized and both counters are reset, indicating the end of one cycle. The main difference between presence and absence of 27 MHz RF input is the period that the quench signal stays "Low". With the RF input, it takes less than 40 μs for the quench signal to stay "Low" compared to the scenario that no RF input is injected. Usually, multiple quench periods are included with and without RF inputs (DATA = "0" or "1")

illustrated in Figure 36b. If the quench signal stays "Low" as 40 μs, the data is demodulated as "0", the duration of which is 360 μs in this application. Once the "Low" state of the quench signal is less than 40 μs, the data is demodulated as "1", the duration of which is 200 μs.

When the SR-Rx detects the RF interference at 27 MHz, the ASIC stops operating at the default 27 MHz and change the active band to 433 MHz. If considerable amount of noise is present at 433 MHz, then 915 MHz will be selected. The link quality of the upper two bands can be detected by the external SDR Rx. If interference is detected at the upper two bands, the Rx will send a packet to the iTDS at 27 MHz. The SR-Rx has the ability to receive and demodulated the packet. Based on the received packet, the MCU is able to change the active band accordingly. This mechanism automatically selects the active band without requiring any user involvement.

4.2.3 Adaptive Matching

Unlike the previous work, in this ASIC, the matching algorithm was implemented on-chip, including a peak detector, a comparator, and a 7-bit up/down counter. The matching circuit topologies are similar for both 433 MHz and 915 MHz PAs, which consist of a choke inductor, LC filter, off-chip π-matching network with two variable on-chip poly-insulator- poly (PIP) capacitor banks, controlled by the on-chip up/down counter. The values of variable capacitor banks are selected. The peak detector is designed to sample the peak voltage of the RF carrier. A large input impedance is required at the detector to avoid degradation of the PA performance and the linear relationship between the magnitude of the input signal and the output voltage. To reduce

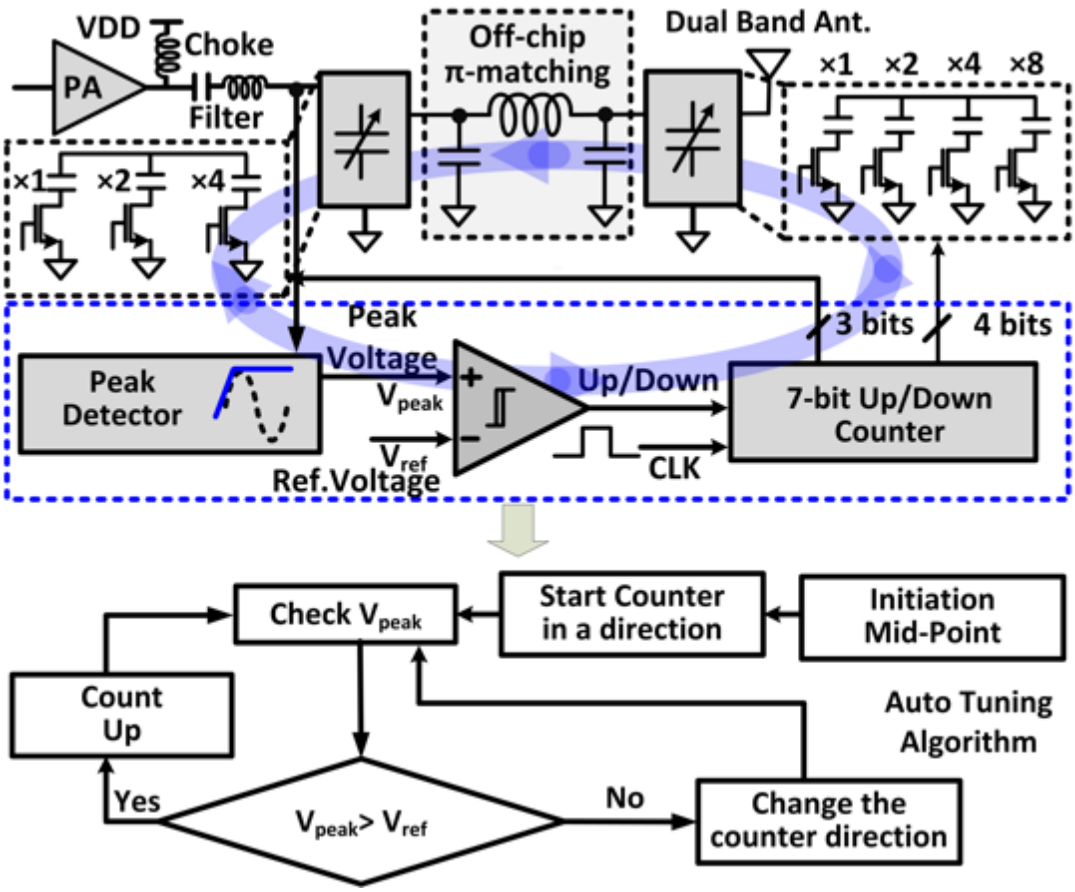

Figure 36 Schematic diagram of the self-adaptive matching block, including on-chip matching algorithm flowchart and off-chip components.

the correction time of the whole process, the peak detector is also required to provide a fast-transient response, less than 0.5 μs. The comparator was also designed to have a fast response time, including the rising and falling times of the output signal.

As stated in [80], there will be only one optimal matching load impedance for the PA. At the optimal matching scenario, the RF signal over the load, which includes tunable capacitor banks, off-chip π-matching network, and the antenna, will generate a unique peak voltage that is used as the reference voltage, V_{ref}. If the antenna impedance is mismatched, the RF signal across the load varies, changing its peak voltage. The adaptive matching algorithm is shown in Figure 36. The peak detector samples the peak voltage

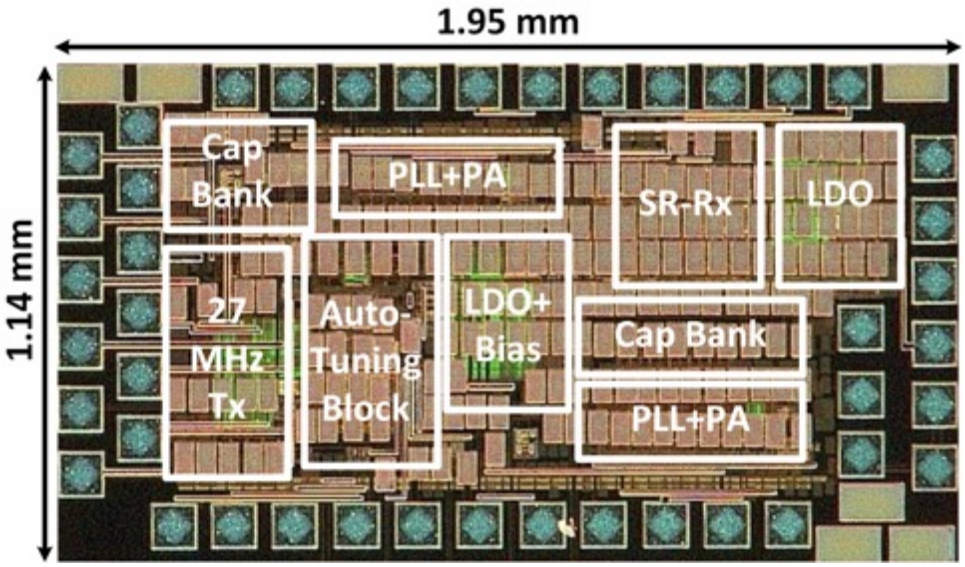

Figure 37 Chip microphotograph of the self-adaptive impedance matching ASIC which has 1.95 mm length and 1.14 mm width.

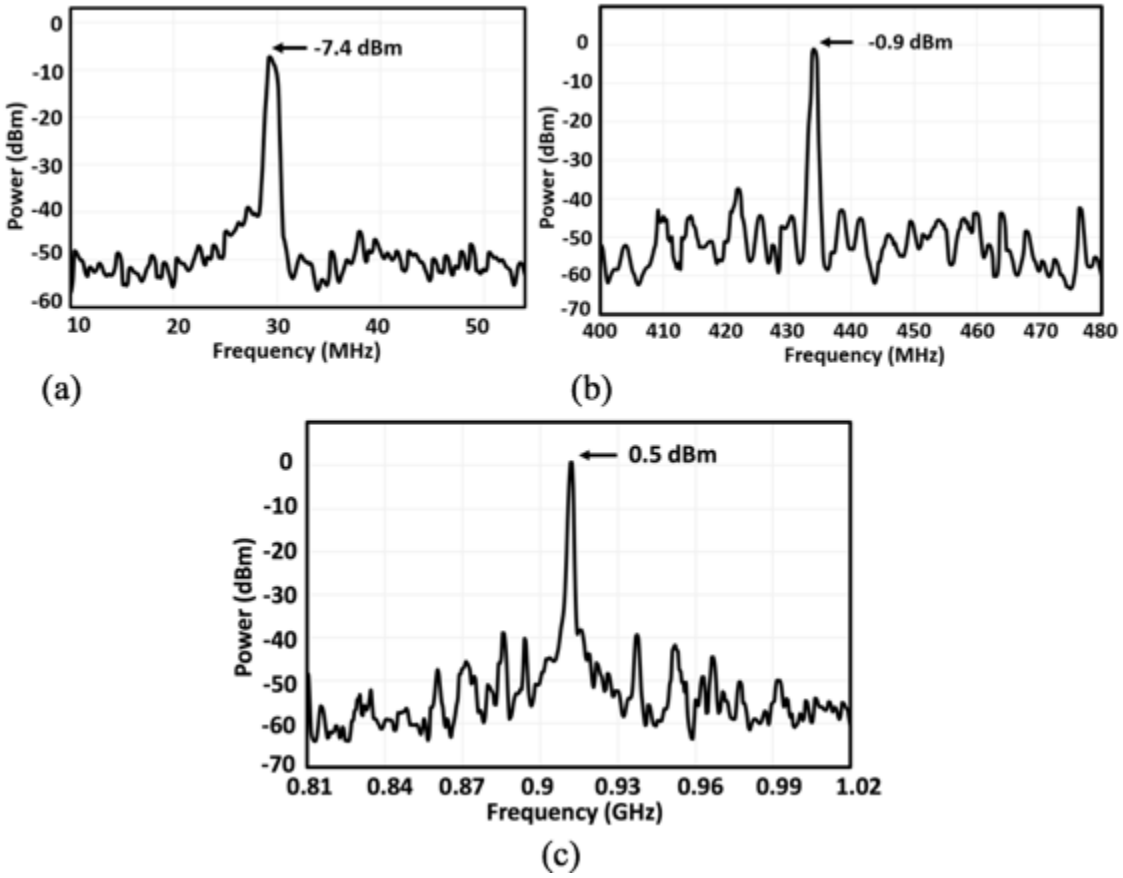

Figure 38 Measurement output spectrum of the Tx ASIC at (a) 27 MHz, (b) 433 MHz, and (c) 915 MHz, when directly loaded at 50 Ω.

and compares it with V_{ref} to determine the counting direction of a 7-bit counter. The 7-bit counter will keep counting in one direction until the peak voltage, V_{peak}, drops below or increases above V_{ref}, changing the status of the output of the comparator. For example, if V_{peak} is higher than V_{ref}, the output of comparator will be high, which enables theUp/Down counter to count up, as illustrated in Figure 36 Schematic diagram of the self-adaptive matching block, including on-chip matching algorithm flowchart and off-chip components.. This simple tracking feedback mechanism ensures the antenna impedance will be tuned near the optimal matching point dynamically, improving the PA output power. Compared with the previous work, by implementing the algorithm on-chip, the peak detector is revised to have a better linear relationship between the RF input and the output voltage. Based on post-layout simulation results and the analysis, it takes a total of 0.41 ms to check all 128 possible combinations.

4.3 Measurement Resutls

The adaptive matching Tx ASIC prototype was fabricated in the TSMC 0.35-μm standard CMOS process, shown in Figure 37, occupying 1.95 mm × 1.14 mm of silicon area. To validate the Tx functionality, we measured the output power spectrum of each individual Tx with 50 Ω spectrum analyzer input port loading, as shown in Figure 38. The peak output power of the Tx at 27 MHz, 433 MHz, and 915 MHz are -7.4 dBm, -0.9 dBm, and 0.5 dBm, respectively. In addition to the Tx functionality, the automated matching ability is measured. First, the voltage amplitude at the output of the PA was measured under 50 Ω loading as the reference voltage, V_{ref}. A load impedance tuner is used to realize the arbitrarily mismatched antenna impedance. Here, we measured the mismatched antenna impedance at $|\Gamma| = 0.6$, Voltage Standing Wave Ratio (VSWR) = 4,

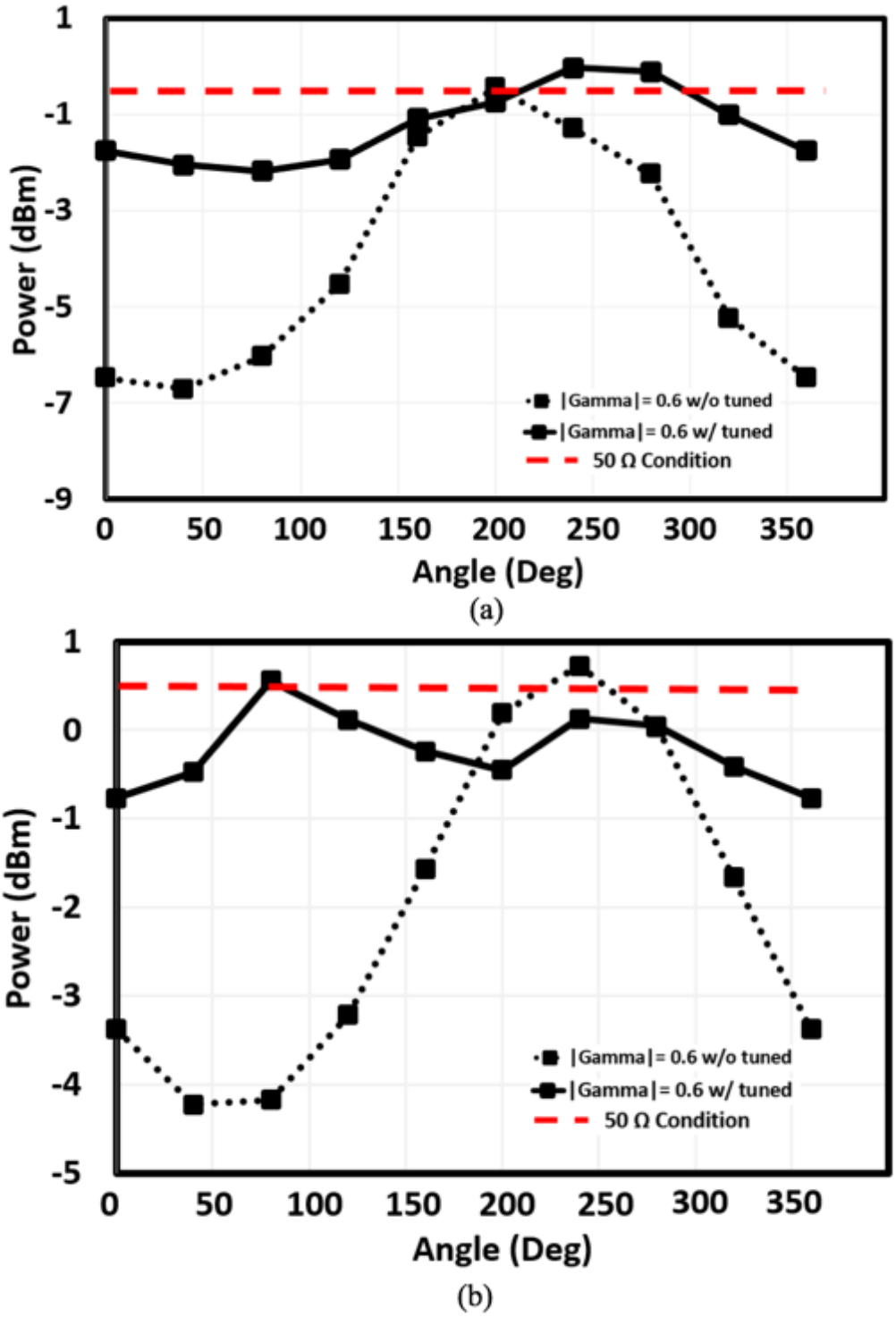

Figure 39 Measured proposed Tx ASIC output power performance with and without matching at (a) 433 MHz and (b) 915 MHz.

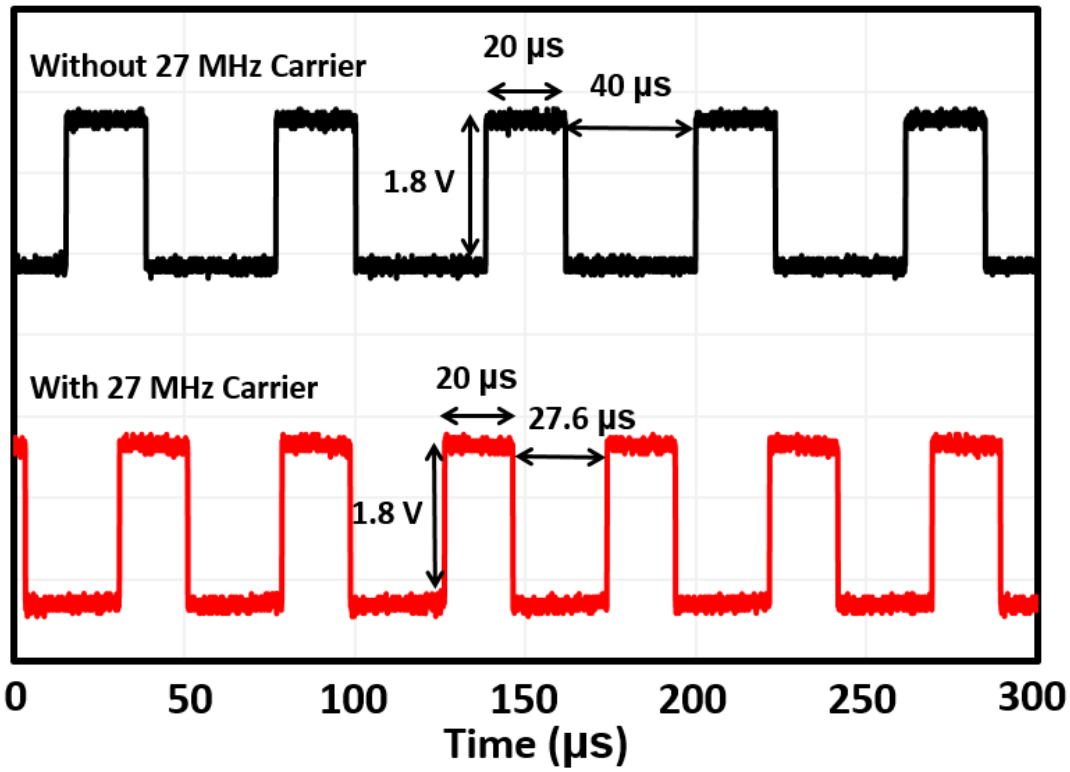

Figure 40 Measured quench signal outputs in the scenarios with and without 27 MHz carrier.

we waited until the output power is relatively stable and at nine different angles (0^o, 40^0, 80^0, 120^0, 160^0, 200^0, 240^0, 280^0, 320^0). After setting up V_{ref}, the impedance matching block was enabled. Since the proposed ASIC dynamically tunes the load impedancerecorded the highest output power after the matching completed. Improvement of the output power with the automated impedance matching mechanism is shown in Figure 39 at 433 MHz and 915 MHz, compared without the matching scenarios. The results show that the output power at both frequencies are improved and closer to the 50 Ω loading condition with a smaller variance compared without the automated matching. The output power is improved up to 4.7 dB at 433 MHz and 3.8 dB at 915 MHz for $|\Gamma|$ = 0.6. Compared with the previous work, this design increases the matching range, allowing more mismatch scenarios. The functionality of SR-Rx is also verified. At the

Table 7 – Benchmarking the matching performance

	ISSCC 2009	TBioCAS 2012	TMTT 2014	JSSC 2014	TBioCAS 2017	TBioCAS 2018	This work
Process	0.18-µm CMOS	0.5-µm std. CMOS	Discrete	0.18-µm std. CMOS	40-nm CMOS	0.35-µm std. CMOS	0.35-µm std. CMOS
Frequency (MHz)	850-2000	27/433	27, 433, 2480	2400	2400	27/433/915	27/433/915
Power Consumption (mW)	31	3.7	-	-	0.83	13.3	11.52
Operating range (cm)	-	75	22, 123, 39	-	-	70	103
Dynamic matching	Yes	No	Yes	Yes	Yes	Yes	Yes
Matching integration	Off-chip	-	Off-chip	On-chip	On-chip	On-chip	On-chip
Detection target	Magnitude	-	Power	Magnitude	Polar	Magnitude	Magnitude
Tuner settings	4096	-	16	128	32	128	128
Tuning range	-	-	-	VSWR of 1.9	VSWR of 3	60jΩ@433MHz 75jΩ@915MHz	VSWR of 4

beginning, without a 27 MHz RF input, the quench signal is shown in Figure 40 upper trace is recorded, which is turned on/off for 20/40 µs. When a 27 MHz RF signal is manually injected into the SR-Rx block, the quench signal time is reduced to 27.6 µs, indicating that it takes less time for the Schmitt trigger to generate 16 oscillations. The performance summary and benchmarking the prototype three- band Tx ASIC is shown in Table 7.

4.4 Summary

To establish a robust wireless communication between the iTDS and SDR-Rx, we have presented an integrated Tx with automated impedance matching and three operating bands (27 MHz, 433 MHz, and 915 MHz) that are automatically activated to mitigate external RF interference without users' involvement. A SR-Rx detects RF signal at 27 MHz and delivers this information by varying the "close" time of the quench signal. To solve the issue of Tx antenna detuning in the dynamic mouth environment, a self-impedance matching algorithm is implemented in the ASIC by adjusting the on-chip capacitor banks for the two upper bands, 433 MHz and 915 MHz. The automated

matching block monitors the matching condition via an on-chip peak detector and controls an on-chip 7-bit up/down counter to interact with the capacitor banks. By adding the automated matching mechanism, the output power is improved, close to that of 50 Ω loading conditions, with small variance under mismatched loading. 4.7 dB and 3.8 dB improvements are achieved at 433 MHz and 915 MHz for $|\Gamma| = 0.6$, respectively.

CHAPTER 5. A STAND-ALONE INTRAORAL TONGUE-CONTROLLED COMPUTER INTERFACE FOR PEOPLE WITH TETRAPLEGIA

5.1 Introduction

Stroke spinal cord injury (SCI) are the main causes of paralysis in the world. In the United States, there are nearly 4,000,000 stroke survivors and their number is growing at the rate of ~800,000 per year. In 2017, there have been ~282,000 individuals affected by SCI, with 17,000 new cases added annually. To improve the quality of life of people with paralysis, assistive technologies (AT) have been developed that can leverage the users' remaining abilities to help them perform daily living tasks independently. One group of ATs that has been heavily researched is brain computer interfacing (BCI) based on electroencephalography (EEG). EEG signals are very weak (<10 μV), however, and thus vulnerable to interference and motion artifacts, resulting in potential safety issues in wheelchair navigation, for instance. Another group of ATs utilize electromyography (EMG) signals to provide users with computer access. However, the muscle fatigue during long-term usage and low number of commands are among limitations of these systems. Speech recognition is now widely available in computers and smart devices for typing and issuing commands. However, these systems are sensitive to acoustic noise, resulting in safety issues in outdoor or noisy environments.

Tongue-controlled ATs are reported to have advantages in terms of sensitivity to noise, less muscle fatigue, and the number of available commands thanks to inherent

abilities of the human tongue. Recently, tongue-controlled AT has been developed to interact with wheelchairs and robotic arms with detailed design. Tongue Drive System (TDS) is one of the tongue-controlled ATs that has been used for a range of applications. By monitoring the position of a small magnetic tracer that is attached ~1 cm posterior to the tip of the tongue, using an array of 3-axial magnetic sensors, TDS is capable of detecting different tongue gestures in real time. These gestures in turn converted to a set of user-defined "tongue commands" to interact with other devices, such as computers, smartphones, and wheelchairs. A version of TDS has been developed in the form of a wireless headset with magnetic sensors mounted on a pair of poles near the cheeks, which is referred to as the external TDS (eTDS). eTDS has been clinically evaluated by our group and shown to be 3 times faster than a popular AT, known as sip'n'puff, but similarly accurate. Another version combines the tongue gestures with head motion and voice recognition all on the same wireless headset, which is called the multimodal TDS (mTDS), and has been evaluated by healthy participants.

There are certain conditions, however, in which headsets may not be optimal for mechanical stability. For example, when users are driving their wheelchairs or riding in vehicles in a rough terrain, the headset position might shift, resulting in deviation of the magnetic sensor positions with respect to the magnetic tracer on the tongue. This requires either more advanced signal processing algorithms that would automatically recognize the shift, or recalibration and retraining of the tongue commands by the users. In addition, based on the results of an eTDS survey, the majority of potential end users with tetraplegia care about their appearance when they choose an AT. Even though headsets are quite common for listening to music, the eTDS/mTDS headset might be

perceived as an indication of disability for a subset of users, and fail to provide them a high enough degree of privacy. Therefore, an AT that would be completely conspicuous and hidden from sight would be preferable for these users.

To address these issues, intraoral Tongue Drive System (iTDS) was introduced as an alternative form factor for the TDS by embedding all of the electronics into a small dental retainer that would clasp onto the teeth. This solution, which is customized based the user's oral anatomy, provide more mechanical stability, while being hidden inside the mouth. The early version of the iTDS was designed to be mounted in the palatal area, where there is more space for the electronics, and clasp onto the upper teeth. However, it occupied a portion of the intraoral space, where the tongue moves, making it more difficult for the users to issue tongue commands. It could also interfere with their speech, at least until they adapted to the new object in their mouth. In this paper, we are adopting the arch-shaped version of the iTDS, which clasps onto the lower teeth with electronics that are small enough to locate in the buccal shelf area of the mouth, without interfering with the tongue motion.

One of the challenges of the iTDS, compared to its eTDS counterparts, is maintaining a robust wireless communication with the external Rx despite the dynamic mouth environment, which constantly changes the Tx antenna impedance and RF power loss. Several ideas have been proposed to solve this issue Here, we have utilized a custom-designed intraoral antenna to address this problem. Moreover, in previous versions of iTDS and eTDS, raw magnetic sensor data had to be wirelessly sent out to the Rx to be processed and converted to tongue commands in the PC or smartphone. In this new iTDS design, an efficient tongue command detection algorithm is implemented

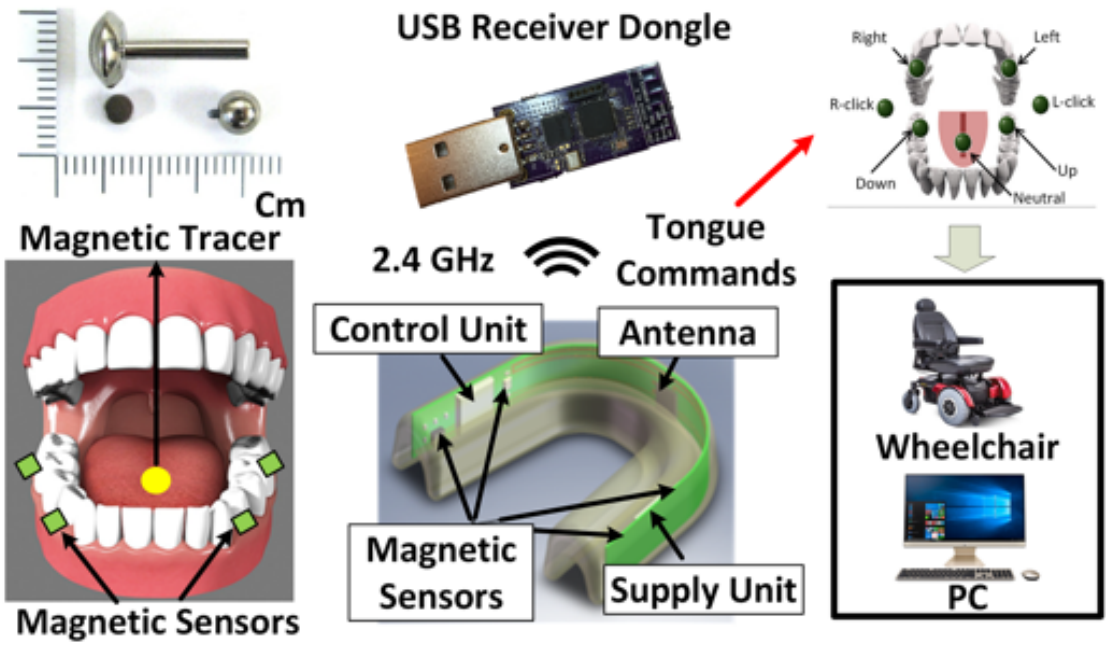

Figure 41 Conceptual view of the standalone intraoral Tongue Drive System (iTDS) with its key components and potential applications.

within the iTDS to process the raw data internally and directly generate tongue commands in real time, independent of the Rx processing capability or software. This has lowered the iTDS power consumption by reducing the amount of data that needs to be sent wirelessly to the Rx, making the iTDS standalone. Moreover, by formatting the iTDS commands to match the Human Interface Device (HID) standard format, they can be universally recognized by the majority of today's computing devices as a peripheral. Finally, a new typing mechanism has been proposed that is specifically designed for the iTDS to help users type faster with lower error rate.

Figure 41 presents a conceptual view of the new standalone iTDS with its main components and target applications. The detailed design of the system is presented in the next subsection, including the hardware and fabrication procedure. The real time

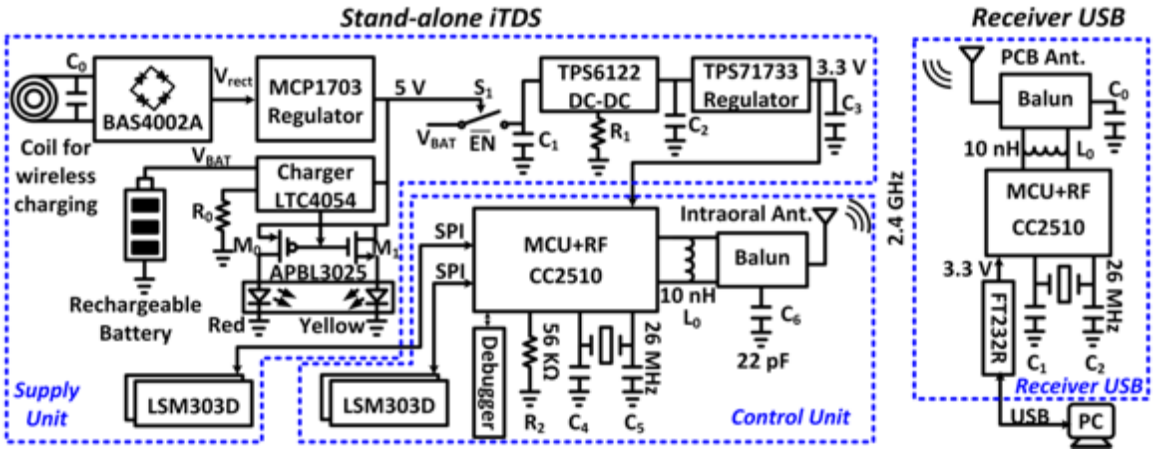

Figure 42 Simplified schematic diagram of the standalone iTDS with its control and supply PCBs that fit in the buccal shelf area as well as the Rx dongle with its serial interface (USB) circuitry with the target device, a PC in this case.

magnetic sensor signal processing (SSP) algorithm has been discussed with details of the firmware architecture will also be discussed. The computer access task to evaluate the system is presented along with the new typing technique. Performance measures and human subject performance results are discussed followed by the conclusion.

5.2 Standalone iTDS Hardware Architecture

Figure 42 shows a simplified schematic diagram of the iTDS, including the intraoral device and external Rx, which is designed as a USB dongle in this prototype to be easily applied to a PC or other embedded systems, such as Raspberry Pi. The magnetic sensors in the standalone iTDS capture the changes in the magnetic field inside the mouth due to tongue motion with the attached magnetic tracer, as raw data, and the built-in microcontroller unit (MCU) converts it to tongue commands in real time, which are then sent to the Rx dongle and eventually delivered to the target device via USB.

5.2.1 Control Unit

The iTDS is divided into two sections, each of which is implemented on a separate trapezoidal PCB, show in Fig. 3. The control PCB houses a CC2510 MCU from Texas Instruments (Dallas, TX) and 2 out of four 3-axial magnetometers, LSM303D from STMicroelectronics (Switzerland), which are placed diagonally across the right side PCB to be as far as possible from one another. The left side PCB, which is slightly smaller is in charge of iTDS power management but it also houses the other two magnetometers. The MCU, which is clocked at 26 MHz by an external crystal oscillator, has a built-in 2.4 GHz radio frequency (RF) transceiver. Magnetic field data streams, which are sampled at 100 Hz and digitized inside the magnetometers, are delivered to the MCU via serial peripheral interface (SPI). A custom-designed 2.4 GHz intraoral antenna, made of Roger 3003 substrate, is provides a gain of -10 dB and 2.4 GHz bandwidth to support robust wireless communication. Before the antenna, a balun is used to convert the differential RF output from the MCU to the single ended connection to the antenna.

5.2.2 Supply Unit

The supply unit provides regulated supply voltage to iTDS components and charges its batteries wirelessly. In this design, two 40 mAh lithium-polymer (Li-Po) batteries ($15\times12\times4$ mm^3) are used, one on each side to balance the volume and weight of the intraoral piece. Two magnetometers are also placed on the opposite corners of the supply PCB. A DC-DC converter (TPS61220DCKR, Texas Instruments, Dallas, TX) followed by a 3.3 V regulator (TPS71733, Texas Instruments, Dallas, TX) is utilized to power the entire system. When the iTDS is placed in a designated wireless charger, it receives RF power at 13.56 MHz through a receiver coil. The received RF signal is rectified by a full-wave rectifier (BAS4002A, Infineon, Germany) and regulated to 5 V (MCP1703,

Microchip, CA, USA). The 5 V regulator output turns off a switch, S_1, that prevents the batteries from supplying the iTDS during charging. It also enables an LTC4054 charger IC (Linear Technology, Milpitas, CA) to charge the batteries, with a programmable current set by the external resistor, R_0. During the charging cycle, the charger turns off the NMOS transistor, M_1 (DMN5L06K, Diode Incorporated, Plano, TX), and turns on the PMOS transistor, M_0 (DMP22D6UT, Diode Incorporated, Plano, TX), by applying a low voltage (~ 20 mV) to the gates of those transistors. Therefore, the red LED in the LED array (APBL3025, Kingbright, Taiwan) is turned on, indicating the charging cycle is in progress. Once the batteries are fully charged, the charger applies a high voltage (~ 5 V) to the gates of the transistors to turn off the PMOS and turn on the NMOS, lighting up the yellow LED to indicate the end of charging cycle. Once the coil stops receiving RF power, the batteries will be used to power up the system again.

5.2.3 Rx Dongle

As for the receiver, a custom-designed USB dongle, which includes the same type of MCU is utilized. Unlike the iTDS, an inverted-F PCB 2.4 GHz antenna was implemented on the Rx. Similarly, a balun is placed in series with the PCB antenna. A USB controller (FT232RQ, FTDI) is used to communicate with PC using a virtual COM port, which is configured at a baud rate of 921.6 kbps.

5.2.4 iTDS Dental Retainer Assembly

Figure 43 shows the iTDS latest prototype, 56.7 gram weighted, with its key components. The control and supply PCBs are connected using a 10-wire flexible cable and the custom designed intraoral antenna is placed over that cable on the front. The oral

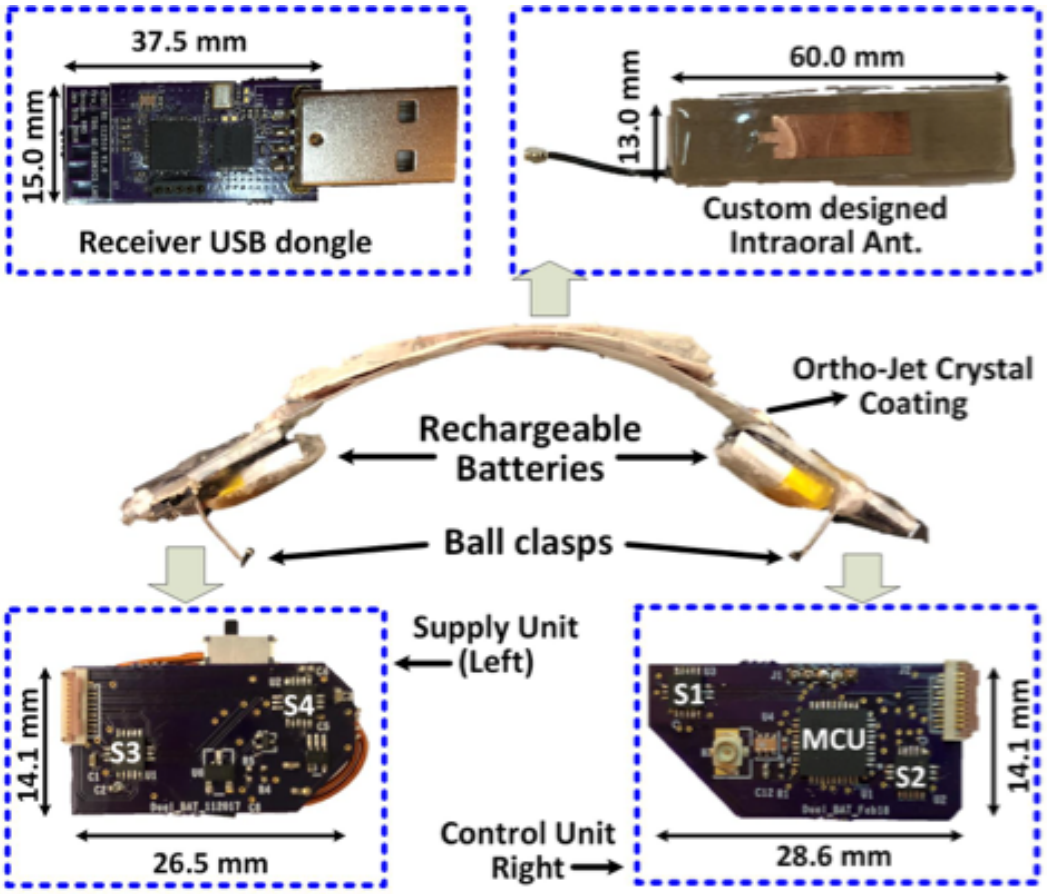

Figure 43 Implementation of the stand-alone iTDS prototype, hermetically sealed inside dental acrylic, including control and supply boards, custom-designed antenna (upper right inset), a pair of rechargeable Li-Po batteries, and ball clasps. The external Rx USB dongle is shown on the upper left inset.

anatomy of each user is unique. To provide them with maximum comfort, it is necessary to customize the outer geometry of the iTDS based on their oral anatomy. Therefore, prior to the experiments, the oral anatomy of each participant was captured using the same method practiced in dentistry. Users' dental impressions are built with dental alginate and dental stone. The geometry of the iTDS is formed using the user's dental impression as a mold. To protect the iTDS electronics from saliva and mechanical forces applied in the mouth, dental acrylic powder and self-curing liquid (Ortho-Jet crystal, Wheeling, Illinois) are applied to cover the electronics. Polydimethyl-siloxane (PDMS) is

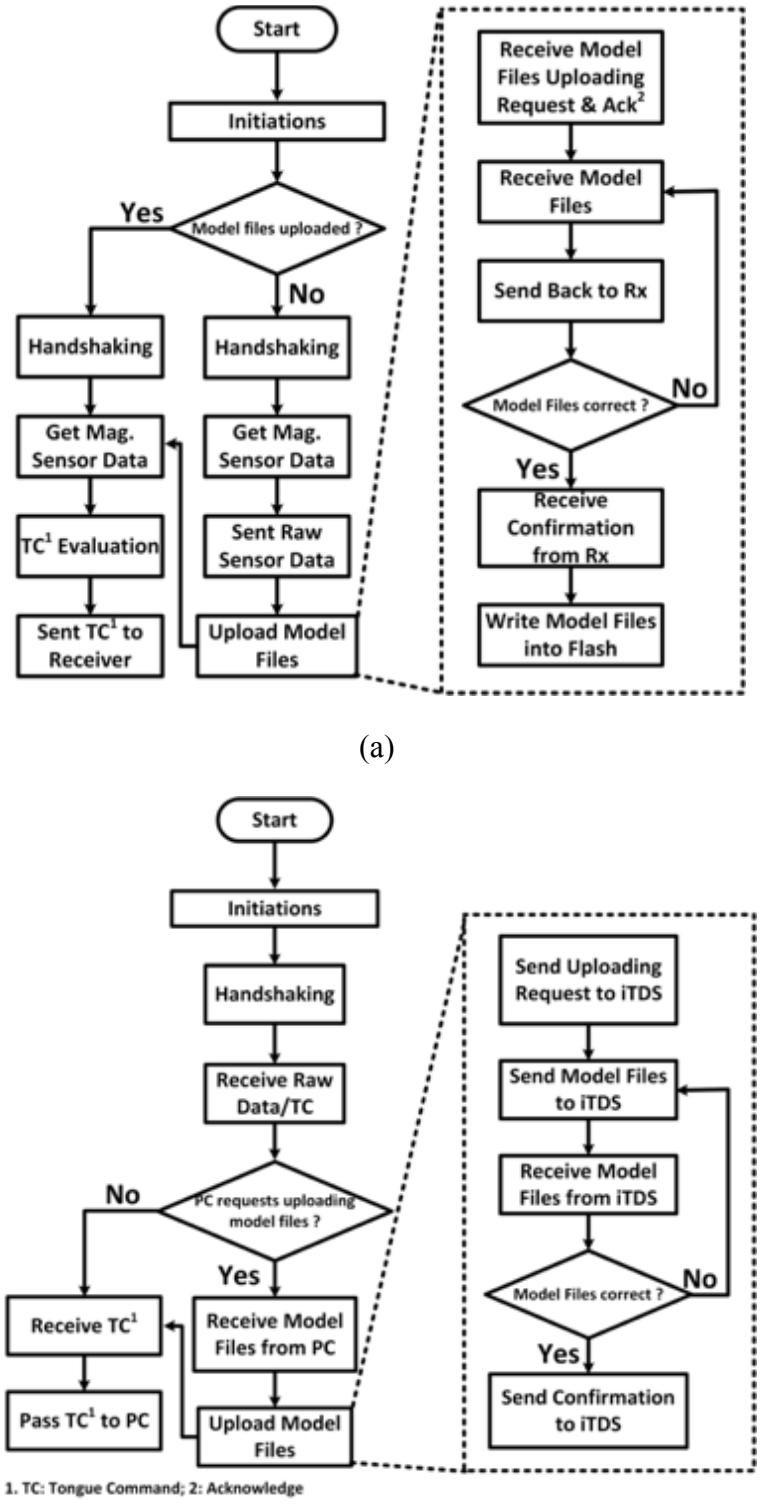

Figure 44 The flowchart of the system firmware architecture: a) stand-alone iTDS firmware, b) receiver USB firmware.

used to coat the intraoral antenna, which is added outside the acrylic coating, to improve flexibility of the device since the acrylic is hard to be bent. Two stainless steel ball clasps are also shaped around the dental impression, and inserted in the iTDS acrylic coating near the two corners of the iTDS between teeth 18-19 and 30-31, as shown in Figure 43, to increase the mechanical stability of the iTDS on the lower teeth.

5.3 Standalone iTDS Software Architecture

In this section, the software implementation of the system is discussed, including the firmware implemented in the main MCU of the stand-alone iTDS unit to read, process, and wirelessly send out the data and the one in the receiver (Rx) USB dongle to receive the data and interact with PC followed by the tongue command processing algorithm.

5.3.1 Standalone iTDS Firmware Architecture

Figure 44a shows the flowchart of the firmware implemented in the stand-alone iTDS. It starts with a set of initialization sequences, such as the clock oscillator, General-purpose input/output (GPIO), SPI communication, sleep timers and the Analog to Digital Converter (ADC), followed by the sensor configuration and initialization. To evaluate the tongue command, it is required that the model files, generated after the training and helped to perform tongue commands evaluation in the MCU, uploaded into the iTDS, therefore, after the configurations, the firmware will check if the model files have been uploaded. If they are, a handshake protocol between iTDS and the Rx USB dongle is used to establish the connectivity. In the handshake stage, 5 repeated broadcasts are initiated by the control unit, waiting for the valid acknowledge packet from the Rx. After

60 broadcasts if the handshaking is still not completed, the MCU will enter into a power saving mode. Otherwise, the MCU gets the raw sensor data, which are processed to generate the corresponding tongue commands in real time. The tongue commands will be sent out wirelessly to the Rx USB dongle. If the model files haven't been uploaded, the handshake still needs to be established, followed by obtaining the sensor data through SPI communication. The raw sensor data will be sent out to the Rx for calibration and training purposes. Once the training has been done and the Rx needs to upload the model files, an upload request will be sent to the iTDS, indicating the start of the uploading model files. After receiving all of the model files, the iTDS will also send them back to the Rx to check the correctness. If some data are missing or incorrect, the model files will be re-uploaded to the iTDS until no errors have been found. A function is created to write all of the model files into the flash drive. After that, the raw sensor data can be evaluated to generate the tongue commands and sent them out to the Rx.

5.3.2 Standalone iTDS signal processing algorithm

Figure 44b presents the firmware architecture of the Rx. Similar to the control unit, it starts with a set of initializations and configurations, including clock oscillator, Universal Asynchronous Receiver/Transmitter (UART), GPIO, and timer. The connection between the iTDS and the Rx will be established with the handshaking protocol which is requested by the PC after initializations. During the handshake, the Rx listens for handshake packets broadcasted by the iTDS. It waits until a valid handshake packet is received and responds back with an acknowledge packet for the completion of handshaking procedure. Once the connection is established, the Rx starts receiving the data, which can be the raw sensor data or tongue commands from iTDS. When the PC

receives raw sensor data, it does either the calibration or training sessions depends on the user's request by the PC UI. After the calibration and training, PC initiates model files transfer request to the Rx. Rx receives model files from the PC and wirelessly uploads to the iTDS control unit. Once done, the model files will also be sent back to the Rx from control unit for validation. In case of an error, the model files will be re-uploaded to the control unit again until error free upload of the model file. Once done, the Rx will start receiving the processed tongue commands from the control unit to interact with the PC.

5.3.3 Tongue Command Processing Algorithm

It is required for the iTDS to perform calibration and training on PC during the first usage. Raw magnetic sensor data are transferred to the PC via Rx USB dongle. Among the four magnetometers shown in Figure 43, two of them (one in supply unit, one in control unit) are used to capture the Earth Magnetic Field (EMF) to attenuate the external magnetic interferences. The other two magnetometers are used to capture the magnetic field generated by the magnetic tracer. During the calibration step, data is captured by placing the magnetic tracer to the "no command" location of the user mouth. Two projection matrices ($PL_{4\times3}$, $PR_{4\times3}$) are found using least square error method from the captured calibration data in the PC [88]. These matrices are utilized during the training and evaluation to capture EMF using two magnetometers, project and subtract from rest two magnetometers to generate noiseless six-dimensional features. Features are used to train 21 (7 commands) one vs. one support vector machines (SVM) with linear kernel during the training session [89]. LIBSVM library is utilized to generate the training model file [90]. This model file is converted to weight, $W_{21\times6}$ and bias, $B_{21\times1}$ matrices.

All of the projection and the training matrices as training model files, $PL_{4\times3}$, $PR_{4\times3}$, $W_{21\times6}$, and

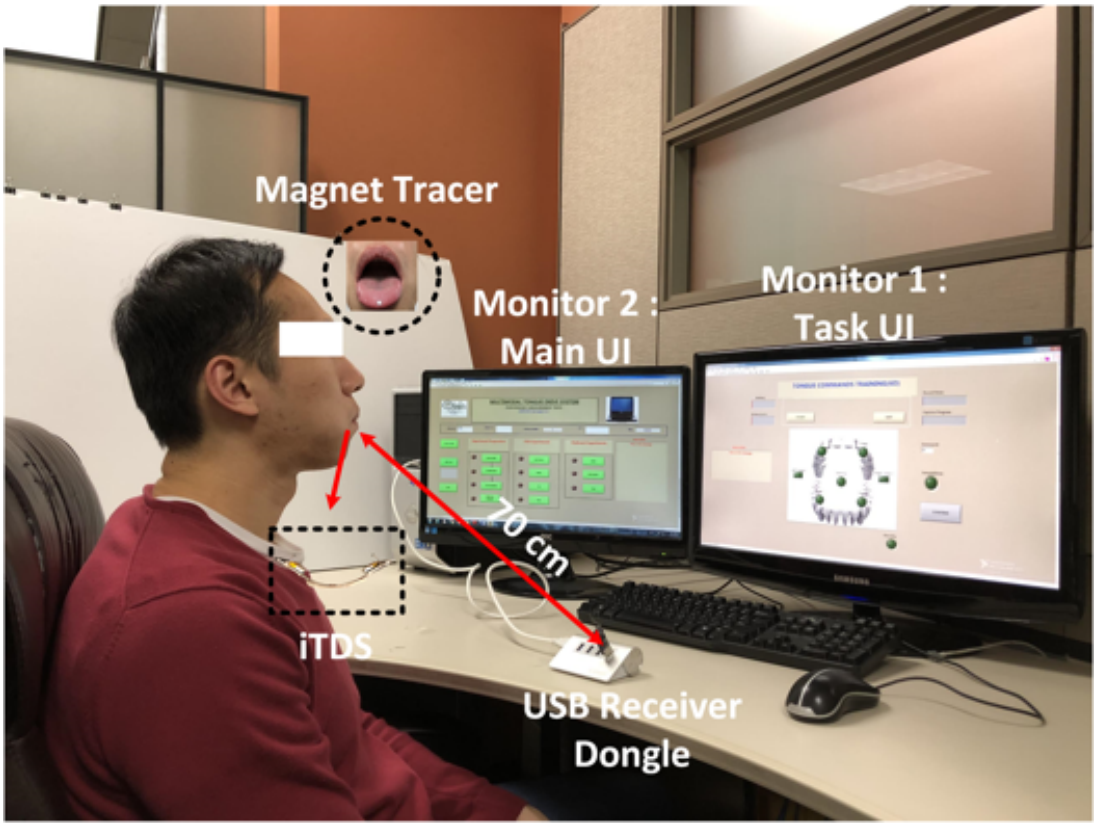

Figure 45 The computer access experimental set up with a subject wearing the iTDS inside the mouth and sitting ~ 70 cm away from the Rx USB dongle (~ 1 m away from the LCD monitor.

$B_{21\times1}$, are transferred to the MCU of iTDS and saved in its flash memory to be utilized later. During the evaluation, which is done in the MCU, the EMF is attenuated using $PL_{4\times3}$ and $PR_{4\times3}$. 6D features, $X_{6\times1}$ are used to find the results from $W_{21\times6}$ and $B_{21\times1}$ matrices using equation (1)

$$res_{21\times1} = W_{21\times6} \times X_{6\times1} - B_{21\times1} \qquad (1)$$

The $res_{21\times1}$ goes through a voting scheme to find the maximum voted class which is considered to be the assigned tongue command by the user. Details regarding the algorithm are presented in [89].

5.4 Experimental Design

The experiment protocol was approved by Georgia Institute of Technology Review Board (IRB). We recruited 4 male able-bodied participants, 2 experienced with eTDS (average 5 hours experienced) and 2 naive. Among the four subjects, one of them is from the authors' group. All subjects completed five sessions in five weeks. The experiment set up is shown in Figure 45. A tiny magnetic tracer (ϕ4.8 mm × 1.5 mm, K&J Magnetics, Jamison, PA) was attached to the tip of the tongue (~ 10 mm) with a cyan acrylic adhesive (3M, St. Paul, MN). The graphical user interface (GUI) of this experiment was implemented in the LabVIEW. All of the experiments were conducted on a desktop PC with two screens, a 22'' LCD monitor (1920 × 1080 pixels) as monitor-1 for the subjects completing the task, monitor-2 for the operator observing the progress of the tasks. The Rx dongle was inserted to the PC, ~ 70 cm away from the subject mouth. At the first session, a 20 s calibration routine was performed by subjects by moving their heads around while keeping the tongue in a stationary position. Once the calibration process was done, seven tongue commands (Left, Right, Up, Down, Left-Select, Right-Select, and Rest) were trained (5 minutes), followed by the model file upload wirelessly. The iTDS was ready to execute after abovementioned steps. The subjects were asked to perform two tasks (Selected Commands and Typing), which took around two hours of total experiment time.

5.4.1 Time Randomly Selected Commands Task

The main purpose of this task is to measure how quickly and accurately a random command can be issued on a visual cue using the iTDS [91]. The participants were asked

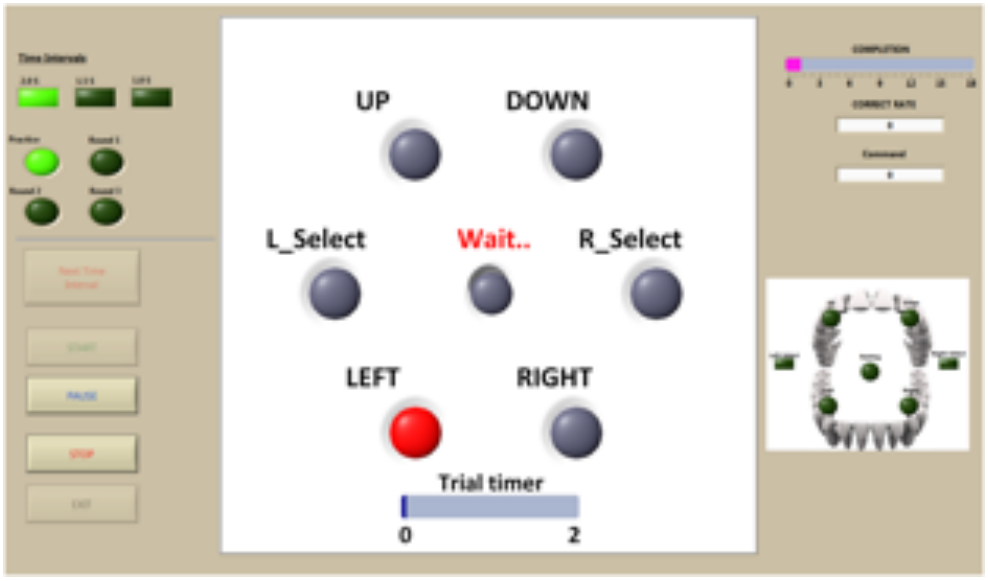

(a)

(b)

Figure 46 GUI screen for timed randomly selected commands task, (a) the stage of showing the random command and preparation and (b) the stage of starting to issue commands.

to issue randomly generated tongue commands that were queued on the GUI which is shown in Figure 46within a given time period, *T*. Three different timeouts (2 s, 1.5 s, and

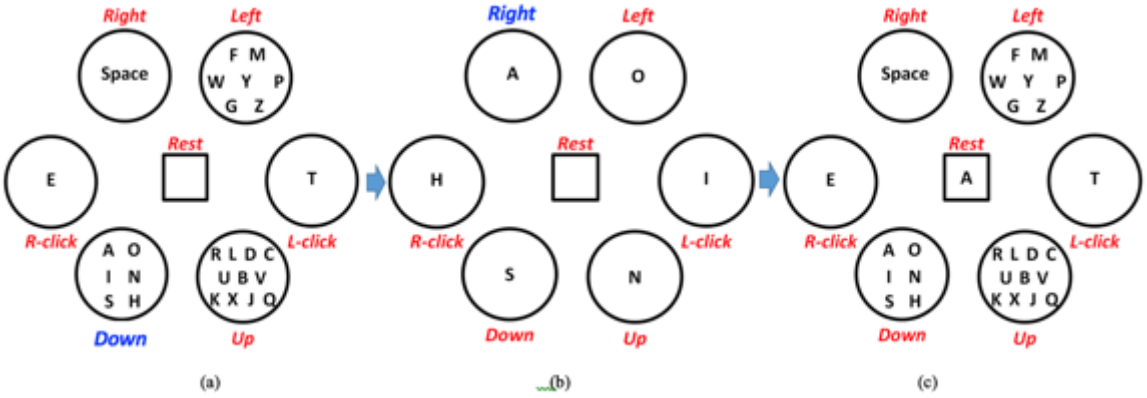

Figure 47 The proposed keyboard layout of iTDS in different stages to type letter A: a) the initial stage, b) after selecting the circle with "Down" command, c) back to initial stage after letter A typed.

1 s) were used as *T*, each with 72 random repetitions. As soon as the next command indicator turns red, the word "Wait" is shown in red on the screen above the center queue (Rest command) for 1 s. Within the 1 s, the participants were able to prepare to move the tongues to the corresponding command position without actually moving the tongue from the "Rest" position. Once the text turned green, saying "Go!", the participants should issue the tongue commands as fast and accurately as possible within the time interval *T*, by reaching the designated command positions that were defined during the training sessions with the tongues.

5.4.2 Text entry task

The idea of the new typing method is to redistribute the letters based on their relative frequencies, which are shown in [92], in English. Less numbers of keystrokes are needed to type frequent letters. We use 6 out of 7 total tongue commands (Rest is not

used to type) as the keystrokes. In this preliminary design, we haven't included punctuations, and the distributions of the letters in the 6 tongue commands are based on the method of constructing the minimum-redundancy code in [93] involving the frequency and probability of individual letter. Each letter will be assigned with a specific code. The codes, which are composed by 6 numbers (1 - 6), are viewed as the 6 tongue commands, also as the keystrokes.

For example, the sequences of typing the letter "A" is shown in Figure 47. The layout of this keyboard is similar to the tongue command structures which are trained at the beginning. Six tongue commands are assigned to each circle, where different number of letters are placed. Fig shows the initial keyboards layout The center square contains the last typed letter. To type letters or switch the layout, the users just simply place their tongues to the corresponding commands. To type letter "A", first, the users need to issue "Down" command, followed by switching to the updated keyboard layout shown in Fig. 7b. In this layout, the letters which are previously in the circle of "Down" command are distributed into each command circle. By issuing the "Right" command, the letter "A" will be typed under the keyboard in Figure 47b. After the letter typed, the layout of the keyboard will be automatically updated to the original one, leaving the letter "A" which is last typed letter in the center. In some scenarios, the users may enter the wrong secondary keyboard by mistake. If it happens, in this design, by leaving the tongue at "Rest" command position 3 s, the keyboard will go back to the initial stage under any other stages. The keystrokes per character (KPSC), which is a common metric for text entry research, is calculated as 1.665 with the method provided in [94].

In the text entry experiment, the reference sentences are randomly picked from the phrase set provided in [95], which contains no punctuation symbols and all lowercase characters. One session of the experiment, designed in LabVIEW environment, has four trials, where the first one is considered as practice. During the task, the subject did not

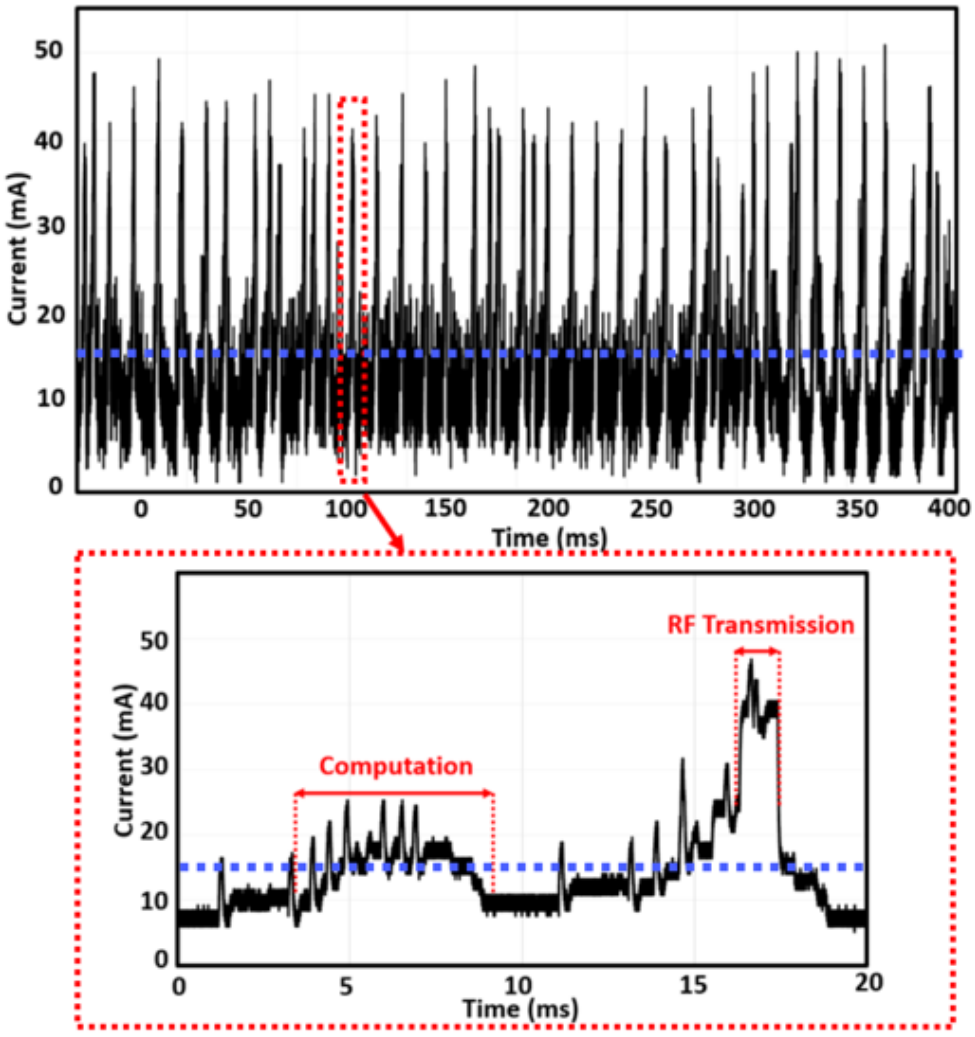

Figure 48 Measured current consumption when the system processes and sends out the tongue commands.

correct their typing errors. The subjects are required to finish total five sessions in five weeks with the proposed typing technique.

5.5 Performance Measures, Results, and Discussions

5.5.1 Stand-alone iTDS Power Consumption

As one of the system performance, the power consumption, which was quantified by obtaining the system total current drawn from the batteries, was measured. By observing the voltage across a 5 Ω resistor, which was series with the batteries, the system total current is able to be computed.

Figure 48 shows the total current when the system is actively sending the tongue commands. The main power consumption during one cycle is the tongue commands computations and RF transmission. Before sending out the tongue commands, the algorithm needs to be run to get sensor data and tongue commands, which takes some of the resources of the MCU, as shown in Figure 48. RF transmission consumes the most of the power since the power amplifier, the most power hungry block, needs to be active. When the system operates, it keeps repeating the cycle that computes and sends out the tongue commands. Based on the data shown in Figure 48, one cycle consumes average 14.2 mA current. A pair of 40 mAh, 3.7 V batteries are used to supply the system. We let the iTDS keeps operating until the batteries are out of power and the duration was recorded. Ten new pairs of batteries were used for this experiment. The average batteries lifetime is 6.01 hours, indicating 13.31 mA average current consumption of the system, which is slightly smaller than the average current in one cycle.

5.5.2 Timed-Randomly Selected Commands

Two performance measures, percentage of correctly completed commands (CCC %) and information transfer rate (ITR) are used in this task for evaluation. ITR presents the rate of information in bits that can be transferred from the users' brain to a computer through a human interface device (HID), which can be calculated with the equation (2)

$$ITR = \frac{1}{T}(\log_2 N) + P\log_2 P + (1-P)\log_2 \frac{1-P}{N-1}, \quad (2)$$

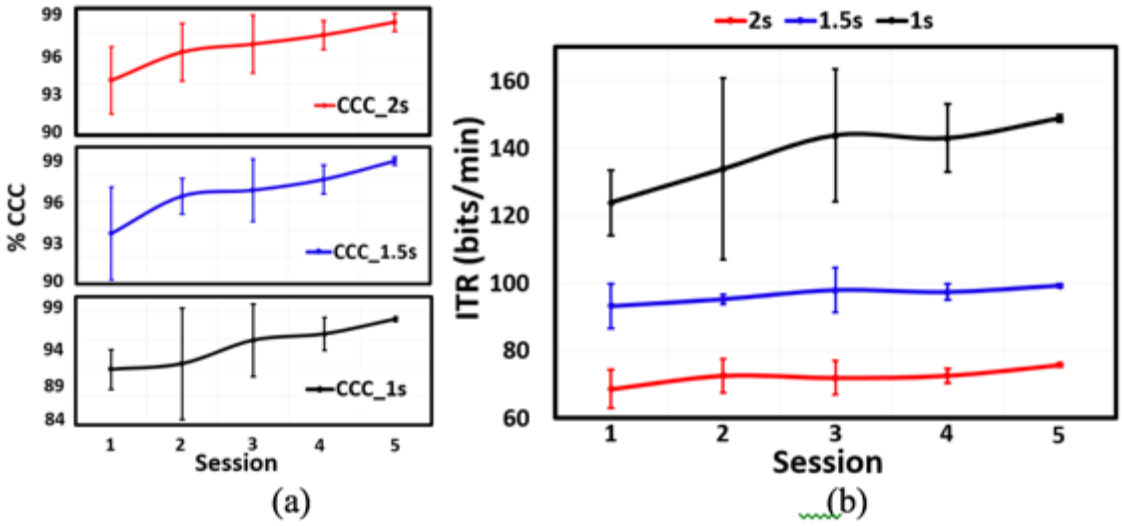

Figure 49 (a) CCC% and (b) ITR results of the timed randomly selected commands task using the standalone iTDS with T = 2 s, 1.5 s, and 1 s.

where N represents the number of simultaneously available commands (N = 6 in this task), P is the CCC % of each trial, and T is the time interval to issue tongue commands. Three participants completed the task of five sessions. Results of this task with its learning ability are shown in Figure 49. It is evident from these graphs that both results of CCC % and ITR are improved and the variations are reduced throughout five sessions, especially for ITR results at small time interval. In the randomly selected tongue commands task, at the first session, the highest ITR was 123.5 ± 9.8 bits/min at T = 1s, which is slightly lower than the results of eTDS. The subjects were not used to the

intraoral devices at the beginning, which may have been initially uncomfortable and slowed usage. Multi-sessions show learning ability by improving the average ITR and reducing its variability among subjects. After the fifth session, the highest ITR had been reached, which is 150.1 ± 1.25 bits/min with CCC = 99.2 % at T = 1s.

5.5.3 Text entry task

In the text entry task, the typing speed and accuracy are the two performance measures that have the greatest interest. Words per minute (*wpm*) is used to quantify the typing speed, which is relative easy to measure [96]. To measure the typing accuracy, we adopted the method presented in [97] by computing the character-level error rate (*ER*) with the following equation:

$$ER = \frac{MSD(SR,\ ST)}{MAL} \times 100\ \%$$

MSD (SR, ST) represents the minimum string distance (*MSD*) between the reference (*SR*) and transcribed text string (*ST*). The MSD between two character strings are defined in terms of editing primitives, which are *insertion*, *deletion*, and *substitution*. Provided two-character strings, the main idea is to find the smallest set of primitives that one can produces another. The *MSD* stands for the number of primitives in the set [96].An algorithm presented in [97] provides the computation of *MSD*. Normally, there are more than one minimum set of transformations from one string to the other given a specific *MSD*. Each transformation is one alignment. *MAL* represents the mean size of alignments which can be calculated based on the algorithm in [97]. Based on the authors' knowledge, not so many ATs research provide the method to calculate the typing error rate. Another

performance measure is the typing throughput (*TP*), measuring the "compensated" words per minute (*cwpm*), by combining the speed and accuracy into a single performance metric [98]. By assuming that one word is composed by five characters in written English, we have the expression from [98]

$$TP = 12\times \frac{(MAL - MSD)^2}{T * MAL}$$

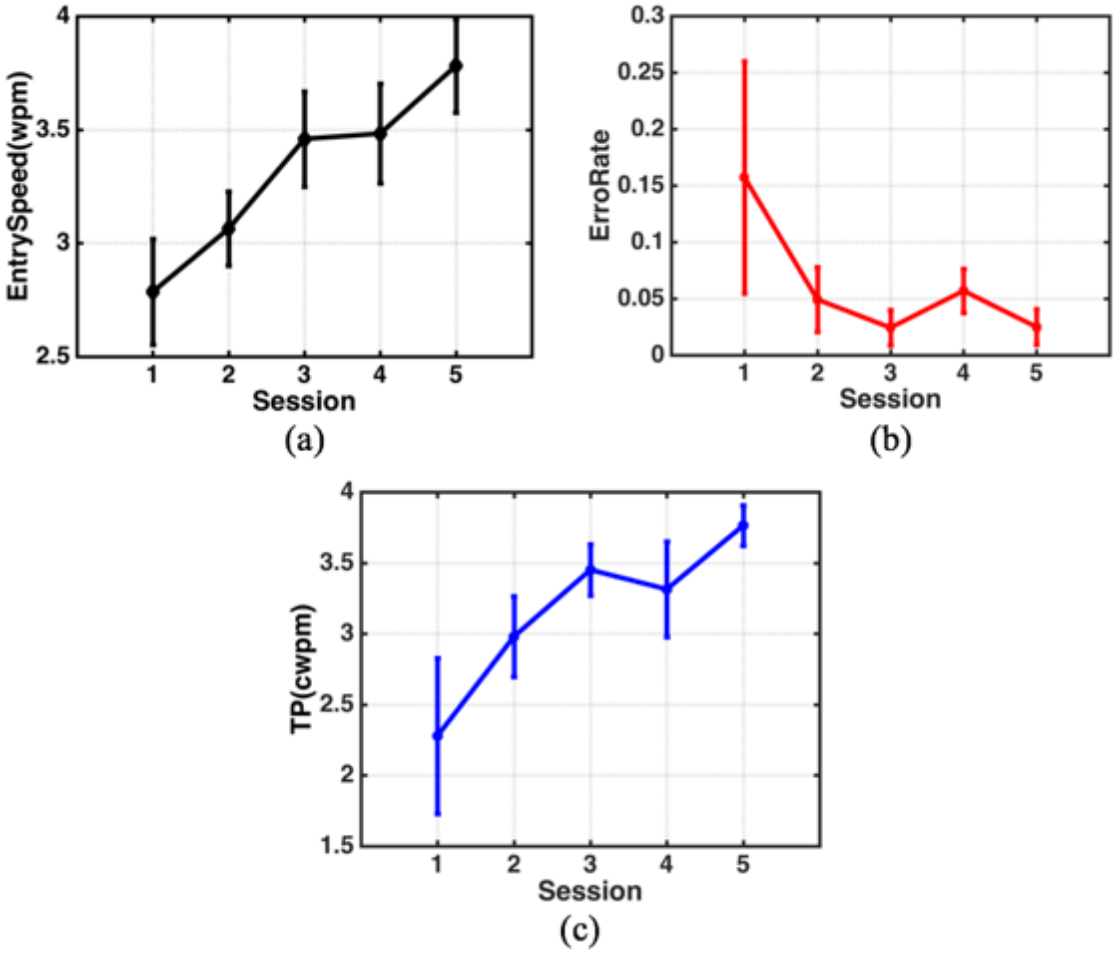

Figure 50 Text entry performance measures over 5 sessions with proposed typing technique in standalone iTDS: (a) Entry speed, (b) Error rate, and (c) Throughput.

T represents the time of typing one complete sentence. The results of all of the performance metrics are shown in Fig. 10. The learning ability of the proposed typing technique is clearly seen based on the presented results over the five sessions.

The goal of the text entry task is to examine the performance of the newly proposed typing technique for the iTDS, also to provide a convenient way for the people with severe disabilities to type efficiently. At the first session, when the subjects were unfamiliar with the typing technique and the device, 16.2 ± 11 % error rate with 2.77 ± 0.25 wpm typing speed and 2.26 ± 0.58 cwpm throughputs were presented. In addition, the first session showed large variances in terms of all of the measurement, indicating the subjects' unfamiliarity of the system and technique. After five sessions which is only 5 hours' experience, all of the performance metrics were improved along with the reduced variations and the learning curve is shown in Fig. 10 for all of the performance metrics. Finally, the typing speed, error rate, and the throughputs reach 3.76 ± 0.25 wpm, 2.23 ± 2.3 %, and 3.74 ± 0.36 cwpm, respectively at the last session. During the experiments, all of the subjects could finish the text entry task within reasonable time. As for the ITCI, it has more than twice commands to select than iTDS in the limited intraoral area. The users can easily forget the commands positions contributing typing error. To use the Head Tracker, the users control their forehead, which is a larger area than tongue, increasing the difficulty to perform accurate control.

5.5.4 Discussion

The main purpose of this work is to present a standalone iTDS prototype, and compare its performance with the other versions of TDS, while observing the learning

process, such as subjects' initial performances, improvement rates, and overall progress through five sessions. Moreover, to assist the end users in typing via iTDS, a new typing method is proposed specific to the iTDS. Unlike the previous versions of TDS, which need to be calibrated and trained at the beginning of every usage session depending on the positioning of the headset, only a one-time training is needed for the standalone iTDS at the first usage. Next time, the user is able to use the device directly without any calibration and training procedures. In addition, by only sending out the tongue commands to the target device (a PC in this case) in a format that the device can easily recognize, as opposed to sending all the raw magnetic sensor data and processing it on

Table 8 – Bench marking typing performance of different assistive technologies computer interface

Interfaces	***Typing Modality***	***Expertise***	***Error Rate***	***Speed (wpm)***
Mouth stick	Mouth	30 hrs	NA	8
Head Tracker	Head	72 hrs	28 %	6.22
Gaze Tracker	Eye	Familiar	NA	5.02
TTK	Tongue	30 hrs	NA	4
ITCI	Tongue	20 hrs	NA	5.6
ITCI	Tongue	53 hrs	0	3.1
TDS	Tongue	Familiar	NA	2.95
mTDS	Speech	2 hrs	NA	107
Standalone iTDS	**Tongue**	**5 hrs**	**2.23 %**	**3.74**

the receiver side, the new iTDS can be universally used with all smart devices, such as smartphones, regardless of their operating system or wireless driver. Compared with eTDS, the new iTDS presents similar ITR and CCC% results with lower standard deviation during the last sessions, when the subjects have gained sufficient experience. Even with 1 s time interval, the subjects were able to reach > 96% accuracy. We hypothesize that the ITR of the iTDS could be significantly higher if smaller time interval had been used.

As a common daily tasks, typing with smart devices through social media or simple texting are very popular methods of communication. However, this is difficult for people with severe physical disabilities. Great effort has been made in today's ATs to provide typing option for the end users, such as eye gaze and voice recognition [99]-[101]. Even though it is simple to type using eye gaze, it suffers from accuracy issues due to interference with vision. Typing with voice recognition is efficient in quiet environments, but it has privacy issues when sensitive information, personal communication, or passwords need to be typed. Considering those issues, we have presented preliminary text entry results using the iTDS and tongue commands, providing acceptable typing speed and low error rate, while protecting the user's privacy. Table 8 compares the typing performance for different ATs. In most of the studies, the typing error rate was not specified, therefore, we use "NA" to present. Even though the typing speed of the standalone iTDS is lower than a mouth stick or head tracker or gaze tracker, it shows sufficient performance within a short learning period. For example, the tongue touch keyboard (TTK) can reach 4 wpm, a result reached after 30 hours of testing **Error! Reference source not found.**. In five hours, participants were able to achieve a

comparable result using the iTDS. Compared to the previous TDS, the new iTDS shows improvement in terms of the typing. Moreover, our system shows a lower error rate compared to all other presented systems. We have also presented the method we used to analyze the typing error rate.

5.6 Summary

We have presented an arch-shaped iTDS in the form of a dental retainer fixed onto the lower teeth. Its electronics are hermetically sealed with dental acrylic and PDMS, and placed in the buccal shelf area of the mouth. The hardware and software design of the iTDS were presented in detail. A custom-designed 2.4 GHz flexible antenna was implemented for the iTDS to establish a robust wireless link with an external Rx. Compared to the previous versions of TDS and iTDS, the stand-alone iTDS is able to detect tongue commands internally send them out to target devices with proper format in real time. With the new algorithm, only one-time training is required instead of performing trainings every time before usage. A new typing technique was proposed for iTDS to enhance the users' ability to access PCs and smartphones. Improved typing speed, error rate, and throughput have achieved compared to other ATs. The standalone iTDS is able to provide an aesthetic solution with better access to the environment for people with tetraplegia. Our future work involves more extensive quantitative performance evaluation of the iTDS in a broader set of widely-accepted human-computer interaction tasks, such as center-out-tapping, maze navigation, and gaming. The users will be asked to speak while doing some of the tasks to compare the performance with no speech interruption. In addition, clinical evaluation of the iTDS with a larger group of potential end users with physical disabilities will be considered.

CHAPTER 6. CONCLUSION AND FUTURE WORK

6.1 Conclusion

In this work, we present a new intra-oral assistive technology, intraoral Tongue Drive System (iTDS), by leveraging the tongue ability of the people with tetraplegia to provide them efficient access to smart phones, computers, and wheelchair. The intra-oral version device not only provides the highest-level privacy for the users, but also the mechanical stability compared with external version of the device. The main tasks of this work are first to present a fully functional device that is able to be used for patients, and second is to provide solutions enhancing the wireless link between the inside mouth device and outside receiver.

In order to establish a very robust wireless communication link, avoiding data packets loss or communication breaking, we first designed a customized intraoral antenna which is able to have high gain. To pick up the best fit antenna solution, three types of antennas (Patch, Dipole, and PIFA) were designed and their performance were compared with the device. The most valuable finding is that patch antenna provides the best performance among all the antennas in terms of gain and directivity. Therefore, the patch antenna was picked up for our system. Another two concerns during the development are the other radio frequencies interfaces and dynamic mouth environment. Both of them adversely affects the quality of the wireless link. Two ASIC were designed to solve these issues by providing multiple transmission bands and dynamic matching components in front of the antenna. The disadvantage of having multiple bands is that the device is able to switch to another relative “clean” band while in the presence of interference. The

dynamic matching components were applied to overcome the dynamic mouth environment. The mouth or tongue movement will change the impedance of the antenna, contributing underside power loss. The matching components are able to match the detuned antenna impedance to the power amplifier, reducing the power loss.

In the end, an advanced signal-processing algorithm was developed to reduce the device power consumption, increasing the battery life time. Another advantages of adopting this algorithm is that the micro-controller unit is able to generate the tongue commands by itself instead of processing it in the PC or other smart devices. By having this, only one training step is required for the users. In the previous versions, every time the users would like to use the device, it is required a 5-min training at the beginning which is tedious and time wasted. This new algorithm is only asked for the users to do one-time training for entire usage, saving the users' effort. In addition to this, the device is able to connect with any other smart devices without any issues since it only sends out the tongue commands, which can be picked up by any smart devices to generate commands accordingly. This new function of the device is validated by a general human computer interaction task with healthy subjects. Moreover, to take advantage of the device most, we proposed a new typing method dedicated for this intraoral tongue controlled assistive technology. Having this typing method, the typing speed goes up and the error rate goes down. At the same time, it is easy for the users to adopt this typing solution.

6.2 Future work

6.2.1 Evaluation: With patients

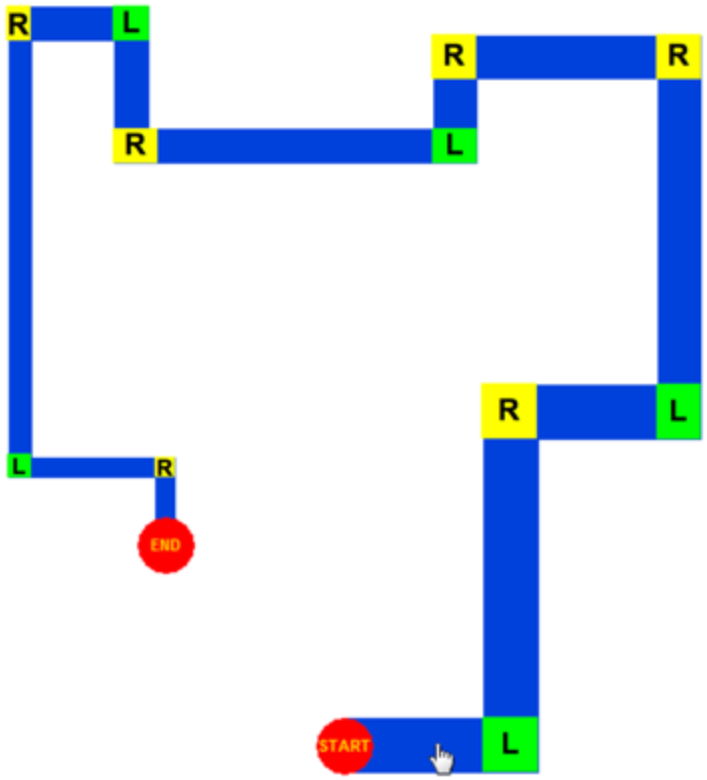

Figure 51 The layout of the maze navigation task on computer screen.

The end users of the device should be the group of people who is with the tetraplegia, it will be more convincing if they are able to test the device and get their performance data. At this point, we don't have any valuable patients' data for our device. Therefore, recording the data from the real end users will definitely provide more accurate evaluation towards the device itself. In addition, having the inputs from the real end users, we can improve our device to the right direction, making it more feasible for the users.

6.2.2 Evaluation: Other human computer interaction tasks

The current evaluation task for the device is only stick to check if the users can issue the correct tongue commands in a certain amount of time. However, there are other

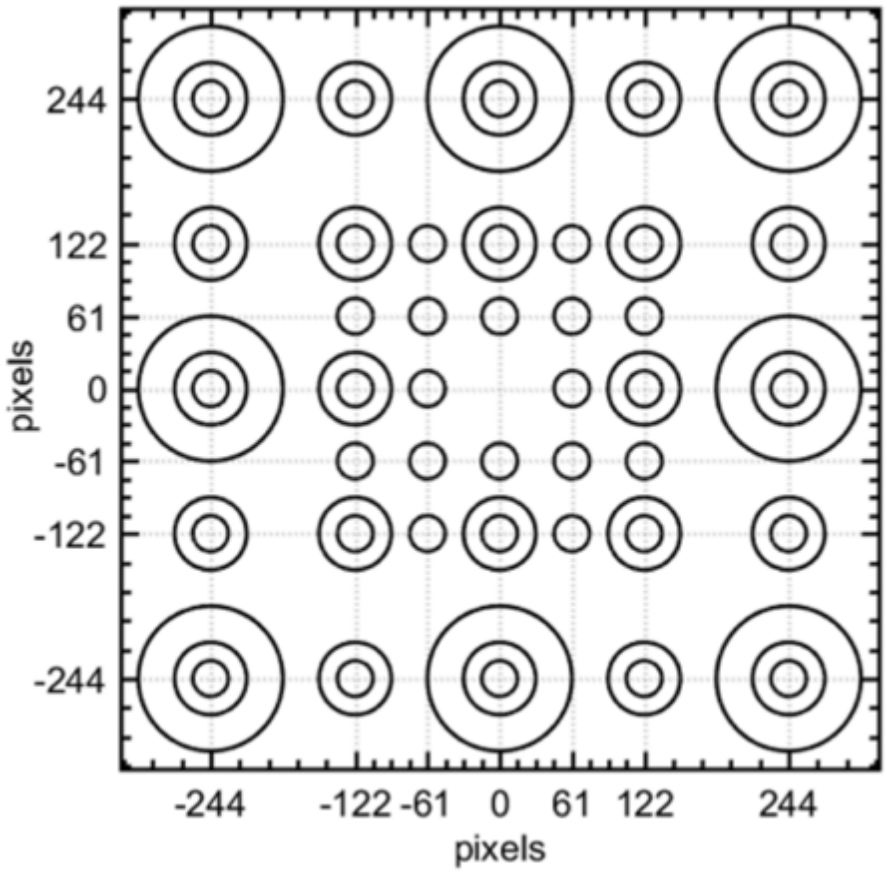

Figure 52 The layout of the center-out tapping task on computer screen.

general tasks that are able to give a better understanding towards the device itself. For example, one of the popular tasks have been used for testing in HCI field is called Maze Navigation task, shown in Figure 51. It is used to evaluate cursor movements within a highly constrained and predefined path using tongue movement. Users moved the cursor from a designated starting point to an endpoint through a maze, trying to stay within the boundaries. The users will be given a time constrained to finish the task within two minutes. If it exceeds the time limitation, the task will stop. The maze throughput combines both speed and accuracy of the input device during cursor navigation in a constrained path. This task also can be used for other devices for comparison.

Another task that can be included is called Center-Out tapping task shown in Figure 52. It is designed to evaluate the performance of pointing devices using Fitts's law. During the tasks, the round targets with different diameters and distances from the center of the screen randomly appeared, one at a time. The subjects will be asked to move the cursor from the center towards the target and click as close as possible to the center of the target. A new random target appeared upon clicking the previous one. Each round includes 48 random targets, which are located either in the cardinal or ordinal direction from the center. This task can be used to quantify information transfer rate from a pointing device to a PC. It is the ratio between the index of difficulty to the average amount of time with the same condition.

6.2.3 Evaluation: Long term study

In our study, the end users performed the study for 5 sessions. It is undoubling that the learning curve can be observed in the most performance metrics. However, we cannot see the saturation of the learning curves. In other words, there should be some scopes to improve those parameters further with more learning/usage. A longer term study will be able to provide better conclusions regarding the device. It can also answer the question that how close the patient can perform using iTDS compared with a person using standard input device, such as keyboard and mouse.

6.3 Publications

Journal publications: (6 total; 4 lead author)

- **F. Kong**, M. N. Sahadat, M. Ghovanloo, and G. D. Durgin, "A Standalone Intraoral Tongue-Controlled Interface for People with Tetraplegia," *IEEE Trans. Biomed. Circuits Syst.,* vol. 13, no. 5, pp. 848-857, Oct. 2019.

- **F. Kong**, M. Ghovanloo, and G. D. Durgin, "An Adaptive Impedance Matching Transmitter for a Wireless Intraoral Tongue-Controlled Assistive Technology," *IEEE Trans. Circuits Syst. II: Express Brief* (Early Acsess)
- **F. Kong**, M. Zada, H. Yoo, and M. Ghovanloo, "Adaptive Matching Transmitter with Dual-Band Antenna for Intraoral Tongue Drive System," *IEEE Trans. Biomed. Circuits Syst*., vol. 12, no. 5, pp. 1279-1288, Dec. 2018.
- **F. Kong,** C. Qi, H. Lee, G. Durgin, and M. Ghovanloo, "Antennas for Intraoral Tongue Drive System at 2.4 GHz: Design, Characterization, and Comparison", *IEEE Trans. Microw. Theory Technology*, vol. 66, no. 5, pp. 2546-2555, May 2018.
- Y. Jia, B. Lee, **F. Kong**, Z. Zhang, M. Connolly, B. Mahmoudi, and M. Ghovanloo, "A Software Defined Radio Receiver for Wireless Recording from Freely Behaving Animal," *IEEE Trans. Biomed. Circuits Syst.,* vol. 13, no. 6, pp. 1645-1654, Dec. 2019.
- Y. Huang**,** L. Zhu**, F. Kong,** C. Cheung, and L. Najafizadeh, "BiCMOS-Based Compensation: Towards Fully Curvature-Corrected Bandgap Reference Circuits," *IEEE TCAS I: Regular Paper*, vol. 65, no. 4, pp. 1210- 1223, Aug. 2017. (Prior to PhD)

Conference publications: (9 total; 5 lead author)

- **F. Kong**, M. N. Sahadat, and M. Ghovanloo, "Development and Preliminary Assessment of an Arch-Shaped Stand-Alone Intraoral Tongue Drive System for People with Tetraplegia," *IEEE Biomedical Circuits and System Conference (BioCAS)*, Cleveland, USA, Oct. 2018.
- M. N. Sahadat, N. Sebkhi, **F. Kong**, and M. Ghovanloo, "Standalone Assistive System to Employ Multiple Remaining Abilities in People with Terapelgia," *IEEE Biomedical Circuits and System Conference (BioCAS)*, Cleveland, USA, Oct. 2018.
- B. Lee, Y. Jia, **F. Kong**, M. Conolly, B. Mahmoudi, and M. Ghovanloo, "Toward a Robust Multi-Antenna Receiver for Wireless Recording from Freely-Behaving Animals," *IEEE Biomedical Circuits and System Conference (BioCAS)*, Cleveland, USA, Oct. 2018.
- **F. Kong,** M. Zada, H. Yoo, M. Ghovanloo, "Triple-Band Transmitter with a Shared Dual-Band Antenna and Adaptive Matching for Intraoral Tongue Drive System.", *IEEE International Symposium on Circuits and System* (*ISCAS*), Florence, Italy, May. 2018.
- **F. Kong**, S. Mirbozorgi, B. Lee, and M. Ghovanloo, "Towards a Robust Data Link for Intraoral Tongue Drive System Using Triple Bands and Adaptive Matching", *IEEE Midwest Symposium on Circuits and System (MWSCAS)*, Boston, USA, Aug. 2017.
- M. Ghovanloo, M.N. Sahadat, Z. Zhang, **F. Kong**, and N. Sebkhi, "Tapping into Tongue Motion to Substitute or Augment Upper Limbs." *SPIE Defense+Security. International Society for Optics and Photonics*, May, 2017.

- Y. Huang, **F. Kong** and L. Najafizadeh, “A Low Drop-out Regulator for Subcutaneous Electrical Stimulation of Nanofibers Used in Muscle Prosthesis,” *IEEE Biomedical Circuits and System Conference (BioCAS)*, Atlanta, USA, Oct. 2015. (Prior to PhD)
- **F. Kong**, Y. Huang and L. Najafizadeh, “A Coil Misalignment Compensation Concept for Wireless Power Transfer Links in Biomedical Implants,” *IEEE Wireless Power Transfer Conference (WPTC), Boulder*, USA, May 2015. (Prior to PhD)
- **F. Kong**, Y. Huang and L. Najafizadeh, “Low-power, Multi-Channel LED Driver for Portable fNIRS Applications,” *IEEE International Conference on Electron Devices and Solid-States Circuits (EDSSC)*, Chengdu, China, June 2014. (Prior to PhD)

APPENDIX A. FIRMWARE DEVELOPMENT OF STANDALONE ITDS

One of the key part of this new stand-alone iTDS is the firmware development since the firmware takes the responsibility of calibration, training, and commands classification. In this appendix, the detailed firmware codes will be presented. At the beginning of the program, the firmware initiated a set of sequences, including clock oscillator, General purpose input/output (GPIO), SPI communications, sleep timers, and the Analog to Digital Converters (ADC). The detailed codes are listed below:

```
#include "per_test_main.h"
#include "iocc2510.h"
#include "sensor.h"
#include "ioCCxx10_bitdef.h"


// Initialization of source buffers and DMA descriptor for
the DMA transfer to sleep register
unsigned        char          __xdata        PM2_BUF[7]        =
{0x06,0x06,0x06,0x06,0x06,0x06,0x04};
unsigned        char          __xdata        dmaDesc[8]        =
{0x00,0x00,0xDF,0xBE,0x00,0x07,0x20,0x42};


UINT8 TimerExpires = 0;
UINT8 TimerCounter = 0;
INT16 Stdby_Upth=2048;                  // Up threshold
INT16 Stdby_Lowth=0;                    // Low threshold
```

```
void delay_us(UINT16 time)
{
  UINT16 i;
  for (i=0;i<time;i++)
  {;}
}
void delay_10us(UINT16 time)
{
  UINT16 i;
  UINT8 j;
  for (i=0;i<time;i++)
  {
    for (j=0;j<12;j++)
    {;}
  }
}
void delay_ms(UINT16 time)
{
  UINT16 i;
  UINT16 j;
  for (i=0;i<time;i++)
  {
    for (j=0;j<895;j++)
    {;}
  }
}
void STInit_IDLE (void) {
  // Set up 1 second sleep timer for IDLE condition
```

```
  UINT16 event0 = 0x041A;       // 1Hz wakeup to blink the
LED or check sensor output.

  WOREVT1 = event0 >> 8;      // Set EVENT0, high byte

  WOREVT0 = event0;           // Set EVENT0, low byte

  WORCTL |= 0x01;

  WORIRQ  |= 0x10;

  EA |= 1;

  STIE |= 1;

}

void init_Timer1(void) {

  // Use the lowest timer clock frequency (1.587kHz) by
setting

  // Both clock divider and timer diver = 128.

  T1CTL = 0x0C;                //suspend the timer 1 and set
divider=128

  T1CNTL = 0x00;              //Clear the counter of timer



  //  T1CC0H = 0xB9;

  //  T1CC0L = 0xF7;             //load the overflow value
for 30s timer

  //  T1CC0H = 0x1E;

  //  T1CC0L = 0xFE;             //load the overflow value
for 5s timer, testing purpose



  T1CC0H = 0x06;

  T1CC0L = 0x32;                  //load for 1s timer to
receive the paramete packet



  TIMIF |= 0x40;

  IEN1 |= 0x02;

}
```

```
void init_Timer1_20ms(void) {

  // Use the lowest timer clock frequency (1.587kHz) by
setting

  // both clock divider and timer diver = 128.

  T1CTL = 0x0C;                //suspend the timer 1 and set
divider=128

  T1CNTL = 0x00;              //Clear the counter of timer

  T1CC0H = 0x0F;

  T1CC0L = 0xDE;               //load the overflow value for
20ms timer

  TIMIF |= 0x40;

  IEN1 |= 0x02;

}


void STInit (void) {

  // UINT16 event0 = 0x0036;    //20 Hz sampling

  //UINT16 event0 = 0x0015;     //50 Hz sampling

  UINT16   event0   =   0x000C;          //90   Hz   sampling
sahadat

  WOREVT1 = event0 >> 8;      // Set EVENT0, high byte

  WOREVT0 = event0;           // Set EVENT0, low byte

  WORCTL |= 0x01;

  WORIRQ  |= 0x10;

  EA |= 1;

  STIE |= 1;

}

void WDTInit(void)

{

  WDCTL = 0x00; // Set 1s timer internal

  WDCTL = 0x08; // Start watchdog
```

```
}
void WDTCLR(void)
{
  WDCTL = 0xA0;
  WDCTL = 0x50; // Clear watchdog counter
}
UINT8 Standby_Check(void)
{
  UINT8 Standby_flag;
  UINT16 X_Sensor;
  UINT16 Y_Sensor;
  UINT16 Z_Sensor;

  // Right back sensor
  X_Sensor = (UINT16)(radioPktBuffer[25]<<8);
  X_Sensor += radioPktBuffer[26];
  Y_Sensor = (UINT16)(radioPktBuffer[27]<<8);
  Y_Sensor += radioPktBuffer[28];
  Z_Sensor = (UINT16)(radioPktBuffer[29]<<8);
  Z_Sensor += radioPktBuffer[30];

  // Left back sensor
  //  X_Sensor = (UINT16)(radioPktBuffer[13]<<8);
  //  X_Sensor += radioPktBuffer[14];
  //  Y_Sensor = (UINT16)(radioPktBuffer[15]<<8);
  //  Y_Sensor += radioPktBuffer[16];
  //  Z_Sensor = (UINT16)(radioPktBuffer[17]<<8);
  //  Z_Sensor += radioPktBuffer[18];
```

```
  Standby_flag                                                    =
(X_Sensor>Stdby_Upth||X_Sensor<Stdby_Lowth)
    || (Y_Sensor>Stdby_Upth||Y_Sensor<Stdby_Lowth) ||
      (Z_Sensor>Stdby_Upth||Z_Sensor<Stdby_Lowth);


  return Standby_flag;
}
void CLK_XOSC(void)
{
  // Power up [HS XOSC] (SLEEP.OSC_PD = 0)
  SLEEP &= ~0x04;
  // Wait until [HS XOSC] is stable (SLEEP.XOSC_STB = 1)
  while ( ! (SLEEP & 0x40) );
  delay_10us(10);
  // Switch system clock source to [HS XOSC] (CLKCON.OSC =
0)
  CLKCON = 0x80;
  // Wait until system clock source has actually changed
(CLKCON.OSC = 0)
  while ( CLKCON & 0x40 );
  // Power down [HS RCOSC] (SLEEP.OSC_PD = 1)
  SLEEP |= 0x04;
}
void CLK_RCOSC(void)
{
  // Power up [HS RCOSC] (SLEEP.OSC_PD = 0)
  SLEEP &= ~0x04;
  // Wait until [HS RCOSC] is stable (SLEEP.HFRC_STB = 1)
  while ( ! (SLEEP & 0x20) );
```

```
  delay_10us(10);

  // Switch system clock source to HS RCOSC (CLKCON.OSC =
1),

  // and set max CPU clock speed (CLKCON.CLKSPD = 1).

  CLKCON = (CLKCON & ~0x07) | 0x40 | 0x01;

  // Wait until system clock source has actually changed
(CLKCON.OSC = 1)

  while ( !(CLKCON & 0x40) );

  // Power down [HS XOSC] (SLEEP.OSC_PD = 1)

  SLEEP |= 0x04;

}

void Enter_PM2(void) //From application notes swra162b
power mode

{

  // Store current DMA channel 0 descriptor and abort any
ongoing transfers,

  // if the channel is in use.

  unsigned char storedDescHigh = DMA0CFGH;

  unsigned char storedDescLow = DMA0CFGL;

  DMAARM |= 0x81;

  // Update descriptor with correct source.

  dmaDesc[0] = (unsigned int)& PM2_BUF >> 8;

  dmaDesc[1] = (unsigned int)& PM2_BUF;

  // Associate the descriptor with DMA channel 0 and arm
the DMA channel

  DMA0CFGH = (unsigned int)&dmaDesc >> 8;

  DMA0CFGL = (unsigned int)&dmaDesc;

  DMAARM = 0x01;


  // NOTE! At this point, make sure all interrupts that
will not be used to
```

```
  // wake from PM are disabled as described in the "Power
Management Control"

  // chapter of the data sheet.

  // The following code is timing critical and should be
done in the

  // order as shown here with no intervening code.

  // Align with positive 32 kHz clock edge as described in
the

  // "Sleep Timer and Power Modes" chapter of the data
sheet.

  char temp = WORTIME0;

  while(temp == WORTIME0);

  // Make sure XOSC is powered down when entering PM{2 - 3}
and that the

  // flash cache is disabled.

  MEMCTR |= 0x02;

  SLEEP = 0x06;

  // Enter power mode as described in chapter "Power
Management Control"

  // in the data sheet. Make sure DMA channel 0 is
triggered just before

  // setting PCON.IDLE.

  asm("NOP");

  asm("NOP");

  asm("NOP");


  if(SLEEP & 0x03)

  {

    asm("MOV 0xD7,#0x01"); // DMAREQ = 0x01;

    asm("NOP"); // Needed to perfectly align the DMA
transfer.

    asm("ORL 0x87,#0x01"); // PCON |= 0x01;

    asm("NOP");
```

```
  } // End of timing critical code

////////////////////////////////////////////////////////////////
/////////////////

  // Enable Flash Cache.

  MEMCTR &= ~0x02;

  // Update DMA channel 0 with original descriptor and arm
channel if it was

  // in use before PM was entered.

  DMA0CFGH = storedDescHigh;

  DMA0CFGL = storedDescLow;

  DMAARM = 0x01;

}
```

Along with the basic initiations, other codes were written to initiate the four magnetic sensors, which are listed as below:

```
#define BATT_VOLT        P0_0       // ADC for the battery
voltage

#define DEN_DCDC       P0_5     // DCDC converter DEN

#define CS1            P1_2     //sensor 1

#define CS2            P2_0     //sensor 2

#define CS6                   P1_0        // sensor LSM9DS1
accelerometer and gyroscope

#define CS5                   P1_1        // sensor LSM9DS1
magnetometer

#define DEN_AG         P0_6     // LSM9D DEN_AG pin

#define SCK            P1_3     // SPI CLK

#define MISO           P1_4     // SPI MISO

#define MOSI           P1_5     // SPI MOSI

#define CS3            P0_3     // sensor 3

#define CS4            P0_4     // sensor 4

#define CS_DISABLED     1
```

```
#define CS_ENABLED      0

#define DISABLED

#define ENABLED      1

#define SPI_BAUD_M  34

#define SPI_BAUD_E  13

void init_Sensor(void) {

  P0SEL &= BIT1 |BIT2 |BIT3 |BIT4 |BIT5;           //set up
general IO

  P1SEL &=  BIT0 | BIT1 | BIT2 | BIT6 | BIT7;     //set up
general IO

  P2SEL &= BIT0;                                    //set up
general IO

  P1SEL = BIT3 | BIT4 | BIT5 ;                          //
peripheral IO pins for SPI

  P0SEL = BIT0;                                         //
Peripheral ADC0

  P0DIR |= BIT1 |BIT2 |BIT3 |BIT4 |BIT5;          // Output
for the sensors chip select

  P1DIR |= BIT0 | BIT1 | BIT2 | BIT6 | BIT7;     // output
for the sensors & LSM9DS1 Chip select

  P2DIR |= BIT0;                                     //Output
for the sensor chip select

}

void InitSensorOutput(void)

{

//  Configure  USART0  for  Alternative  2  =>  Port  P1
(PERCFG.U0CFG = 1).

    PERCFG = 0X01;


// Set USART to SPI mode and Master mode.

    U0CSR &= ~(U0CSR_MODE | U0CSR_SLAVE);


  // Set:
```

```
  // - mantissa value

  // - exponent value

  // - clock phase to be centered on first edge of SCK
period

  // - negative clock polarity (SCK low when idle)

  // - bit order for transfers to LSB first

    U0BAUD =  SPI_BAUD_M;

    U0GCR  =  (U0GCR  &  ~(U0GCR_BAUD_E  |  U0GCR_CPOL  |
U0GCR_CPHA)) | U0GCR_ORDER | SPI_BAUD_E;
```

Once all of the initiations have been done, the iTDS will start talking with the receiver USB dongle. The training matrix will be uploaded to the iTDS for commands processing. The detailed codes are presented below:

```
while(TRUE)

 {

  T1CTL |= 0x02;                                          //
Starts the 1s timer

  FT_flag=0;

  UINT8 ack = 0;


  while (FT_flag == 0)

  {

   CHANNR = CHANNR_HS;

   // Switch to RX mode;

   mode = RADIO_MODE_RX;

   // Set up the DMA to move packet data from radio to
buffer

   dmaRadioSetup(RADIO_MODE_RX);


   IRCON &= ~0x80;                          //clear interrupt
flag
```

```
   WORIRQ &= ~0x01;


   // Start receiving
   DMAARM = DMAARM_CHANNEL0;           // Arm DMA channel 0
   RFST    = STROBE_RX;                   // Switch radio to
RX


   // Wait till either 1s timer is expired or a receive
something.
    while((!TimerExpires)&&(!HS_flag))
    {
      if (pktRcvdFlag) {
        pktRcvdFlag = FALSE;
      //Check if it has received the USB ACK packet
       if((radioPktBuffer[3] == 0xB5) && (radioPktBuffer[4]
== 0x5B))
       {
         ack = 1;                        //Update the ACK.
         FT_flag = 1;                           //Update the
receiving status.
         j=0;
       }
       else
       {
        FT_flag = 1;


        FILE_BUF = radioPktBuffer[3];    //Get the data.
       }
      }
    }
```

```
    TimerExpires = 0;

    DMAARM |= 0x81;                          // Disarm current
DMA channel 0

    RFST = STROBE_IDLE;                       // Switch radio
to IDLE

    delay_ms(1);

    //IF receive a packet which is not he ACK, starts data
tansfer.

    if ((FT_flag == 1) && (ack ==0))

     {

      //set up the packet to transfer the data back for
confirmation.

      radioPktBuffer[0]           =           PACKET_LENGTH;
// Length byte

      radioPktBuffer[1]    =    (BYTE)    (NETWORK_ID_KEY>>8);
// Network identifier

      radioPktBuffer[2] = (BYTE) NETWORK_ID_KEY;

      radioPktBuffer[3] = FILE_BUF+10;


      // Switch to TX mode;

      mode = RADIO_MODE_TX;


      // Set up the DMA to move packet data from buffer to
radio

      dmaRadioSetup(RADIO_MODE_TX);


      // Transmit 5 times

      for (i=0;i<5;i++)

      {

        // Send the packet with old frequency

        DMAARM |= DMAARM_CHANNEL0;  // Arm DMA channel 0

        RFST = STROBE_TX;           // Switch radio to TX
```

```
        while(!pktSentFlag);
        pktSentFlag = FALSE;
      }
      if (!(FILE_BUF == 0))          //Store the data if it
equals to the header. It can be changed customized.
      {                              // This is for storing
the correct data.
       FILE_Store[j] = FILE_BUF;
       j++;
      }
      if(j>=DATA_LENGTH)
      {
        j=0;
      }

      // Update the parameter
      // Update standby threshold (0-1024)
      Standby_TH =  (radioPktBuffer[5]<<8)+radioPktBuffer[6];
      Stdby_Upth = 2048 + Standby_TH;
      Stdby_Lowth = 2048 - Standby_TH;

      CHANNR_TX = radioPktBuffer[7];

    }
  }
  //If it receives USB ACK packet, it will move to this
loop and send its own ACK packet back.
  while(ack == 1)
   {
```

```
    DMAARM |= 0x81;                          // Disarm current
DMA channel 0

    RFST = STROBE_IDLE;                       // Switch radio
to IDLE

    delay_ms(1);

    //Tx mode

    mode = RADIO_MODE_TX;

    dmaRadioSetup(RADIO_MODE_TX);

    //Set up its own ACK Packet.

    radioPktBuffer[0] = PACKET_LENGTH;                    //
Length byte

    radioPktBuffer[1] = (BYTE) (NETWORK_ID_KEY>>8);       //
Network identifier

    radioPktBuffer[2] = (BYTE) NETWORK_ID_KEY;

    radioPktBuffer[3] = 0xA0;

    radioPktBuffer[4] = 0x0A;

    //send this packet 5 times.

    for (i=0;i<5;i++)

     {

       // Send the packet with old frequency

       DMAARM |= DMAARM_CHANNEL0;  // Arm DMA channel 0

       RFST = STROBE_TX;           // Switch radio to TX

       while(!pktSentFlag);

       pktSentFlag = FALSE;

     }

     ack = 0;                     // update ACK parameter

   }

  FT_flag = 0;                        //Update packet revceive
parameter.

 }

}
```

At last, the voting mechanism, which is the algorithm used to generate tongue commands is also presented here:

```
uint8 vote (float *dec_values)
{
        uint8 i = 0;
        uint8 j = 0;
        uint8 nr_class = 7;
       // uint8 p = 0;
        uint8 vote[7] = {0};
        uint8 vote_max_idx = 0;
                //for(i=1;i<nr_class;i++)

 /*       for(i=0;i<nr_class;i++)
        {
            vote[i] = 0;
        }

   */
        for(i=0;i<nr_class;i++)
        {
            for( j=i+1;j<nr_class;j++)
            {

                if( *(dec_values) > 0)
                {
                    ++vote[i];
```

```
                }
                else
                {
                    ++vote[j];
                }
                dec_values++;
            }
        }


        for(i=1;i<nr_class;i++)
        {
            if(vote[i] > vote[vote_max_idx])
            {
                vote_max_idx = i;
            }
        }

        return vote_max_idx;

}
```

REFERENCES

[1] Model System Knowledge Translation Center, "SCI factsheet booklet edition 3 final," [Online document], 2016. Available: http://www.msktc.org/lib/docs/Booklet.

[2] R. Barea, L. Boquete, and M. Mazo, "System for assisted mobility using eye movements based on electrooculography," *IEEE Trans. Neural Syst Rehabil Eng*., vol. 10, no. 4, pp. 209-218, Dec. 2002

[3] J. R. Wolpaw, N. Birbaumer, D. J. McFarland, G. Pfurtscheller, and T. M. Vaughan, "Brain-computer interfaces for communication and control," *Clin. Neurophysiol*, vol. 113, pp. 767–791, Jun. 2002.

[4] M. R.Williams and R. F. Kirsch, "Evaluation of head orientation and neck muscle EMG signals as command inputs to a human-computer interface for individuals with high tetraplegia," *IEEE Trans. Neural Syst. Rehabil. Eng*., vol. 16, no. 5, pp. 485–496, Oct. 2008.

[5] Adaptive Switch Labs, Inc. [Online]. Available: http://www.asl-inc. com/catalog

[6] NaturalPoint, Inc. [Online]. Available: http://www.naturalpoint.com/ smartnav.

[7] Origin Instrument: Sip/Puff Switch [Online]. Available: http://www. orin.com/access/sip_puff/index.htm.

[8] L. R. Hochberg et al., "Neuronal ensemble control of prosthetic devices by a human with tetraplegia," *Nature*, vol. 442, no. 7099, pp. 164–171, Jul. 2006.

[9] J. Donoghue, "Bridging the brain to the world: A perspective on neural interface systems," *Neuron*, vol. 60, no. 3, pp. 511–521, Jul. 2008.

[10] C. Choi, S. Micera, J. Carpaneto, and J. Kim, "Development and quantitative performance evaluation of a noninvasive EMG computer interface," *IEEE Trans. Biomed. Eng*., vol. 56, no. 1, pp. 188–191, Jan. 2009.

[11] M. R. Ahsan, M. I. Ibrahimy, and O. O. Khalifa, "EMG signal classi- fication for human computer interaction: A review," *Eur. J. Sci. Res*., vol. 33, no. 3, pp. 480–501, 2009.

[12] C. M. Karat, C. Halverson, D. Horn, and J. Karat, “Patterns of entry and correction in large vocabulary continuous speech recognition systems,” in *Proc. SIGCHI Conf. Human Factors Comput. Syst*., pp. 568–575, 1999.

[13] S. Harada, J. A. Landay, J. Malkin, X. Li, and J. A. Bilmes, “The vocal joystick: Evaluation of voice-based cursor control techniques,” in *Proc. Int. ACM SIGACCESS Conf. Comput. Accessibil*., pp. 197–204, Oct.2006.

[14] A. Acero, L. Deng, T. T. Kristjansson, and J. Zhang, “HMM adaptation using vector Taylor series for noisy speech recognition,” *in Proc. INTERSPEECH*, pp. 869–872, Oct. 2000.

[15] X. Huo, M. Ghovanloo, "Tongue Drive: a wireless tongue-operated means for people with severe disabilities to communicate their intentions," *IEEE Comm Mag*, vol. 50, no. 10, pp. 128-135, Oct. 2012.

[16] J. Kim, H. Park, et al., “Tongue enables computer and wheelchair access for the people with high-level disabilities,” *Sci Translat. Med*, vol. 5, no.21 3, pp. 213ra166, Nov. 2013.

[17] E. R. Kandel, J. H. Schwartz, and T. M. Jessell, *Principles of Neural Science*, 4th ed. New York: McGraw-Hill Medical, 2000.

[18] M. Liancai, and I. Sanders. "Human tongue neuroanatomy: nerve supply and motor endplates." *Clinical Anatomy,* vol. 23, no. 7, pp. 777-791, Oct. 2010.

[19] H. Park, J. Kim, and M. Ghovanloo, “Development and preliminary evaluation of an intraoal tongue drive system,” in *Proc. IEEE 34th Conf. Eng. Med. Biol. Soc*., pp. 1157-1160, Aug. 2012.

[20] J. Kim *et al*. “Qualitative assessment of tongue drive system by people with high-level spinal cord injury,” *J. Rehabil. Res. Develop*., vol. 51, no. 3, pp. 451-466, Jun. 2014.

[21] L. N. S. A. Struijk, “An inductive tongue computer interface for control of computers and assistive devices,” *IEEE Transactions on Biomedical Engineering*, vol. 53, no. 12, Dec. 2006.

[22] Y. Lee, et.al, “Wireless, intraoral hybrid electronics for real-time quantification of sodium intake toward hypertension management,” *Proceedings of National Academy of Sciences of the United States of America*, May. 2018.

[23] This smart mouthguard can monior concussions, Online: https://www.wired.com/story/this-smart-mouthguard-can-monitor-concussions/.

[24] Mouth devices for sleep apnea, Online: https://www.webmd.com/sleep-disorders/sleep-apnea/mouth-devices-for-sleep-apnea#1

[25] H. Xueliang, W. Jia and M. Ghovanloo, "Introduction and preliminary evaluation of the tongue drive system: wireless tongue-operated assistive technology for people with little or no upper-limb function," *Journal of rehabilitation research and development,* vol. 45, no. 6, p. 921, 2008

[26] X. Huo, J. Wang, and M. Ghovanloo, "A magneto-inductive sensor based wireless tongue-computer interface," *IEEE transactions on neural systems and rehabilitation engineering,* vol. 16, pp. 497-504, 2008.

[27] J. Kim, X. Huo, and M. Ghovanloo, "Wireless control of smartphones with tongue motion using tongue drive assistive technology," in *Engineering in Medicine and Biology Society (EMBC), 2010 Annual International Conference of the IEEE*, 2010, pp. 5250-5253.

[28] X. Huo, J. Wang, and M. Ghovanloo, "A wireless tongue-computer interface using stereo differential magnetic field measurement," in *Engineering in Medicine and Biology Society, 2007. EMBS 2007. 29th Annual International Conference of the IEEE*, 2007, pp. 5723-5726.

[29] X. Huo, J. Wang, and M. Ghovanloo, "A magnetic wireless tongue-computer interface," in *Neural Engineering, 2007. CNE'07. 3rd International IEEE/EMBS Conference on*, 2007, pp. 322-326.

[30] L. N. A. Struijk, E. R. Lontis, B. Bentsen, H. V. Christensen, H. A. Caltenco, and M. E. Lund, "Fully integrated wireless inductive tongue computer interface for disabled people," in *Engineering in Medicine and Biology Society, 2009. EMBC 2009. Annual International Conference of the IEEE*, 2009, pp. 547-550.

[31] E. R. Lontis, M. E. Lund, H. V. Christensen, B. Bentsen, M. Gaihede, H. A. Caltenco, and L. N. A. Struijk, "Clinical evaluation of wireless inductive tongue computer interface for control of computers and assistive devices," in *Engineering in Medicine and Biology Society (EMBC), 2010 Annual International Conference of the IEEE*, 2010, pp. 3365-3368.

[32] M. E. Lund, H. V. Christiensen, H. A. Caltenco, E. R. Lontis, B. Bentsen, and L. N. A. Struijk, "Inductive tongue control of powered wheelchairs," in *Engineering in Medicine and Biology Society (EMBC), 2010 Annual International Conference of the IEEE*, 2010, pp. 3361-3364.

[33] L. NS Andreasen Struijk, E. R. Lontis, M. Gaihede, H. A. Caltenco, M. E. Lund, H. Schioeler, and B. Bentsen, "Development and functional demonstration of a wireless intraoral inductive tongue computer interface for severely disabled persons," *Disability and Rehabilitation: Assistive Technology,* pp. 1-10, 2016.

[34] D. Fortune, J. E. Ortiz, and H. N. Tran, "Tongue activated communications controller," ed: Google Patents, 1996.

[35] T. T. Keypad, "newAbilities Systems Inc," Santa Clara, CA, available online www. newabilities. com.

[36] Saponas, T. Scott, Daniel Kelly, Babak A. Parviz, and Desney S. Tan. "Optically sensing tongue gestures for computer input." In *Proceedings of the 22nd annual ACM symposium on User interface software and technology*, pp. 177-180. ACM, 2009.

[37] Nutt, Wolfgang, et al. "Tongue-mouse for quadriplegics." *Journal of Micromechanics and Microengineering* 8.2 (1998): 155.

[38] Salem, Chris, and Shumin Zhai. "An isometric tongue pointing device." *Proceedings of the ACM SIGCHI Conference on Human factors in computing systems*. ACM, 1997.

[39] R. Chandra and A. J. Johansson, “In-mouth antenna for tongue con- trolled wireless devices: Characteristics and link-loss,” in *Proc. IEEE 33rd Conf. Eng. Med. Biol. Soc.*, pp. 5598–5601, Aug. 2011.

[40] R. Chandra and A. J. Johansson. "Antennas and propagation for in-mouth tongue-controlled devices in wireless body area networks." *IEEE Antennas and Wireless Propag. Lett.* vol. 14, pp. 1518-1521, Oct. 2014.

[41] Z. Yang and S. Xiao. "A single-fed miniaturized circularly polarized implantable antenna for ISM band biomedical application." *in Proc. IEEE MTT-S int. Microw. Workshop*., Oct. 2016.

[42] H. Park, and M. Ghovanloo. "Wireless communication of intraoral devices and its optimal frequency selection." *IEEE Trans. Microw. Theory Tech.*, vol. 62, no. 12, pp. 3205-3215, Dec. 2014.

[43] M. Song, C. Lu, A. Ba, X. Wang, Y. Liu, K. Shibata, C. Bachmann, and K. Philips, “An energy-efficient antenna impedance detection using electrical balance for single-step on-chip tunable matching in wearable/implantable applications,” *IEEE Trans. Biomed. Circuits Syst.,* vol. 11, no. 6, pp. 1236-1244, Dec. 2017.

[44] Y. Yoon, H. Kim, H. Kim, K. Lee, C. Lee, and J.S. Kenny, “A 2.4 GHz CMOS power amplifier with an integrated antenna impedance mismatch correction system,” *IEEE J. Solid-State Circuits*, vol. 49, no. 3, pp. 608-620, March 2014.

[45] H. Park, and M. Ghovanloo. "An arch-shaped intraoral Tongue Drive System with built-in tongue-computer interfacing SoC." *Sensors*, vol 14, no. 11, pp 21565-21587, Nov. 2014.

[46] A. Laumann, J. Holbrook, J. Minocha, D. Rowles, B. Nardone, D. West, J. Kim, J. Bruce, E.J. Roth, and M. Ghovanloo, “Safety and efficacy of medically performed tongue piercing in people with tetraplegia for use with tongue-operated assistive technology,” *Topics in Spinal Cord Injury Rehabilitation*, vol. 21, no. 1, pp. 61-76, Feb. 2015.

[47] Y. Behnaz, X. Huo, and M. Ghovanloo. "Preliminary assessment of Tongue Drive System in medium term usage for computer access and wheelchair control." in *Proc. IEEE 33rd Conf. Eng. Med. Biol. Soc.*, pp. 5766–5769, Aug. 2011.

[48] E. R. Kandel, J. H. Schwartz, and T. M. Jessell, *Principles of Neural Science*, 4th ed. New York: McGraw-Hill Medical, 2000.

[49] M. Liancai, and I. Sanders. "Human tongue neuroanatomy: nerve supply and motor endplates." *Clinical Anatomy,* vol. 23, no. 7, pp. 777-791, Oct. 2010.

[50] M. N. Sahadat, A. Alreja, P. Srikrishnan, and M. Ghovanloo, “A multimodal human computer interface combining head movement, speech and tongue motion for people with severe disabilities.” *IEEE Biomed. Circ. Sys. Conf*., pp.1-4, Oct. 2015.

[51] H. Park, et al., "A wireless magnetoresistive sensing system for an intraoral tongue-computer interface." *IEEE Trans. Biomed. Circuits Syst.,* vol. 6, no. 6, pp. 571-585, Dec.2012.

[52] H. Park, and M. Ghovanloo. "An arch-shaped intraoral Tongue Drive System with built-in tongue-computer interfacing SoC." *Sensors*, vol 14, no. 11, pp 21565-21587, Nov. 2014.

[53] M. Giraldi. "Independence day: Tongue-touch controls give Ben a more satisfying self-sufficient lifestyle." *Teamrehab Rep. Mag,* pp. 1417, 1997.

[54] J. Daniel, C. Cipriani, D. B. Popovic, and L. N. S. A. Struijk "Control of a robotic hand using a tongue control system-a prosthesis application." *IEEE Trans. Biomed Eng.*, vol 63, no. 7, pp. 1368-1376, July 2016.

[55] Q. Peng and T. F. Budinger, “ZigBee-based wireless intra-oral control system for quadriplegic patients,” in *Proc. Int. Conf. Eng. Med. Bio. Soc*., pp. 1647–1650, Aug. 2007.

[56] C. Lau and S. O’Leary, “Comparison of computer interface devices for persons with severe physical disabilities,” *Amer. J. Occupat. Therapy*, vol. 47, pp. 1022–1030, Nov. 1993.

[57] M. Kuribayashi, Y. Kitasako, K. Matin, A. Sadr, K. Shida, and J. Tagami, “Intraoral pH measurement of carious lesions with qPCR of cariogenic bacteria to differentiate caries activity,” *J. Dentistry*, vol. 40, pp. 222–228, Dec. 2011.

[58] L. N. S. A. Struijk, E. R. Lontisand, B. Bentsen, H. V. Christensen, H. A. Caltenco, and M. E. Lund, “Fully integrated wireless inductive tongue computer interface for disabled people,” in *Proc. IEEE 31st Conf. Eng. Med. Biol. Soc*., pp. 547–550, Sep. 2009.

[59] Z. Yang and S. Xiao. "A single-fed miniaturized circularly polarized implantable antenna for ISM band biomedical application." *in Proc. IEEE MTT-S int. Microw. Workshop*., Oct. 2016.

[60] M. Francesco, L. Bolomey, and J. Zurcher, "Design, realization and measurements of a miniature antenna for implantable wireless communication systems." *IEEE Trans. Antenna Propag.* vol 59, no. 10, pp. 3544-3555, Oct. 2011.

[61] F. Merli, L. Bolomey, E. Meurville, and A. K. Skrivervik, “Implanted antenna for biomedical applications,” in *IEEE Antennas Propag. Soc. Int. Symp*., pp. 1–4, 2008.

[62] Molex, “Product specifications of the 0.5 mm center FFC jumper cable,” FFC Jumper Cable datasheet, Sept. 2010 [Revised April 2014].

[63] Hirose Electric, “Ultra small surface mount coaxial connectors”, U.FL-R-SMT-1 datasheet, Feb. 2008.

[64] A. O. Rahn, J. R. Ivanhoe, and K. D. Plummer, “*Textbook of complete dentures*”, 6th ed. Shelton, Connecticut, People’s Medical Publishing House. 2009.

[65] S. A. Fernandes, F. Vellini-Ferreira, H. Scavone-Junior, and R. I. Ferreira, “Crown dimensions and proximal enamel thickness of mandibular second bicuspids”, *Braz. Oral Res*, vol. 25, pp.324-440, July, 2011.

[66] T. Miyabara, “An anthropological study of the masticatory system in the Japanese: The teeth”. *Dent. Cosmo* vol. *58*, pp. 739–749, July, 1916.

[67] J. He, T. Chou, H. Chang, J. Chen, Y. Yang, and D. Moore, "Predictable reproduction of the buccal shelf area in mandibular dentures." *Int. J. Prosthodont*. Vol. 20, pp. 535-537, Sept. 2007.

[68] B.M. Zide. "The mentalis muscle: an essential component of chin and lower lip position." *Plastic and reconstructive surgery,* vol. 105, no. 3, pp. 1213-1215, March, 2000.

[69] Rogers Corporation, "RO3000® Series Circuit Materials", RO3000 Laminate datasheet, 2015.

[70] A. K. Bhattacharyya, "Long rectangular patch antenna with a single feed." *IEEE Trans. Antenna Propag.* vol 38, no. 7, pp. 987-993, July 1990.

[71] J. Liu, and Q. Xue, "Broadband long rectangular patch antenna with high gain and vertical polarization" *IEEE Trans. Antenna Propag.* vol 61, no. 2, pp. 539-546, Oct. 2012.

[72] C. A. Balanis, "*Antenna theory: analysis and design*." 4th ed. Hoboken, New Jersey, John Wiley & Sons. 2016.

[73] F. Merli, L. Bolomey, J. Zürcher, G. Corradini, E. Meurville, and A. K. Skrivervik, "Design, realization and measurements of a miniature antenna for implantable wireless communication systems," *IEEE Trans. Antennas Propag*, vol. 59, no. 10, pp. 3544-3555, Oct. 2011.

[74] C. Liu, Y. Guo, and S. Xiao. "Capacitively loaded circularly polarized implantable patch antenna for ISM band biomedical applications." *IEEE Trans. Antenna Propag.* vol. 62, no. 5, pp. 2407-2417, May. 2014.

[75] Texas Instruments, "SmartRF Studio 7 Overview", [Online], 2010. Available: http:\\ www.ti.com/lit/ug/swru195b.

[76] Texas Instruments, "CC debugger User's Guide," [Online], 2014. Available: http:\\ www.ti.com/lit/ug/swru197h.

[77] F. Kong, C. Qi, H. Lee, G. D. Durgin, and M. Ghovanloo, "Antennas for intraoral Tongue Drive System at 2.4 GHz: design, characterization, and comparison," *IEEE Trans. Microw. Theory Tech.*, vol. 66, no. 5, pp. 2546-2555, May 2018.

[78] Federal Communications Commision, "FCC online table of frequency allocations," [Online]. Available: https://transition.fcc.gov/oet/spectrum/table/fcctable.pdf.

[79] Internationl Commision on Non-Ionizing Radiation Protection, “Guidelines for limiting exposure to time-varying electric, magnetic, and electromagnetic fields,” *Health Phys*., vol. 74, pp. 494-5229, 1998.

[80] Y. Yoon, H. Kim, H. Kim, K. Lee, C. Lee, and J.S. Kenny, “A 2.4 GHz CMOS power amplifier with an integrated antenna impedance mismatch correction system,” *IEEE J. Solid-State Circuits*, vol. 49, no. 3, pp. 608-620, March 2014.

[81] P. Sjoblom and S. Henrik, “An adaptive impedance tuning CMOS circuit for ISM 2.4-GHz band,” *IEEE Trans. Circ. Sys. I: Regular Papers* , vol. 52, no. 6, pp.1115-1124, Jun. 2005.

[82] Texas Instruments, “Mixed signal microcontroller,” MSP430 datasheet, May 2013.

[83] S. A. A. Shah and H. Yoo, “Scalp-implantable antenna system for intracranial pressure monitoring, ” *IEEE Trans. Antennas Propag.*, vol. 66, no. 4, pp. 2170-2173, April 2018.

[84] F. Kong, S. A. Mirbozorgi, B. Lee, and M. Ghovanloo, “Towards a robust data link for intraoral Tongue Drive System using triple bands and adaptive matching,” *IEEE Int. Midwest Symp. Circuits Syst.,* pp. 491-494, Aug. 2017.

[85] I. Gani and H. Yoo, “Multi-frequency antenna system for skin implant,” *IEEE Microw. Wireless Compon. Lett.*, vol. 26, no. 4, pp. 294-296, April 2016.

[86] Linx Technology, “ANT-433-MHW-xxx-x,” ANT-433-MHW-SMA-S datasheet, March 2013.

[87] RF Solutions, “Stubby Quad Band Antenna GSM +4dB,” ANT-GSMSTUB4 datasheet.

[88] M. N. Sahadat, N. Sebkhi, D. Anderson and M. Ghovanloo, "Optimization of Tongue Gesture Processing Algorithm for Standalone Multimodal Tongue Drive System," in *IEEE Sensors Journal.*

[89] M. N. Sahadat, N. Sebhki, and M. Ghovanloo, “Simultaneous multimodal access to wheelchair and computer for people with tetraplegia,” in *Proc. 20th ACM International Conference on Multimodal Interaction*, pp. 393-399, Oct. 2018.

[90] C.-C. Chang and C.-J. Lin, "LIBSVM: a library for support vector machines," *ACM transactions on intelligent systems and technology (TIST),* vol. 2, p. 27, 2011.

[91] B. Yousefi, X. Huo, J. Kim, E. Veledar, and M. Ghovanloo, "Quantative anc comparative assessment of learning in a tongue-opreated computer input device-part II: navigation tasks," *IEEE Trans. Inf. Technol. Biomed*., vol.14, no. 4, pp. 633-643, July. 2012.

[92] I. S. Mackenzie, R. W. Soukoreff, and J. Helga, "1 thumb, 4 buttons, 20 words per minute: design and evaluation of H4-writer," in *Proc. 24th annual ACM symposium on User Interface software and technology*, pp. 471-480, Oct. 2011.

[93] D. A. Huffman, "A method for the construction of minimum-redundancy codes," in *Proc. of the IRE*, pp. 1098-1101, 1952.

[94] I. S. Mackenzie, "KPSC (keystrokes per character) as a characteristic of text entry techniques," in *Proc. of the 4th International Symposium of Human-Computer Interaction with Mobile Devices*, pp. 195-210, 2002.

[95] I. S. Mackenzie and R. W. Soukoreff, "Phrase sets for evaluating text entry techniques." in Proc. *extended abstracts on Human Factors in Computing Systems*, pp. 754-755, Apr. 2003.

[96] R. W. Soukoreff, "Measuring errors in text entry tasks: an application of the levenshtein string distance statistic," in *Proc. extended abstracts on Human Factors in Computing Systems*, pp. 319-320, Apr. 2001.

[97] I. S. Mackenzie and R. W. Soukoreff, "A character-level error analysis technique for evaluating text entry methods," in *Proc. second Nordic conference on Human-computer interaction*, pp. 243-246, Oct. 2002.

[98] H. A. Caltenco, B. Breidegard, and L. N. S. A. Struijk, "On the tip of the tongue: learning typing and pointing with an intra-oral computer interface," *Disability and Rehabilitation: Assistive Technology*, vol. 9, no. 4, pp. 307-317, 2014.

[99] S. Anelis, A. Malek, C. Mercedes, A. Melvin, and B. Armando, "Adaptive eye-gaze tracking using neural-network-based user profiles to assist people with motor disability," *J. Rehabil. Res. Dev*., vol. 45, pp. 801-817, Apr. 2008.

[100] Z. Zhu and Q. Ji, "Novel eys gaze tracking techniques under natural head movement," *IEEE Trans. Biomed. Eng*., vol. 54, no. 12, pp. 2246-2260, Dec. 2007.

[101] S. Harada, J. A. Landay, J. Malkin, X. Li, and J. A. Bilmes, "The vocal joystick: Evaluation of voice-based cursor control techniques for assistive technology," *Disability Rehabil. Assistive Technol*., vol. 3, nos. 1-2, pp. 22-34, 2008.